

https://dspace.org/

Development of an enhanced calcination, optimised leaching process for the improved recovery of rare earth elements from South African discard coal

Harrar, Hamza

2022
https://hdl.handle.net/10539/34419

Downloaded from a DSpace repository. https://dspace.org/



Development of an enhanced calcination, optimised leaching process for the improved recovery of Rare Earth Elements from South African discard coal.

Prepared by:

Hamza Harrar

1429563

Submitted to:

A Dissertation Submitted to the School of Chemical and Metallurgical Engineering, Faculty of Engineering and the Built Environment, University of the Witwatersrand, Johannesburg, in Fulfilment of the Requirements for the Degree of Master of Science in Engineering.

Supervisor: Prof. Samson Bada

17th May 2022

DECLARATION

I declare that this dissertation is my own unaided work, unless otherwise stated and acknowledged. It is being submitted for the degree of Master of Science in the School of Chemical and Metallurgical Engineering, to the University of Witwatersrand, Johannesburg. It has not been submitted before for any degree or examination to any other university.

Signature of candidate: ……. on the 17th day of: May, Year: 2022.

ABSTRACT

Globally there has been a rapid surge in demand for rare earth elements (REE) due to their numerous high-tech applications. China holds more than 43% of global conventional REE reserves and supplies 97% of the world's REE. Research into other sources of REE is important in responding to society demands, coupled with China's REE export restrictions and unique commodity applications. Mechanised mining in South Africa produces about 60 million tonnes of coal discard each year that is left in discard dumps. Thus, there is an innovative need to reuse discard coal to reduce its pollution and impact on the health of society and the environment.

In this study, a Run of Mine (ROM) and discard coal were evaluated for their REE contents, distribution and association with the inorganic mineral and organic coal constituents. The Tescan Integrated Mineral Analyser was used to investigate the REE associations and distributions. X-ray diffraction provided information on mineral phases and Inductively coupled plasma-mass spectrometry was used to quantify the amount of REE in the coals and subsequent leachate samples. Varying lixiviates under the optimised leaching parameters were investigated using the response surface methodology (RSM) to recover REE from the coal samples. The data attained was used to optimise the leaching process to improve the REE leaching recovery. The same optimised leaching approach was applied to coal samples calcined between 500 ^{o}C to 800 ^{o}C.

The Total REE (TREE) content of each of the two medium rank C bituminous coal samples exceeded 225 ppm. In addition, kaolinite, pyrite and hematite were the main REE-bearing minerals in the discard and ROM coal samples. Heavy REE (HREE) showed a weak ion-adsorbed association with clay minerals (kaolinite) finely dispersed in the organic matrices and fractures of both samples. Furthermore, HREE displayed a strong affinity for the organic macerals and were slightly enriched in the ROM coal, with the discard coal containing higher concentrations of TREE. The encouraging results of this study suggest that both coal sources contain more Critical REE than Uncritical REE, which are in greater demand internationally.

The optimised leaching experiments for both coals indicated that an increase in lixiviate concentration (0.5 M to 2 M) and leaching temperature (30 ^{o}C to 50 ^{o}C), along with a decrease in solid:liquid ratio (40 g/l to 10 g/l), improved the percentage (%) recovery of REE. The RSM and statistical analysis of the leaching data were satisfactorily indicated by an error % of less

than 1.26%. The optimised leaching parameters (2 M, 10 g/l and 50 ^{o}C) manifested a 18.95% REE recovery and 41.35% TREE recovery in the discard and ROM samples, respectively. The low recovery of REEs on the raw samples had indicated that significant quantities of the weekly ion adsorbed REEs were recovered. The study indicated that the best lixiviate was HCl, as it achieved a higher REE recovery than $HClO_4$ and is relatively inexpensive compared to HNO_3.

The % REE leaching recovery increased as the calcination temperature increased from 500 ^{o}C to 700 ^{o}C, with optimal calcination at 700 ^{o}C. At this temperature (700 ^{o}C), the REE leaching recovery achieved was 94.73% (ROM) and 98.17% (discard). Calcination also increased the concentration of REE for ROM sample from 225 ppm to 347 ppm and discard sample from 245 ppm to 363 ppm at 700 ^{o}C. At 800 °C, the REE concentration increased to 362 ppm (ROM) and 390 ppm (discard). Leaching time was reduced as the majority of the REE were recovered under the optimised leaching conditions in the first 15 minutes of the process. The significant effect of calcination on REE recovery suggests that REE-bearing minerals were solubilised and oxidised during calcination.

The discard coal used in this study had a significantly higher potential than the ROM coal for REE recovery, as it had higher REE abundance and greater recovery. It also establishes a potentially economically viable secondary REE source as no mining is required and contributes to the international pollution reduction target.

ACKNOWLEDGEMENTS

First and foremost, my gratitude and thanks to the Almighty Allah (God), the most merciful, the most beneficent who has given me the capacity and good health to complete this study. The journey was a beautiful bumpy challenge through which my belief in Allah continues to help me overcome the challenges.

To my mother, Khadija, and my father, Abderrahim Harrar, thank you for all the support, encouragement and prayers. Thank you to my five sisters (Fatima, Aa'ishah, Zainab, Saudah and Boushrah) who motivated me, inspired me, supported me on tedious days, for humour and happiness during difficult times, coupled with the editing of the English grammar in the study. I truly appreciate all the assistance, love, encouragement and support.

I acknowledge with immense pleasure and appreciation the assistance, guidance and contributions provided by my principal supervisor, Prof. Samson. O Bada. Thank you for always providing me with drive, energy and good work ethic, together with all the suggestions and motivations. I would like to thank Dr Jibril Abdulsalam for his contributions and the University of Witwatersrand's Clean Coal Technology Group for its support. Special thanks to Mr. Kingsley for becoming a close friend and research colleague who provided me with complex advice and support throughout my study.

I wish to extend my appreciation for the immeasurable contributions to the completion of my research to the following persons: Prof. Rosemary Falcon, Mr. Phillip Pieterse, Prof. Nicola Wagner, Mrs. Petra Dinham, Mr. Paul Den Hoed, Mr. Motlatsi Phali, Mr. Bruce Mothibedi, Miss Ntokozo Dube, Mrs. Reghana Burns, Miss Sibongile Maswanganye and Mr. Phathutshedzo Sikhwari, Mr. Rodney Gurney.

I extend my gratitude to the National Research Foundation of South Africa's SARChI Clean Coal Technology Grant (Grant Number: 86421) for their financial support for this project. Lastly, the opinions, findings, and conclusions expressed and are not necessarily to be attributed to the National Research Foundation (NRF) as they accept no liability in this regard.

PUBLICATIONS

The following journal articles were developed from this study:

I. Orevaoghene Eterigho-Ikelegbe, **Hamza Harrar**, Samson Bada. (2021) 'Rare earth elements from coal and coal discard – A review', *Minerals Engineering*. Pergamon, 173, p. 107187. doi: 10.1016/J.MINENG.2021.107187.

II. **Hamza Harrar**, Orevaoghene Eterigho-Ikelegbe, Samson Bada. 'Mineralogy and distribution of rare earth elements in the Waterberg Coalfield discard coal' (**Accepted May 2022**).

III. **Hamza Harrar**, Orevaoghene Eterigho-Ikelegbe, Samson Bada, Jibril Abdulsalam 'Development of an optimisation leaching process for the improved recovery of Rare Earth Elements from South African discard coal and Run of Mine coal' (Prepared).

IV. **Hamza Harrar**, Orevaoghene Eterigho-Ikelegbe, Samson Bada. 'Development of an enhanced calcination optimised leaching process for the improved recovery of Rare Earth Elements from South African discard coal and Run of Mine coal' (In preparation).

TABLE OF CONTENTS

DECLARATION i

ABSTRACT ii

ACKNOWLEDGEMENTS iv

PUBLICATIONS v

LIST OF FIGURES xi

LIST OF TABLES xiv

NOMENCLATURE xv

CHAPTER 1: INTRODUCTION 1

1.1 Background and motivation 1

1.2 Problem statements 3

1.3 Research questions 3

1.4 Aim and research objectives 4

1.5 Hypothesis 4

1.6 Dissertation layout 5

CHAPTER 2: LITERATURE REVIEW 6

2.1 Introduction 6

2.2 What are Rare Earth Elements 6

2.2.1 Application and demand for REE 8

2.2.2 Occurrences of REE 11

2.2.2.1 Bastnaesite 13

2.2.2.2 Monazite 13

2.2.2.3 Xenotime 13

2.2.3 Alternative REE-bearing minerals. 14

2.2.4 REE in coal 17

2.2.4.1 The abundance of coal and REE in coal-related sources 18

2.3 Background of coal 21

2.3.1 Formation of coal 21
2.3.2 Origin of coal macerals (organic matter) 23
2.3.3 Coal microlithotypes 23
2.3.4 Mineral matter in coal 24
2.3.4.1 Formation of mineral matter in coal 25
2.3.5 Rank of coal 27
2.3.6 Coal grade 29
2.4 Overview of South African coals 29
2.4.1 South African coal reserves 29
2.4.2 Geological setting of coalfields in South Africa 30
2.5 Occurrence of REE and REE-bearing minerals in South African coal reserves 31
2.5.1 Modes and formation of REE minerals present in coal 33
2.6 Physicochemical separation and physical separation of REE minerals 34
2.6.1 Froth flotation 34
2.6.2 Magnetic separation 36
2.6.3 Spiral, shaking table and multi-gravity separators 37
2.6.4 Electrostatic separation 38
2.7 Chemical beneficiation and thermal pre-treatment of REE 39
2.7.1 Hydrometallurgical techniques for REE recovery 39
2.7.1.1 Ion-exchange leaching of REE 40
2.7.1.2 Sequential digestion/leaching of REE 40
2.7.1.3 Acid leaching of REE 42
2.7.1.4 Alkaline pre-treatment before leaching 45
2.7.2 Thermal pre-treatment and leaching of REE (pyrometallurgy) 47
2.8 Summary 50
CHAPTER 3: METHODOLOGY 52
3.1 Introduction 52
3.1.1 Origin and collection of samples 52

3.1.2 Sample preparation 52
3.1.3 Sample relative densities 52
3.2 Analytical techniques 53
3.2.1 Particle size distribution analysis 53
3.2.2 Proximate analysis 53
3.2.3 Ultimate and total sulphur analysis 53
3.2.4 Forms of sulphur analysis 54
3.2.5 Petrography 54
3.2.6 X-ray diffraction analysis 54
3.2.7 Fourier transform infrared spectroscopy 55
3.2.8 Tescan Integrated Mineral Analyzer analysis 55
3.2.9 Inductively coupled plasma mass spectrometry 55
3.3 Experimental procedure 56
3.3.1 Summary of Experimental Procedures 57
3.4 Beneficiation and recovery of REE 58
3.4.1 Part 1: Leaching of the non-calcined samples 58
3.4.1.1 Stage 1: varying concentration, solid:liquid ratio and temperature 58
3.4.1.2 Stage 2: leaching of non-calcined samples under DOE optimal conditions 61
3.4.2 Calcination method and apparatus 61
3.4.3 Part 2: Leaching of the calcined samples at optimal parameters 62
3.5 List of apparatus and equipment required for the leaching tests 62
CHAPTER 4: RESULTS AND DISCUSSION 63
4.1 Introduction 63
4.2 Coal characterisation results 63
4.2.1 Physico-chemical properties and petrography results 63
4.2.2 Mineralogical composition of the coals 65
4.2.3 Fourier transform infrared spectroscopy results. 72
4.3 REE contents 74

4.3.1 Comparative quantitative results of REE....74
4.3.2 Comparative quantitative REE results for the two calcined coal samples....75
4.3.3 Estimation of the quality of RC1 and DC1 as an REE source....77
4.4 Depositional environment of REE....80
4.5 Hydrometallurgical treatment of RC1 and DC1 for REE recovery....83
4.5.1 Particle size distribution of samples used in the leaching tests....83
4.5.2 Part 1 and stage 1 of the leaching results from non-calcined RC1 and DC1....84
4.5.3 Leaching mechanisms of the REE-bearing minerals....86
4.6 Experimental design and statistical analysis results from DOE....88
4.6.1 Optimisation of the REE leaching recovery from DC1 and RC1....88
4.6.1.1 Suitability and adequacy of the model (ANOVA)....90
4.6.1.2 Linear model equations for predicting % REE leaching recovery....92
4.6.1.3 Response plots for determining the effect of HCl concentration on the % REE leaching recovery....95
4.6.1.4 Response plots for determining the effect of solid:liquid ratio on the % REE leaching recovery....96
4.6.1.5 Response plots for determining the effect of leaching temperature on the % REE leaching recovery....97
4.6.1.6 Response surface methodology plots for the interactions between the leaching factors and the % REE leaching recovery....98
4.6.1.7 Determination of the optimal leaching parameters....103
4.7 Percentage REE recovery under optimised leaching conditions for discard and ROM coals....106
4.7.1 Effect of HCl on the recovery of REE from RC1 and DC1 coals....106
4.7.2 Effect of acid type on the percentage REE recovery under optimal leaching parameters....110
4.8 The effect of calcination pre-treatment on the subsequent % REE leaching recovery…..112
4.8.2 The effect of calcination pre-treatment on the subsequent % HREE and LREE leaching recovery....115

4.9 Summary 117
CHAPTER 5: CONCLUSION AND RECOMMENDATIONS 118
5.1 Overview 118
5.2 Key findings of the research 118
5.3 Recommendations for future studies 120
REFERENCES 122
APPENDICES 139
Appendix A1 139

LIST OF FIGURES

Figure 2-1: REE industrial market demand per element during 2015 (adapted from Goodenough *et al.*, 2018)……..10
Figure 2-2: Forecast of REE market demand estimate per element for 2025 (adapted from Goodenough *et al.*, 2018)……..11
Figure 2-3: SEM-EDX analysis of a non-calcined coal sample from Western Kentucky USA (Zhang and Honaker, 2020)……..18
Figure 2-4: Variation in the key coal properties for rank advancement (adapted from Ward and Suárez-Ruiz (2008))…….29
Figure 2-5: Illustration of the 19 coalfields situated in South Africa (adapted from Snyman (1998))……..31
Figure 2-6: XRD spectrum for raw coal from the Tutuka Power Station (Akinyemi *et al.*, 2012)…….32
Figure 2-7: Variation of the minerals by depth in the Grootegeluk formation based on XRD and petrographic analysis (Faure, 1993)……...33
Figure 2-8: The sequential extraction procedure for REE recovery from coal (adapted from Zhang and Honaker, 2019b)……42
Figure 2-9: Representation of REE recovery based on their mode of occurrence in sequential extraction tests (Zhang and Honaker, 2019b)……42
Figure 2-10: Acid leaching of coarse refuse coal and middlings coal at different calcination temperatures (Zhang and Honaker, 2019a)……...49
Figure 3-1: Overview of the calcination and leaching methodology applied in the study……57
Figure 3-2: Image of the experimental leaching set-up…….59
Figure 3-3: Image of the microfilter-syringe employed for leachate extractions……...60
Figure 4-1: Petrography images 1a, b, c, d (RC1) and 1e, f, g, h (DC1)…….67
Figure 4-2: XRD diffractograms for RC1 and DC1……..69
Figure 4-3: TIMA image results of REE-bearing minerals for RC1 (BSE image a and c, and SE image b and d) and DC1 (BSE image e and g, and SE image f and h)……...71
Figure 4-4: FTIR spectrum for the ROM (RC1) and discard coals (DC1)…….73
Figure 4-5: Categorisation of the RC1 (representing the ROM coal) (denoted by the **red star**) and DC1 (representing the discard coal) (denoted by the **red star as well, similar position on chart**) by employing the $C_{outlook}$ in conjunction with the $REY_{def,\ rel}$ % (Seredin and Dai,

2012)…….78
Figure 4-6: Normalised REE:UCC for RC1 and DC1…….…..79
Figure 4-7: REE chondrite (Schmitt *et al.*, 1963) normalised plot for ROM coal (represented by RC1), discard coal (represented by DC1), USA coals (Finkelman, 1993) and Chinese coals (Dai *et al.*, 2008)……...82
Figure 4-8: PSD analysis curve for RC1 and DC1…….83
Figure 4-9: The % REE recovery of RC1 (A, B and C) and DC1 (D, E and F) after leaching…85
Figure 4-10: Normal probability plots of the % REE leaching recovery for RC1 (A) and DC1 (B)…….93
Figure 4-11: Residuals vs predicted plot for % REE leaching recovery for RC1 (A) and DC1 (B)…….94
Figure 4-12: Linear regression plots for the predicted vs actual % of REE leaching recovery for RC1 (A) and DC1 (B)……..95
Figure 4-13: % REE leaching recovery vs HCl concentration for RC1 (A) and DC1 (B)……..96
Figure 4-14: % REE recovery leaching vs solid:liquid ratio for RC1 (A) and DC1 (B)…….97
Figure 4-15: % REE leaching recovery vs leaching temperature for RC1 (A) and DC1 (B)…..98
Figure 4-16: Contour plots for the relationship between HCl concentration and leaching temperature with respect to % REE leaching recovery for RC1 (A) and DC1 (B)……...……..99
Figure 4-17: 3D surface plots of the relationship between temperature, HCl concentration and their impact on the % REE leaching recovery for RC1(A) and DC1(B)……..100
Figure 4-18: Contour plots for the relationship between solid:liquid ratio and leaching temperature with respect to % REE leaching recovery for RC1 (A) and DC1 (B)……..101
Figure 4-19: 3D surface plots of the relationship between leaching temperature, pulp density (solid:liquid ratio) and their impact on the % REE leaching recovery for the RC1(A) and DC1(B) coals……..101
Figure 4-20: ROM (RC1) (A) and Discard (DC1) (B) coals contour plots for the relationship between solid:liquid ratio (g/l) and HCl (M) concentration with respect to REE recovery…..102
Figure 4-21: 3D surface plots of the relationship between leachate concentration, pulp density (solid:liquid ratio) and their impact on the % REE leaching recovery for the RC1(A) and DC1(B)……...102
Figure 4-22: Contour plots of desirability for varying solid:liquid ratios and HCl concentrations for RC1 (A) and DC1 (B)……104
Figure 4-23: Contour plots of desirability for varying solid:liquid ratios and leaching temperatures for RC1 (A) and DC1 (B)……...105

Figure 4-24: RC1 and DC1 % REE leaching recovery under the optimised leaching parameters (HCl concentration of 2 M, solid:liquid ratio of 10 g/l, leaching temperature of 50 ^{o}C, D_{90} = - 106 μm, stirrer speed 550 rpm)……...107
Figure 4-25: RC1 and DC1 % HREE (A) and % LREE (B) leaching recovery under the optimised leaching parameters (HCl concentration of 2 M, solid:liquid ratio of 10 g/l, leaching temperature of 50 ^{o}C, D_{90} = - 106 μm, stirrer speed 550 rpm)……..109
Figure 4-26: RC1 and DC1 % REE leaching recovery under the optimised leaching parameters ($HClO_4$/HNO_3 concentration of 2 M, solid:liquid of 10 g/l, leaching temperature of 50 ^{o}C, D_{90} = - 106 μm, stirrer speed 550 rpm)……..110
Figure 4-27: RC1 and DC1 % HREE (A) and % LREE (B) leaching recovery under the optimised leaching parameters ($HClO_4$/HNO_3 concentration of 2 M, solid:liquid ratio of 10 g/l, leaching temperature of 50 ^{o}C, D_{90} = - 106 μm, stirrer speed 550 rpm)……111
Figure 4-28: The effect of calcination of RC1 (A) and DC1 (B) on the % REE leaching recovery under the optimised leaching parameters (HCl concentration of 2 M, solid:liquid of 10 g/l, leaching temperature of 50 ^{o}C, D_{90} = - 106 μm, stirrer speed 550 rpm)……...113
Figure 4-29: Calcined RC1 (A) and DC1 (B) % HREE leaching recovery under the optimised leaching parameters of (HCl concentration of 2 M, solid:liquid ratio of 10 g/l, leaching temperature of 50 ^{o}C, D_{90} = - 106 μm, stirrer speed 550 rpm)……..115
Figure 4-30: Calcined RC1 (A) and DC1 (B) % LREE leaching recovery under the optimised leaching parameters of (HCl concentration of 2 M, solid:liquid ratio of 10 g/l, leaching temperature of 50 ^{o}C, D_{90} = - 106 μm, stirrer speed 550 rpm)……..116
Figure A1-1: PSD curve for RC1 coal sample calcined at 500^{o}C……139
Figure A1-2: PSD curve for RC1 coal sample calcined at 600^{o}C. ……...……...…139
Figure A1-3: PSD curve for RC1 coal sample calcined at 700^{o}C...…….……...…139
Figure A1-4: PSD curve for RC1 coal sample calcined at 800^{o}C……140
Figure A1-5: PSD curve for DC1 coal sample calcined at 500^{o}C. ……140
Figure A1-6: PSD curve for DC1 coal sample calcined at 600^{o}C……140
Figure A1-7: PSD curve for DC1 coal sample calcined at 700^{o}C……141
Figure A1-8: PSD curve for DC1 coal sample calcined at 800^{o}C……141

LIST OF TABLES

Table 2-1: List of 17 REE, illustrating their valence states and ionic radii (Shannon, 1976)…...7
Table 2-2: Applications and uses of REE in the industry (Naumov, 2008)……..9
Table 2-3: Common and predominant, economic or potentially economically feasible REE-bearing minerals (Long et al., 2012)……..……..15-16
Table 2-4: Minerals in coal deposits (adapted from Saxby (2000) and Xiuyi (2011))……...27
Table 3-1: Experimental design matrix (from DOE) for the leaching of non-calcined RC1…..60
Table 3-2: Experimental design matrix (from DOE) for the leaching of non-calcined DC1…..61
Table 4-1: Summary of the characteristics of the ROM coal (RC1) and coal discard (DC1)….64
Table 4-2: TIMA modal liberation analysis results for the quantities of the various mineral species present in RC1 and DC1……...70
Table 4-3: ICP-MS results for individual REE contents and TREE, outlook coefficient ($C_{outlook}$), together with important REE ratios……...75
Table 4-4: ICP-MS results for individual REE contents and the TREE, outlook coefficient ($C_{outlook}$) and REE ratios for the calcined coal samples……..77
Table 4-5: Enrichment patterns and anomalies for individual REE of RC1 and DC1……79
Table 4-6: Experimental vs predicted % REE leaching recovery from RC1…….89
Table 4-7: Experimental vs predicated % REE leaching recovery from DC1……...89
Table 4-8: ANOVA table of the % REE recovery for RC1 with respect to the various leaching factors……...91
Table 4-9: ANOVA table of the % REE recovery for DC1 with respect to the various leaching factors……...91
Table 4-10: Leaching parameter settings for the optimised response of RC1 and DC1……...103
Table 4-11: Leaching conditions of the optimised solution for RC1 and DC1……103
Table 4-12: Point prediction table for the optimised selected solutions……...105

NOMENCLATURE

List of abbreviations

Abbreviations and Acronyms	*Full meaning*
ASTM	American Society for Testing and Materials
BSE	Backscattered Electron
CFA	Coal fly ash
CREE	Critical Rare Earth Elements
DC1	Discard coal sample
DOE	Design of Expert
EDX	Energy-dispersive X-ray
FTIR	Fourier transform infrared
H_2SO_4	Sulphuric acid
H_3PO_4	Phosphoric acid
HCl	Hydrochloric acid
$HClO_4$	Perchloric acid
HGMS	High gradient magnetic separator
HHS	Hydrophobic hydrophilic separation
HNO_3	Nitric acid
HREE	Heavy Rare Earth Elements
ICP-MS	Inductively coupled plasma mass spectrometry
IEA	International energy agency
ISO	International Organization for Standardization
LREE	Light Rare Earth Elements
MGS	Multi-gravity separator
NaOH	Sodium hydroxide
NdFeB	Neodymium-iron-boron alloy
PSD	Particle size distribution
RC1	Run of Mine coal sample
REE	Rare Earth Elements
REO	Rare earth oxide
ROM	Run of Mine
RSM	Response surface methodology

SE	Secondary Electron
SEM	Scanning Electron Microscopy
SG	Specific Gravity
TEM	Transmission Electron Microscopy
TIMA	Tescan Integrated Mineral Analyzer
TREE	Total Rare Earth Elements
UCC	Upper continental crust
UCREE	Uncritical Rare Earth Elements
USA	United States of America
WEEE	Waste Electrical and Electronic Equipment
XRD	X-ray diffraction

Units of measure

Symbols	*Meaning*
^{o}C	degrees Celsius
g	grams
g/l	grams/litre
>	greater than
hrs	hours
kg	kilograms
<	less than
l	litre
kA/m	magnetic field intensity (kilo amp per metre)
T	magnetic field strength (Tesla)
µg/g	microgram/gram
µg/ml	microgram/millilitre
µm	micrometres
ml	millilitres
mm	millimetre
min	minute
M	molar concentration (mol/litre)
No.	number

-	particle size and below the specific particle size
ppm	parts per million
%	percentage
C_{RS}	REE/elemental concentration
rpm	revolutions per minute
s	second
SG	specific gravity
C_L	TREE/elemental concentration
V_L	volume of leachate
vol. %	volume percentage
M_{RS}	weight of the coal
% wt.	weight percentage

CHAPTER 1: INTRODUCTION

1.1 Background and motivation

The international demand for Rare Earth Elements (REE) was approximately 256 000 tonnes in 2021 (Statista, 2022). As of 2019, China had an estimated 44 million metric tonnes of rare-earth oxide, with South Africa owning 0.79 million metric tonnes (Garside, 2021). The demand for REE is based on its high-technology applications, as well as its benefits and economic value (Reid, 2018). The research into the mining, beneficiation and utilisation of this commodity will continue to gain more attraction due to its importance in the 4th industrial revolution. REE have unique intrinsic properties that are used in high-tech applications, including phosphors and electronic displays, high strength permanent magnets and the generation of renewable energy sources (wind and solar power) (Humphries, 2013).

For many years REE have been mined conventionally from the ion-adsorbed clay deposit predominantly found in China, Mongolia and Australia (Zaimes *et al.*, 2015; Reid, 2018). The high concentration of these elements in one location or region is rare, apart from in China. This has led China to be the dominant global market for this commodity (JackLiftonReport, 2019). The Light Rare Earth Elements (LREE) are obtained from minerals like Bastnaesite and Monazite (LREE: Cerium (Ce), Lanthanum (La), Neodymium (Nd)), whilst the Heavy Rare Earth Elements (HREE) are obtained from Xenotime (HREE: Yttrium (Y), Dysprosium (Dy), Erbium (Er), Ytterbium (Yb) and Holmium (Ho)) (Akdogan *et al.*, 2019). With the economic exploitation of conventional ores in many countries, as well as the limited supply and importance of the commodity, there is a growing interest globally to find alternative sources for extraction and enrichment of REE. Approximately 20 years ago, the first detection of REE from coal deposits was conducted in the Russian coal basin by Seredin (1991). Subsequently, other sources, such as fly ash (Kolker *et al.*, 2017), the roof and floor of coal seams (Seredin and Dai, 2012), coal discard and acid mine drainage effluent (Zhang and Honaker, 2018) have been identified as potential sources for beneficiating REE.

Significant research has been conducted on extracting and recovering REE from Run of Mine (ROM) coarse and fine coal discard (Huang *et al.*, 2018; Zhang and Honaker, 2018) . With global coal production estimated at 8.13 billion tonnes in 2019 (Prime, 2019), it is expected that production of discard coal will increase and, thus could be a potential supply of REE. This

is significant for South Africa, where 60 million tonnes of coal waste or discard is generated annually (Nogzina, 2001).

REE are also present in post-combustion fly ash, in which they are bound with other minerals or in an ion-adsorbed/ion-substitution form (Kolker *et al.*, 2017). This form of REE require large amounts of energy for grinding and concentration of the REE at a fine particle size less than 10 µm (Huang *et al.*, 2018). The distribution of REE at fluctuating concentrations was observed in phosphorite, shells, corals, coal and carbonatites. According to Schofield and Haskin (1964), phosphorite was found with the highest concentration of lanthanides (160 ppm), whilst coal was at 49.9 ppm, followed by shells at 3.3 ppm, corals at 0.13, 0.08 and 0.052 ppm, and carbonatites within 76 and 181 ppm.

A shift in the application of coal solely for power generation is required if coal will continue to retain its dominance as the cheapest and most abundant fossil fuel. Using coal for non-energy applications such as the synthesis of high-value products is the only way that coal will continue to contribute to the South African economy for decades to come. A recent study by Wagner and Matiane (2018) revealed that Witbank and Highveld coalfields were high in REE with Total REE (TREE) levels for both samples exceeding 111 ppm. Thus, a potential source for REE recovery. Seventeen other coalfields in South Africa require investigation in terms of their REE-bearing content. Wagner and Matiane (2018), as well as others (Akinyemi *et al*., 2012; Akdogan *et al.*, 2019; van Breugel *et al*., 2019), investigating REE in South Africa, have only focused on the distribution and acid leaching of REE in ROM coal and fly ash, respectively.

The current study conducted, employed the integration of calcination before an optimised leaching process for improving REE recovery from a South African discard and ROM coals. South African coal discard has not been previously investigated for REE extraction using this procedure. Samples from discard and ROM coal were analysed for their physicochemical coal and mineralogy properties, REE distribution and abundance. Hydrochloric acid (HCl) leaching was applied to the raw coal samples according to conditions attained from Design of Expert (DOE) to optimise the leaching parameters (concentration, temperature and solid:liquid ratio) and to improve REE recovery. The pre-treatment method to increase the solubility of REE by calcination was adopted to mitigate the characteristic low REE recovery from raw coal. The REE contents of the leachate samples were analysed using Inductively coupled plasma mass spectrometry (ICP-MS).

1.2 Problem statements

I. Due to the rapid rise in global demand for REE and declining conventional reserves, the supply of high-value REE has become a concern that needs to be addressed. Furthermore, China, the major international supplier of REE, has now imposed restrictions on REE export, driving the recovery of REE from other sources such as coal and coal discard.

II. Coal is South Africa's primary electricity generation resource. The mechanised mining of coal and whole coal seam rather than mining the high-quality seam has led to the generation of tonnes of fines and coarse discard tailing streams from beneficiation plants. These coals or tailings dumps are an environmental concern for mining companies and surrounding communities. These dumps may contain REE that can be mined economically and used as a source of income for the community and the mining sector and may be employed for rehabilitation costs.

III. Another predominant problem is the ultrafine dispersion of REE within coal sources. It was noted that even with extreme particle liberation finer than 10 µm, physical separation methods manifest poor REE recovery (Jordens *et al.*, 2013). Hence, acid leaching has been identified as a better method for REE recovery, but the recovery rate depends on the coal constituents (Jordens *et al.*, 2013). Because the types of bonds and mineral associations differ from one coal to another, the recovery rate is not expected to be the same for all coals. Also, the acid concentration required for maximising REE recovery is expected to differ from coal to coal. Improving REE recovery requires optimising the acid leaching process in terms of concentration, temperature and solid:liquid ratio.

IV. The recovery of REE also depends on the mineralogy of the discard and ROM coals in terms of the distribution of REE in the coal constituents.

1.3 Research questions

The following questions were addressed in this study:

I. Will a South African discard and ROM coal provide a substantial concentration of REE before pre-treatment? Thus, indicating whether these coals are a good source for REE extraction.

II. What does the mineralogy reveal about the occurrence of REE, their associations with the mineral matter and organic matter, and is HREE or LREE more dominant in this South African ROM and discard coal?
III. Based on the association of REE with different minerals, can REE be recovered via leaching?
IV. Which acid lixiviate will achieve the highest REE recovery?
V. What effect will different leaching conditions (concentration, temperature and solid:liquid ratio) have on the percentage (%) REE leaching recovery?
VI. Will the calcination step improve the % REE leaching recovery of the two coal samples, and will this treatment technique reduce leaching time?

1.4 Aim and research objectives

This research aimed to develop an enhanced calcination and optimised acid leaching process route to recover REE from a South African discard and ROM coals. The objectives of this study were:

I. To identify the particle size distribution (PSD) of the REE present in discard and ROM coals.
II. To understand the REE associations with mineral and organic matter in the two coal samples.
III. To determine the effect of acid concentration, temperature and solid:liquid ratio on the % REE leaching recovery.
IV. To derive a statistically optimised leaching model for REE recovery.
V. To establish the most effective lixiviate for improving REE recovery.
VI. To determine the effect of calcination at optimal leaching conditions on the % REE leaching recovery from calcined discard and ROM coals.

1.5 Hypothesis

Acidic leaching of coal samples is expected to recover REE, though not in high quantities. Furthermore, with the integration of calcination before an optimised leaching process, it is expected that the % REE leaching recovery will improve for both discard and ROM coal.

1.6 Dissertation layout

This dissertation comprises of five chapters:

I. **Chapter 1:** The background and motivation for this study are outlined. The research problems, questions, aim, objectives and hypothesis evaluated in this study are presented.

II. **Chapter 2:** This chapter provides an extensive review of REE; their demand, applications, occurrences in coal and conventional minerals and associations with organic and mineral coal fractions. The chapter also presents the background of coal and its properties, the physical, chemical and thermal beneficiation methods for REE recovery from coal and other sources.

III. **Chapter 3:** This chapter provides in-depth methodology, characterisation techniques and apparatus used in the leaching and calcination experiments. The chapter further describes the experimental design for optimising modelled leaching parameters (acid concentration, temperature and solid:liquid ratio, and lixiviate) to determine the optimal parameters for improving REE recovery.

IV. **Chapter 4:** The chapter describes the coal characterisation, mineralogy and REE associations. In addition, the chapter presents the experimental and optimised results of the leaching parameters achieved, as well as the effect of calcination on improving the % REE leaching recovery.

V. **Chapter 5:** This section highlights the overall findings of the study, coupled with recommendations for future research.

CHAPTER 2: LITERATURE REVIEW

2.1 Introduction

The chapter provides a broader perspective on REE, their occurrences in conventional ores and coal sources, and their applications and benefits. Furthermore, it includes information on the association of REE with minerals in coal, together with the methods of extracting and increasing their recovery from various conventional resources and coal-related sources.

2.2 What are Rare Earth Elements

REE, in the past, were only known to chemists and material scientists, as their applications and intrinsic qualities were not well known. At the beginning of the 21st century, REE received more recognition due to the media and development of the internet (Long *et al.*, 2010). Their increasing recognition is due to their intrinsic and specialised properties, making them useful in many high-tech applications (Van Gosen *et al.*, 2017).

There are 17 REE, depicted on the periodic table as the lanthanide series from atomic number 57 to 71, including scandium (Sc, atomic number 39) and Y (atomic number 21) (Humphries, 2013; De Lima and Leal Filho, 2015). Y and Sc are considered REE due to their physical and chemical similarities, along with their affinity and association with REE minerals in nature (Dushyantha *et al.*, 2020). However, promethium (Pm, atomic number 61) does not occur naturally and thus is not regarded in the group of REE (De Lima and Leal Filho, 2015). REE spontaneously occur together in nature as they share a common trivalent charge ($^{+3}$) and primarily have similar ionic radii (Long *et al.*, 2010; Table 2-1). Cerium (Ce; atomic number 58) and Europium (Eu; atomic number 63) are exceptions, as they can also occur in different valence states (Ce^{4+} and Eu^{2+}) (Shannon, 1976). Elements on the periodic table typically increase in ionic radii as their atomic weights increase (Long *et al.*, 2010). However, with REE, their ionic radii decrease with increasing atomic weight, termed the lanthanide contraction (Gupta and Krishnamurthy, 2005; Jordens *et al.*, 2013).

Table 2-1: List of 17 REE, illustrating their valence states and ionic radii (Shannon, 1976).

Atomic number	Symbol	Name	Valence state/ Ionic radii (Å)
21	Sc	Scandium	Sc^{3+}: 0.87
39	Y	Yttrium	Y^{3+}: 1.02
57	La	Lanthanum	La^{3+}: 1.16
58	Ce	Cerium	Ce^{3+}: 1.14, Ce^{4+}: 0.87
59	Pr	Praseodymium	Pr^{3+}: 1.13
60	Nd	Neodymium	Nd^{3+}: 1.11
61	Pm	Promethium	
62	Sm	Samarium	Sm^{3+}: 1.08
63	Eu	Europium	Eu^{2+}: 1.25, Eu^{3+}: 1.07
64	Gd	Gadolinium	Gd^{3+}: 1.05
65	Tb	Terbium	Tb^{3+}: 1.04
66	Dy	Dysprosium	Dy^{3+}: 1.03
67	Ho	Holmium	Ho^{3+}: 1.02
68	Er	Erbium	Er^{3+}: 1.00
69	Tm	Thulium	Tm^{3+}: 0.99
70	Yb	Ytterbium	Yb^{3+}: 0.99
71	Lu	Lutetium	Lu^{3+}: 0.98

REE are classified according to their geochemical properties and economic stance (Seredin and Dai, 2012; Zhang *et al.*, 2015). The geochemical classification separates REE into LREE and HREE based on their atomic number (Gupta and Krishnamurthy, 1992). LREE are elements with an atomic number from 57 to 63, which include the following elements: La, Ce, Praseodymium (Pr), Nd, Samarium (Sm) and Europium (Eu) (Gupta and Krishnamurthy, 2005). Whilst HREE are elements with an atomic number of 21, 39 and from 64 to 71: Sc, Gadolinium (Gd), Terbium (Tb), Dy, Ho, Erbium (Er), Thulium (Tm) Yb, Lutetium (Lu) and Y (Gupta and Krishnamurthy, 2005). Even though Y (atomic number 39) is light, it is still in the HREE category due to the chemical and physical affiliation that it shares with HREE (Van Gosen *et al.*, 2017). LREE are found more commonly in nature than HREE, reflecting why HREE are more valuable than LREE (Reid, 2018).

The United States of America (USA) Department of Energy also categorised REE into Critical REE (CREE) and Uncritical REE (UCREE) based on their importance to global development and for supply within the next five to twenty years (Reid, 2018). According to the USA Department of Energy, the CREE include Nd, Tb, Y, Dy, Er and Eu based on their high demand and specialised characteristics (Ekmann, 2012).

2.2.1 Application and demand for REE

The surge in global demand for REE is due to their increased use in high-tech applications (Dushyantha *et al.*, 2020). In the 1890s, the first documented application of REE was the use of lanthanum oxide as a commercialised gas mantle in Vienna (Neary and Highley, 1984; Szabadvary, 1988). Since then, many scientists have been evaluating the characteristics and intrinsic properties of REE for application in different industrial sectors (Humphries, 2013; Van Gosen *et al.*, 2017). This has led to the industrial use of these elements in many different chemical forms, such as oxides, chlorides and metal alloys (Kołodyńska *et al.*, 2019).

Modern societies are becoming increasingly reliant on REE due to their strong magnetism, high thermal stability, high electrical conductivity and optical properties (Goonan, 2011; Dushyantha *et al.*, 2020). These characteristics are used in manufacturing products for primary end-consumer usage such as fluorescent light bulbs and light-emitting diodes (Humphries, 2013). Glass industries use cerium oxide for polishing and as additives to provide colour and special optical properties to glass (Goonan, 2011; Van Gosen *et al*., 2017). Manufacturing camera lenses requires REE such as La (Van Gosen *et al*., 2017). La and Ce are also used as catalysts for petrol refining and in automotive catalytic converters (Haque *et al.*, 2014; Mancheri *et al.*, 2019).

Worldwide, the rapidly growing demand for permanent magnets has led to the development of neodymium-iron-boron alloy (NdFeB) magnets, which are the most powerful magnets known today (Humphries, 2013). NdFeB magnets are used in several products such as hard drives, cell phones, windmills (Morris, 2011), hybrid vehicles, and as actuators in aircraft (Long, 2011), and approximately 75% of these magnets are manufactured in China (Humphries, 2013). Furthermore, the rise in demand for renewable energy resources has, in turn, increased the demand for REE (Haque *et al.*, 2014). Solar panels make use of REE as they absorb lower-energy photons, thereby increasing the efficiency of the solar panels (Strümpel *et al.*, 2007; Dushyantha *et al.*, 2020). Wind turbines require REE-based strong permanent magnets to design more reliable lightweight turbines with reduced maintenance costs (Heier, 2014).

REE are also used in the manufacturing of military equipment such as actuators, missiles, and smart bombs (Humphries, 2010). Agricultural activities use REE as they are vital in biological structural and functional molecules (Abdelnour *et al.*, 2019; Dushyantha *et al.*, 2020). In the

agricultural sector, they are fed as additives to farmed animals to assist in fattening and enhancing the growth of livestock (Abdelnour *et al.*, 2019). The many major end uses of REE (Table 2-2) indicate their important role in developing more efficient equipment and systems and are regarded as vitamins and a corner stone for future technologies.

Table 2-2: Applications and uses of REE in the industry (Naumov, 2008).

Chemical symbol	**Name**	**Applications**
Sc	Scandium	High-strength Al–Sc alloys, electron beam tubes
Y	Yttrium	Capacitors, phosphors, microwave filters, glasses
La	Lanthanum	Glasses, ceramics, car catalysts, phosphors, pigments
Ce	Cerium	Polishing powders, ceramics, phosphors, glasses, catalysts
Pr	Praseodymium	Ceramics, glasses, pigments
Nd	Neodymium	Constant magnets, catalysts, IR filters, pigments for glass
Pm	Promethium	Sources for measuring devices, miniature nuclear batteries
Sm	Samarium	Constant magnets, microwave filters, nuclear industry
Eu	Europium	Phosphors
Tb	Terbium	Phosphors
Dy	Dysprosium	Phosphors, ceramics, nuclear industry
Ho	Holmium	Ceramics, lasers, nuclear industry
Er	Erbium	Ceramics, dyes for glass, optical fibres, nuclear industries
Tm	Thulium	Electron beam tubes, visualisation of images in medicine
Yb	Ytterbium	Metallurgy, chemical industry
Lu	Lutetium	Single-crystal scintillators, catalysts

REE applications in end products have increased drastically over the last ten to fifteen years due to its vast applications in industry. In 2015, Ce has the highest market demand (Figure 2-1) (Goodenough *et al.*, 2018). In the next six years, the use of REE in hybrid electric vehicles will lead to their increased demand (Roskill, 2017). By 2027 it is expected that approximately 10.1 million hybrid vehicles will be manufactured by various automotive manufacturers (Goodenough *et al.*, 2018). The increase in demand for Nd (Figures 2-1 and 2-2) is attributed to the extensive use of NdFeB magnets (Roskill, 2017; Goodenough *et al.*, 2018). This magnet will be the driving force behind the increase in the value of REE internationally due to its vast applications (wind turbines, automotive hybrid vehicles etc.).

Furthermore, a 5% increase in REE demand growth rate is forecasted for 2021, with global REE demand continuing to grow in the years to follow (Zhou *et al.*, 2017). Thus, new conventional REE deposits or alternate REE-bearing secondary resources need to be explored

to meet the future commercial extraction and production demands of these resources (Seredin and Dai, 2012; Goodenough *et al.*, 2018). Given the growing demand and potential future economic benefits of REE, this literature review also explores other non-conventional sources of REE, especially coal-related sources.

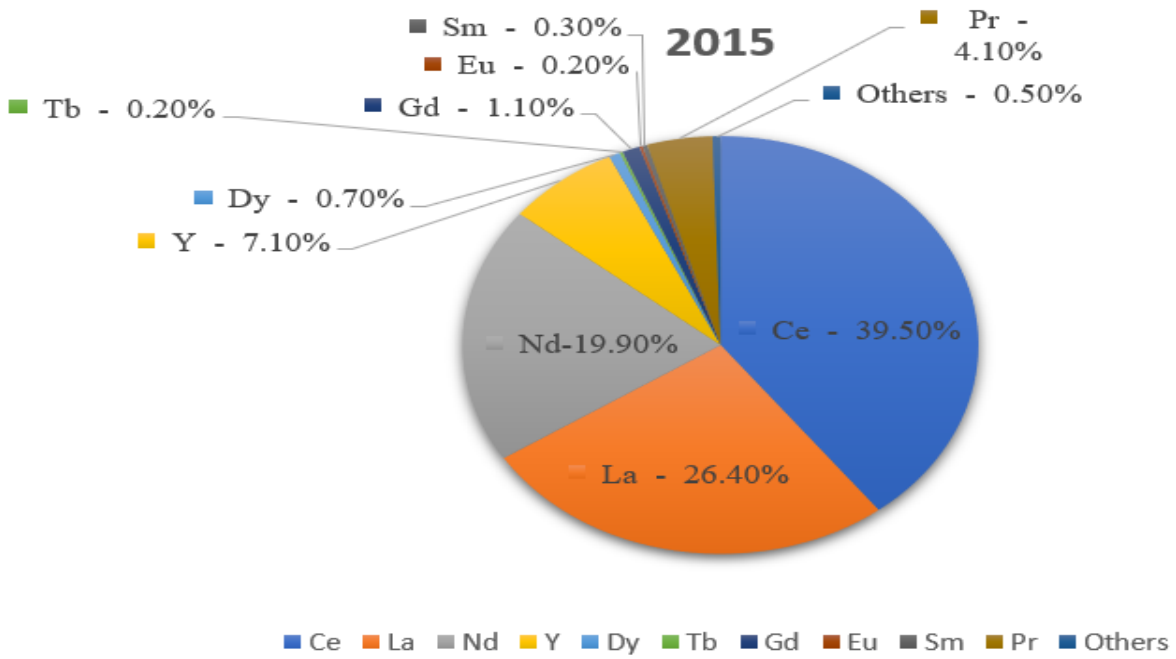


Figure 2-1: REE industrial market demand per element during 2015 (adapted from Goodenough *et al.*, 2018).

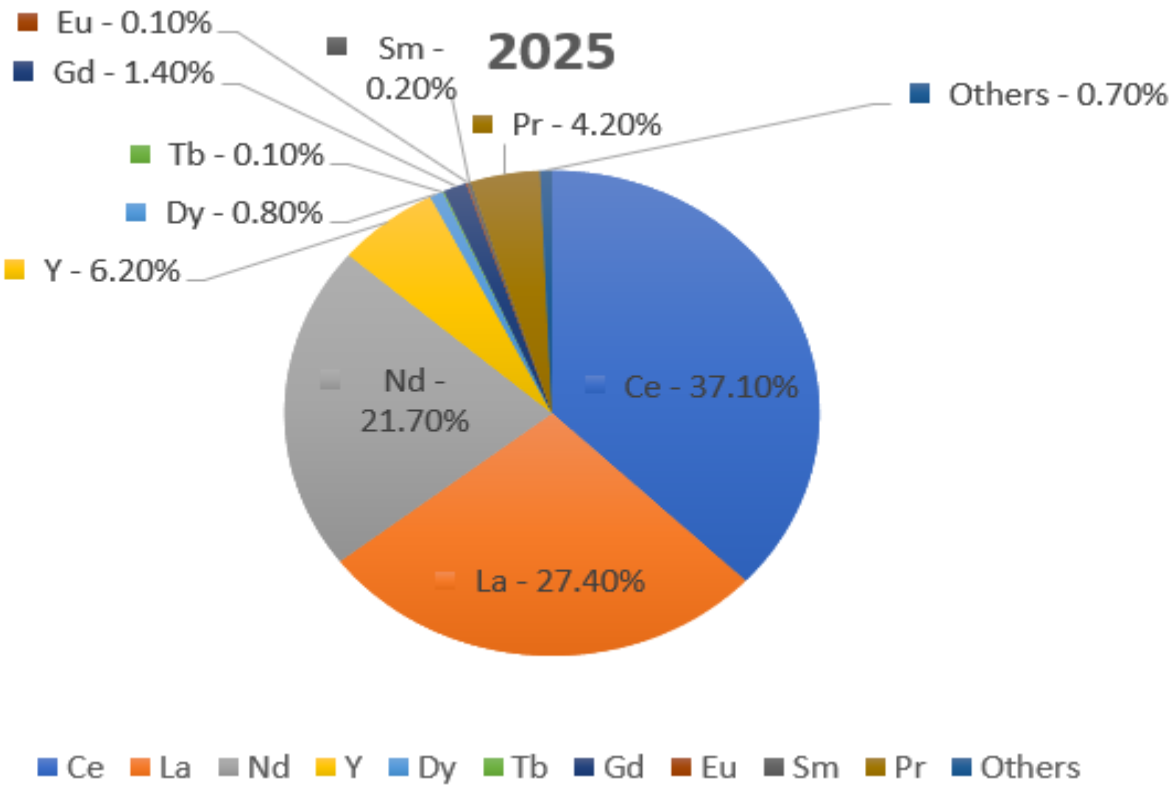


Figure 2-2: Forecast of REE market demand estimate per element for 2025 (adapted from Goodenough *et al.*, 2018).

2.2.2 Occurrences of REE

The occurrence of REE are, in fact, not as scarce or rare as the name suggests, but rather are found in abundance in ultra-dispersive forms, and thus they are seldom concentrated in easily recoverable forms or in economically mineable deposits (Yang, 2019). Although REE are considered rare, they are originally found in Earth's entire crust and are found in greater abundance than gold, platinum and silver (de Wit, 2015; Yang, 2019). In nature, REE do not originate in their elemental metallic forms but are associated with mineral compounds (Jordens *et al*., 2013).

To date, approximately 250 REE-bearing mineral forms have been discovered (Gupta and Krishnamurthy, 2005; Jordens *et al.*, 2013) in carbonate, silicate, oxide, phosphate, and halide forms (Van Gosen *et al.*, 2017; Al-Ani *et al.*, 2018; Dushyantha *et al.*, 2020). Nonetheless, only a few minerals (monazite, xenotime and bastnaesites) have been established for commercial production of REE due to their significant economic content and recovery (Seredin and Dai, 2012; Jordens *et al.*, 2013; Van Gosen *et al.*, 2017). REE can be recovered as primary products or secondary by-products from REE-bearing mineral deposits and mining wastes. In addition,

they can be recovered as by-products from heavy mineral extractions of rutile, ilmenite and pyrite, which typically comprise REE-bearing minerals (Dushyantha *et al.*, 2020). The REE-bearing mineral ores are found worldwide, with frequently large deposits in China, Australia, Mongolia, Russia, Finland, Brazil, India and Malaysia (Seredin and Dai, 2012; Van Gosen *et al.*, 2017; Al-Ani *et al.*, 2018).

The fact remains that in 2018 China accounted for approximately 71% of REE production internationally (Shen *et al.*, 2020) and since the late 1990s China contributed approximately 90% to the world REE production on average (Van Gosen *et al.*, 2017). The world REE reserve is estimated to be over 130 million tonnes (Van Gosen *et al.*, 2017), with China holding 43% (Ekmann, 2012) and Mongolia accounting for a further 17% (Kim *et al.*, 2016). In 2016, China's export restrictions affected the global demand for this resource, as out of the 210 000 tonnes produced in 2016, China supplied approximately 130 000 tonnes (Humphries, 2013). This restriction and the indispensable applications of REE have led to new efforts by several scientists (Van Gosen *et al.*, 2017). The efforts of these scientists and scholars (such as Zhang *et al.*, 2015; Honaker *et al.*, 2016; Dushyantha *et al.*, 2019) include exploring alternative sources, new deposits, secondary sources and REE wastes for the extraction and recycling of REE (Long *et al.*, 2010; Seredin and Dai, 2012).

An alternate conventional resource to REE-bearing minerals is ion-adsorbed clay ores, mined exclusively in China (Bao and Zhao, 2008) and first detected in the 1970s (Dushyantha *et al.*, 2020). These ores exhibit extremely low concentrations of REE (0.035 % to 1 % Rare Earth oxides (REO)) but are advantageous in terms of manifesting easily leachable forms of REE (Bao and Zhao, 2008). Ion-adsorbed clay ores, also identified as weathered crust elution deposits, consist of low-grade Rare Earth ions that are adsorbed onto negatively charged alumina-silicate minerals and exhibit high economic potential consisting predominantly of HREE in easily extractable forms (Moldoveanu and Papangelakis, 2013). Many of these deposits in China are close to being exhausted, citing the need to explore alternate REE-bearing deposits (Seredin and Dai, 2012). Today, nearly all REE come from the weathered crust elution deposit and three viable REE-bearing minerals, namely bastnaesite, monazite and xenotime (Seredin and Dai, 2012). These REE-bearing minerals are discussed in the following section.

2.2.2.1 Bastnaesite

Bastnaesite [REE(CO_3)F] contains approximately 70 % of REO and is the largest source of REE available for economic extraction (Jordens *et al.*, 2013; Dushyantha *et al.*, 2020). Bastnaesite is a flouro-carbonate mineral that consists mainly of LREE and comprises 50 % Ce, 20 % La and does not contain any toxic minerals such as thulium and uranium (Gupta and Krishnamurthy, 2005). Bastnaesite deposits are distributed mainly in the USA Mountain Pass, California region and Mianning, Sichuan Province, China (Gupta and Krishnamurthy, 2005; Dushyantha *et al.*, 2020). Bastnaesite bearing deposits are currently one of the main sources of LREE (Jordens *et al.*, 2013).

2.2.2.2 Monazite

Monazite [(REE)PO_4] tend to be dispersed in South Africa, Australia, Sri Lanka, China, Brazil, Thailand and the USA (Kumari *et al.*, 2015; Pandey, 2011). Monazite is ubiquitous in beach sands, metamorphic and granitic rocks and is a significant mineral present in carbonatite, iron oxide, aluminosilicates and apatite related deposits (Chen *et al.*, 2017; Dushyantha *et al.*, 2020). Monazite is a phosphate-dominant mineral comprising LREE predominantly and typically 10 % to 38 % La, 10 % to 30% Ce and 8 % to 15 % Nd (Thompson *et al.*, 2011; Chen *et al.*, 2017). REE-bearing monazite ores contain 50 % to 70% REO prior to physical treatment (Jordens *et al.*, 2013). Nonetheless, monazite ores contain significantly elevated amounts of radioactive thorium (4 % to 12 %) and uranium (Thompson *et al.*, 2011; Kumari *et al.*, 2015), thus limiting the viability of REE extraction from monazite.

2.2.2.3 Xenotime

Xenotime, an additional key REE-bearing mineral highly enriched in HREE and Y, comprises 67% REO (Gupta and Krishnamurthy, 2005; Jordens *et al.*, 2013). Xenotime [(Y, HREE)PO_4], a phosphate-dominant mineral, is commonly found with monazite and contains lower amounts of radioactive waste (Jordens *et al.*, 2013). Nonetheless, xenotime is a mineral containing significant amounts of HREE like ion-adsorbed clay ores, despite its scarcity (Jordens *et al.*, 2013). Xenotime placer deposits are distributed across the globe in China, Mongolia, Indonesia, USA, Scandinavia, South Africa and Australia (Gupta and Krishnamurthy, 2005; Lolon and Rahman, 2014; Mudd and Jowitt, 2016).

These three main REE-bearing minerals are presently being mined in a few countries for REE extraction, and the techniques used in processing these minerals and other REE mineral deposits are discussed in Sections 2.6 and 2.7.

2.2.3 Alternative REE-bearing minerals.

As stated earlier, there are approximately 250 identified minerals associated with REE (Gupta and Krishnamurthy, 2005; Jordens *et al.*, 2013; Dushyantha *et al.*, 2020). These REE-bearing minerals, such as allanite, euxenite, loparite, cheralite, phosphorites, eudialyte, samarskite and others, are further described in Table 2-3 (Long *et al.*, 2012; Jordens *et al.*, 2013). These minerals occur in the forms of oxides, carbonates, phosphates, silicates, hydroxides and halides (fluorides) that are observed and identified in commercial or potentially commercial REE deposits (Van Gosen *et al.*, 2017; Dushyantha *et al.*, 2020).

Table 2-3: Common and predominant, economic or potentially economically feasible REE-bearing minerals (Long *et al.*, 2012).

Mineral	**Chemical formula**	**REO %**	**ThO_2 %**	**UO_2 %**	**Mineral**	**Chemical formula**	**REO %**	**ThO_2 %**	**UO_2 %**
Oxides and hydroxides					*Carbonates*				
Aeschynite	(Ce,Th,Ca…)[(Ti,Nb,Ta)$_2$O$_6$]	-	-	-	Ancylite	Sr(Ce,La)(CO$_3$)$_2$(OH)(H$_2$O)	46–53	0–0.4	0.1
Brannerite	(U,Ca,Y,Ce)(Ti,Fe)$_2$O$_6$	4	4	63	Bastnäsite	(Ce, La,Y)CO$_3$F	70–74	0–0.7	–
Cerianite	(Ce^{4+},Th)O$_2$	82	5	–	Parisite	Ca(Ce,La)$_2$(CO$_3$)$_3$F$_2$	59	0–0.5	0–0.3
Euxenite	(Y,Er,Ce,U,Pb,Ca)(Nb,Ta,Ti)$_2$(O,OH)$_6$	–	–	–	Synchysite	Ca(Ce,Nd,Y,La)(CO$_3$)$_2$F	51	–	–
Fergusonite	YNbO$_4$	42–52	0–0.9	1–2.5	Tengerite	Y$_2$(CO$_3$)$_3$·n(H$_2$O)	–	–	–
Loparite	(Ce,Na,Ca)(Ti,Nb)O$_3$	32–34	0.8	–	*Phosphates and fluorides*				
Perovskite	(Ca,REE)TiO$_3$	<37	0–2	≤0.05	Britholite	(Na,Ce,Ca)$_5$(OH)[(P,Si)O$_4$]$_3$	33–61	0.5–21	0.2–1.5
Pyrochlore	(Ca,Na,REE)$_2$Nb$_2$O$_6$(OH,F)	2.6	0.2	0–10	Brockite	(Ca,Th,Ce)(PO$_4$)·H$_2$O	7–24	24–45	3
Samarskite	(Y,Er,Fe,Mn,Ca,U,Th,Zr)(Nb,Ta)$_2$(O,OH)$_6$	–	–	–	Cheralite	(Ca,Ce,Th)(P,Si)O$_4$	27–43	28–32	4
Uraninite	(U,Th,Ce)O$_2$	0.9–5	0.2–14	70–91	Churchite	YPO$_4$·H$_2$O	50–53	–	–

Mineral	**Chemical formula**	**REO %**	**ThO_2 %**	**UO_2 %**	**Mineral**	**Chemical formula**	**REO %**	**ThO_2 %**	**UO_2 %**
Phosphates and fluorides					*Silicates*				
Britholite	$(Na,Ce,Ca)_5(OH)[(P,Si)O_4]_3$	33–61	0.5–21	0.2–1.5	Allanite	$Ca(Ce,La,Y,Ca)Al_2(Fe^{2+},Fe^{3+})(SiO_4)(Si_2O_7)O(OH)$	3–51	0–5	0–3
Brockite	$(Ca,Th,Ce)(PO_4)\cdot H_2O$	7–24	24–45	3	Chevkinite	$(Ca,Ce,Th)_4(Fe^{2+},Mg)_2(Ti,Fe^{3+})_3Si_4O_{22}$	40–45	0.7–0.8	–
Cheralite	$(Ca,Ce,Th)(P,Si)O_4$	27–43	28–32	4	Eudialyte	$(Na,Ca,REE)_5(Fe^{2+}Mn)(Zr,Ti)[(Si_3O_9)_2](OH,Cl)$	0.4–7	–	≤0.09
Churchite	$YPO_4\cdot H_2O$	50–53	–	–	Gadolinite	$Y_2Fe^{2+}Be_2Si_2O_{10}$	51–55	0–0.9	–
Crandallite	$CaAl_3(PO_4)_2(OH)_5\cdot H_2O$	–	–	–	Gerenite	$(Ca,Na)_2(Y,REE)_3Si_6O_{18}\cdot 2H_2O$	–	–	–
Florencite	$(La,Ce)Al_3(PO_4)_2(OH)_6$	18–32	1.4	–	Iimorite	$Y_2(SiO_4)(CO_3)$	69	–	–
Fluocerite	(La,Ce)F	83	1.6	–	Kainosite	$Ca_2(Ce,Y)_2(SiO_4)_3CO_3\cdot H_2O$	38	0.03	–
Gagarinite	$NaCaY(F,Cl)_6$	55–57	–	–	Sphene	$(Ca,REE)TiSiO_5$	0–4.5	–	0.06
Gorceixite	$(Ba,REE)Al_3[(PO_4)_2(OH)_5]\cdot H_2O$	–	–	–	Steenstrupine	$Na_{14}Ce_6Mn_2Fe_2(Zr,Th)(Si_6O_{18})_2(PO_4)_7\cdot 3H_2O$	30–31	2	–
Goyazite	$SrAl_3(PO_4)_2(OH)_5\cdot H_2O$	–	–	–	Thalenite	$Y_2[Si_2O_7]$	63–64	–	–
Monazite	$(Ce,La,Th,Nd,Y)PO_4$	35–71	0–20	0–16	Thorite	$(Th,U)SiO_4$	≤3	72–82	8–16
Rhabdophane	$(Ce,La)PO_4\cdot H_2O$	58–69	0.7	0.4	Zircon	$(Zr,REE)SiO_4$	0–10.5	0–2	0–5
Xenotime	YPO_4	52–57	0.4	0–5					

2.2.4 REE in coal

Over the past three decades, several researchers have observed that REE are abundant in different coal types and grades (Seredin and Dai, 2012; Dai and Finkelman 2018). Coal naturally contains low concentrations of REE that are typically two and half times less in concentration related to the Earth's upper continental crust (Seredin and Dai, 2012). In the past two decades, the existence, mineralogy and geochemistry of REE in coal have been well studied (Dai *et al.*, 2012; Zhang *et al.*, 2015; Hoshino *et al.*, 2016). This had led to further developments of modern analytical techniques (Thompson *et al.*, 2011; Dai *et al.*, 2012; Dai *et al.*, 2020) in detecting elevated concentrations of REE in coal. Ketris and Yudovich (2009) reported an average REE concentration of 68.5 ppm for world coals, whilst Seredin (1996) and Zheng *et al*. (2007) estimated that the average REE concentration in coal globally is 46 ppm. Seredin and Dai (2012) and Karayigit *et al.* (2000) reported an average REE content of 101 ppm and 116 ppm in Chinese and Turkish coal, respectively. Some coals in the USA have been reported with a concentration of 62 ppm. Nonetheless, the differences in the concentration of REE in world coals arise as a result of the variation in coal geochemistry due to environmental factors prevailing during its formation (Zhang *et al.*, 2015).

According to Zhang *et al.* (2015), the cut-off grade for REE in coal-related sources is around 115 ppm to 130 ppm, which depicts whether an ore is appropriate or suitable for REE recovery. A few scholars have suggested an outlook coefficient for REE ores to evaluate the market value and quality of the ore (Seredin and Dai, 2012; Zhang *et al.*, 2015). The outlook coefficient (depicted in equation 2-1) employs a criterion that portrays the CREE for supply divided by excessive and UCREE of the ore of interest (Seredin and Dai, 2012; Dai and Finkelman 2018).

$$C_{outlook} = \frac{\left(\frac{(\sum CREE)}{(\sum REE)}\right)}{\left(\frac{(\sum UCREE)}{(\sum REE)}\right)} \quad (2\text{-}1)$$

From the equation 2-1, a higher $C_{outlook}$ would dictate an ore rich in CREE, meaning more CREE can be recovered at an increased profit. Ketris and Yudovich (2009) estimated the average $C_{outlook}$ for world coals to be 0.64. Moreover, an increase in REE content of coals will reflect a higher $C_{outlook}$.

2.2.4.1 The abundance of coal and REE in coal-related sources

The deposition of REE within coal-bearing strata is understood to be an outcome of sedimentation mechanisms that include chemical and physical rock weathering (Li *et al.*, 2019). This is followed by the deployment of REE with humic matter during coalification and diagenesis (Pourret *et al.*, 2007). Many investigations reported considerably elevated concentrations exceeding 300 ppm REE in individual sites situated in the Illinois, Northern Appalachian and Central Appalachian Basins in the USA (Reid, 2018). Likewise, numerous scholars, for example, Zhang and Honaker (2019a), Montross *et al.* (2020) and Yang and Honaker (2020), have employed different analytical techniques such as SEM-EDX (scanning electron microscopy energy-dispersive X-ray spectroscopy), TEM (transmission electron microscopy) together with petrography to view the REE size distribution, site and association with mineral or organic matter in coal. These techniques determine the occurrence of REE in coal, as seen in Figure 2-3 (Zhang and Honaker, 2020). The SEM-EDX and TEM micrographs (depicted in Figure 2-3) indicate that REE occur in ultrafine particle size of 0.5 µm to 5 µm (Zhang and Honaker, 2020) and are predominantly concentrated in coal minerals such as monazite, xenotime, allanite, zircon and clay minerals like kaolinite and illite.

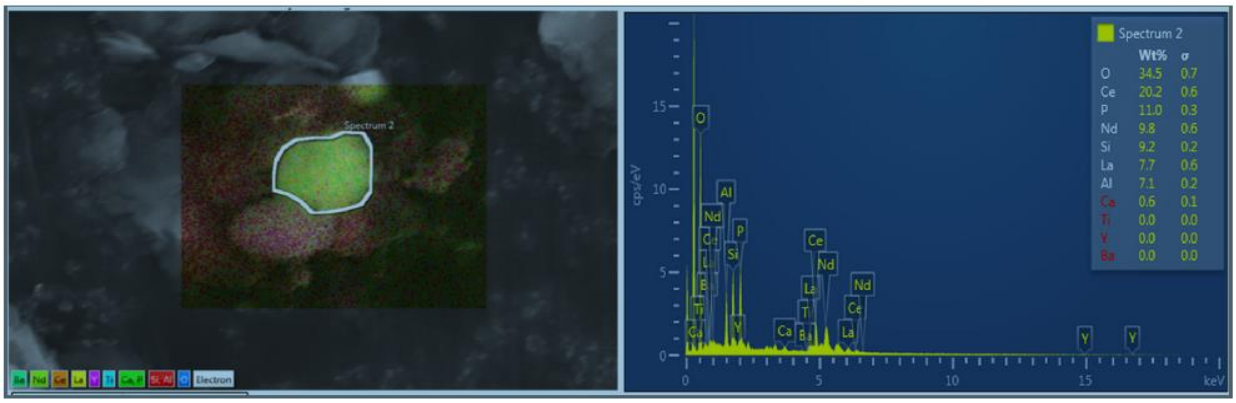


Figure 2-3: SEM-EDX analysis of a non-calcined coal sample from Western Kentucky USA (Zhang and Honaker, 2020).

In 2019, first-world developed countries in the European Union observed a decline in coal production, whereas countries like Indonesia and other Asian and African countries experienced increased coal production (IEA, 2019). China has been the dominant coal producer for the last three and half decades, and by May of 2020, China mined 3 960 million tonnes of raw coal (TheCoalHub, 2020).

South Africa, a dominant player in coal production, is the 7th largest coal producer globally, producing 254 megatonnes of coal in 2019 (Wood, 2019). Furthermore, South Africa holds the 6th largest recoverable coal deposits of 53 gigatonnes, 5% of the world's total coal reserves and 97% of Africa's hard coal (Mills, 2010). Coal generates 90% of the country's electricity, provides a feedstock for Sasol's gasification processes and is also used as coking coal for the production of steel in the country (Mills, 2010). The total reserves of REE in coal sources worldwide exceeds 50 million tonnes, which is nearly 50% of the conventional REE-bearing mineral reserves available (Zhang *et al.*, 2015; Honaker and Groppo, 2016); thus, illustrating the economic potential of coal as a source of REE.

The target REE resource from coal production and mining can be found in many different coal resources and by-products. These resources include acid mine drainage, which occurs from coal mining and discard coal stockpiles and hence assists in the natural leaching of REE (Reid, 2018; Zhang and Honaker, 2018). Coal fly ash (CFA), another resource generated as a by-product of coal combustion, is highly enriched in REE (Kolker *et al.*, 2017). CFA manifests substantially high concentrations surpassing 400 ppm due to combustion, which leads to the consumption of the organic matter and hence leaves behind REE-rich mineral matter (Seredin and Dai, 2012; Kolker *et al.*, 2017; Reid, 2018). Alternative target REE resources include coal tailings (discard coal), which is the by-product of the coal beneficiation plants (Reid, 2018). The clean product from the beneficiation plant is enriched in carbon, whilst the discard contains significant amounts of mineral matter, thus a potential high-grade resource of REE relative to the raw coal.

Extracting REE from coal wastes forms part of an overall international goal to reduce land pollution and contamination from coal discards. Many factors indicate why extracting REE from discard coal is more advantageous than extracting from post-combustion CFA (Reid, 2018). By concentrating only on CFA, most of the REE associated with the discard coal would not have been accounted for, as this fraction would have been deposited in the discard dump before the cleaned coal was used for combustion. The fact is that the bulk of REE in coal (75%) is located in the mineral matter rather than the organic fraction, which would have been removed at the coal washing plant (Reid, 2018). The REE in CFA requires high-temperature thermal processes such as sintering for separating REE from their original co-anions, potentially improving the ease of leaching acid recovery (Zhang *et al.*, 2020). The main challenge in concentrating REE from CFA is that REE silicates and phosphates in CFA are

fused into alumina-silicate glass matrices, thus resisting acid leaching and leading to a very costly process for the extraction of REE (Reid, 2018; Yang, 2019). Another reason for using discard coal is that the surrounding rock located on the roof and floor of coal seams are rich in REE, leading to optimised REE recovery during beneficiation into the high relative density fraction (Faure *et al*., 1996; Seredin and Dai, 2012; Reid, 2018; Yang *et al*., 2019).

The occurrence and existence of REE in coal are either associated with the mineral matter or organic (maceral) matter, determining the beneficiation route for REE recovery (Zhang *et al.*, 2015). There has been much discussion regarding whether REE are associated with mineral matter or organic macerals. Karayigit *et al.* (2000) reported that LREE in thirteen Turkish coal samples displayed a strong positive correlation with high ash yield, whereas HREE had no real correlation with ash yield. Furthermore, it was noted that HREE are enriched in coals with low clay content, thus depicting coals with low ash content have enriched levels of HREE (Seredin, 1996; Moldoveanu and Papangelakis, 2013). Furthermore, Karayigit *et al.* (2000) used an organic solvent extraction procedure to extract REE from coal. The result depicted a low LREE:HREE ratio; more HREE extracted implies HREE have a strong affinity for associating with organic matter. Based on these outcomes, it is evident that HREE possess a stronger affinity for the organic fraction of coal than LREE. Nevertheless, an investigation conducted by Wang *et al.* (2008) used the concept of organic solvent extraction of coal using carbon disulphide and N-methyl-2-pyrrolidone and reported that less than 5% of the TREE are associated with the organic matter. The bulk of the literature shows that REE distribution in coal is associated with the incombustible mineral matter, which fills in cracks and cleats within the organic matrices, rather than the organic matter (Zhang *et al.*, 2015).

Previous characterisation studies conducted on seams in the Southern Appalachian Basin in the USA found elevated concentrations of REE exceeding 700 ppm (Van Gosen *et al.*, 2017). Nonetheless, previous research conducted in 2013 on coal from 20 preparation plants situated in the central and Northern Appalachian coalfields showed TREE in combined feed to all 20 plants at 9900 tonnes annually (Luttrell *et al.*, 2016). The total amount of REE in the discard coal to these 20 plants was 63% (6825 tonnes), and these REE were always in the coarse discard coal after beneficiation (Honaker *et al.*, 2017). The study showed that the REE within the coal fed into the coal preparation plants are separated and mainly concentrated into the coarse discard coal fraction. Based on this, the most promising economic potential avenue for REE recovery is the use of coal discard as a feedstock.

2.3 Background of coal

2.3.1 Formation of coal

Coal is a sedimentary complex heterogeneous rock material consisting of different organic entities known as macerals together with variable amounts of inorganic matter (Taylor *et al*., 1998; Kossovich *et al.*, 2020). Coal is classified as a fossil fuel due to its combustible properties, thus providing a source of energy in many industries (Epshtein *et al.*, 2015). The organic structure of coal is primarily composed of carbon, hydrogen, nitrogen, oxygen and sulphur elements (Taylor et al., 1998; Maledi, 2017). Coal forms over millions of years when vegetation dies and is subsequently buried due to the build-up of silt and other sediments (World Coal Association, 2010). When vegetation is buried below ground level, the plant matter is altered due to the combined effects of high temperatures and pressures. This results in chemical and physical alterations of the plant matter, transforming the vegetation initially into peat and later into coal (World Coal Association, 2010).

Approximately 360 million to 290 million years ago, during the Carboniferous Period (recognised as the first coal age), coal formation began in the Northern Hemisphere (i.e., the Laurussian region) (Taylor *et al*., 1998; World Coal Institute, 2005). During the Permian Period, about 250 million years ago, coal development began in the Southern Hemisphere (i.e., the Gondwana region) (World Coal Institute, 2005). The global coal deposits vary in characteristics and properties (organic maturity and maceral composition) because of different burial conditions experienced by the dead vegetation due to tectonic plate movements, climatic conditions, type of vegetation and the subsequent temperatures and pressures after coalification (Falcon, 1986).

Initially, over millions of years, peat is converted to lignite, which is coals exhibiting a poor organic maturity (World Coal Institute, 2005). Lignite is a soft coal and varies in colour from brown to dark black. The continuous and progressive effects of variations in temperatures and pressures further transform lignite coal into sub-bituminous coal of increased organic maturity. Furthermore, progressive physical and chemical changes result in the formation of bituminous (hard) coals. Subsequently, the gradual increase in organic maturity establishes the formation of anthracite, which is coal with the highest carbon content (World Coal Institute, 2005; Zeng, 2008).

Southern African coals and coals from the Gondwana region vary significantly in rank (which reflects the organic content of the coal), host an increased amount of minerals and are relatively tricky to beneficiate (Pickel *et al*., 2018; Falcon, 1986). These features are responsible for the differences between Southern Hemisphere Gondwana coals and Northern Hemisphere Carboniferous coals. These differences are attributed to variations in conditions during coal formation and the subsequent historic different geological events occurring. Coal in the Northern Hemisphere was formed under humid, hot coastal forming swamps. Coals in the Gondwana region were formed under cold temperate conditions ascribed to the massive Ice Age (Falcon and Ham, 1988).

A study conducted by Zeng (2008) reported that all coal-bearing deposits were formed in peat swamps. Coal-bearing deposits accumulated over time occurred in continental depressions along margins of glacial valleys, lakes and shallow seas (Falcon and Ham, 1988). With the burial of vegetation matter, highly diverse topographic and sedimentary environments existed, thus leading to numerous degrees of degradation of plant matter. Some plant matter accumulated in-situ, whilst seasonal floods carried other forms of vegetation into rivers, lakes and shallow seas (Zeng, 2008). The latter resulted in large amounts of mineral matter and smaller sediments being swept from mountainous regions into lower-lying lakes, low tidal seas and lagoons (Zeng, 2008; Ward, 2002). Plant matter in the Gondwana region was typically composed of cold-cool-temperate deciduous (probably hardwood) forests to warm savannah woodlands with reed-infested swamps (Falcon and Ham, 1988). Vegetation in swamps in the Laurussian region mainly arose from abundant ferns, lycopods, horsetails and fleshy-barked trees (Falcon and Ham, 1988).

As time evolves, under the effect of temperature and pressure, vegetation increases in rank and organic maturity (Falcon and Ham, 1988). Northern hemisphere coals are higher in rank and maturity due to the deep burial of coal-bearing strata and the effects of elevated geothermal temperatures for long periods. Whereas Southern Hemisphere coal-bearing strata are predominantly buried in shallow environments and were exposed to the intrusion of hot volcanic lava, resulting in uneven rank and maturity (Falcon and Ham, 1988). The important constituents of coal are classified into three fundamental categories: organic matter, mineral matter and rank. These are discussed in Section 2.3.2.

2.3.2 Origin of coal macerals (organic matter)

Macerals are optically homogeneous organic material with partially decomposed organic remains from vegetative material (Taylor *et al*., 1998; Zeng, 2008). All macerals are categorised into three groups: vitrinite, liptinite and inertinite (Zeng, 2008). Vitrinite, a significantly important maceral group that frequently occurs in bituminous coals, is obtained from the plant's woody tissues (Falcon and Ham, 1988; Zeng, 2008). Vitrinite has a medium reflectance with a higher carbon and hydrogen content than the other two groups of macerals. The important sub-maceral groups of vitrinite include collinite, tellinite and pseudo-vitrinite (Scott, 2002). Vitrinite constituents present in South African coals vary with an average amount of approximately 40% wt. (Falcon and Ham, 1988).

Liptinites are derived from resins, pollen coats, cuticles, algae and other fatty excretions and are distinguished from vitrinite due to a higher hydrogen content and increased volatile matter (Falcon and Ham, 1988; Scott, 2002). Liptinite sub-maceral groups include sporinite, alginate, suberinite, cutinite, resinite and liptodetrinite (Pickel *et al*., 2018; Scott, 2002). Typically, South African coals reflect a minimum of 10% wt. and a maximum of 15% wt. of liptinites (Falcon and Ham, 1988). Inertinites are formed from the partial carbonisation of various flora tissues in the peat swamp stage by fire (Zeng, 2008). They are differentiated from the other macerals by their characteristic optical properties making them highly reflective. The inertinite maceral group includes fusinite, semi-fusinite, inertodetrinite, micrinite and sclerotinite (Zeng, 2008). A study conducted by Holland *et al.* (1989) illustrated that South African coals constitute 20% to 80% wt. of inertinites. Vitrinite and liptinite are reactive groups as they readily ignite under combustion conditions (Falcon and Ham, 1988). However, inertinites are unreactive as they require more oxygen and heat to ignite. The macerals play an important role in the application of coal, and much research has identified minute amounts of REE associated with coal’s organic macerals. Therefore, it is important that this study provided a review of the coal’s constituents.

2.3.3 Coal microlithotypes

Microlithotypes, or the types of maceral association, are regarded as the natural assemblages of macerals at a microscopic level (Taylor *et al*., 1998). They contain a minimum of 5% maceral and more than 20% mineral matter. Together with the maceral content, microlithotypes are composed of 20 vol. % to 60 vol. % of silicate or carbonate minerals or 5% sulphide, thus they are regarded as carbominerite irrespective of the macerals present (Suárez-Ruiz and Ward,

2008). Microlithotypes play an integral role in the density, liberation, gasification, combustion, strength and coking behaviour of coal (Falcon and Ham, 1988). The chemical characteristics of microlithotypes are similar to their prevailing macerals, whereas their physical properties exhibit a combined effect of their occurrence with macerals (Falcon and Falcon, 1987). The nature and extents of the organic forms establish the coal type (Falcon and Ham, 1988).

2.3.4 Mineral matter in coal

Improvements in highly efficient analytical techniques have led to identifying various minerals associated with coal strata. Approximately 200 different minerals have been identified in coal seams globally (Finkelman *et al.*, 2020). According to Ward (2002) and Xiuyi (2011), mineral matter in coal is referred to as the inorganic matter distributed and associated with the coal, which typically occurs in five different forms:

I. Crystalline mineral particles
II. Non-crystalline inorganic particles
III. Inorganic elements associated with organic macerals
IV. Inorganic elements dissolved in pore water and surface water in coal
V. Dissolved salts

Analogous to organic matter, mineral matter in coal is formed via complicated geological processes and events (Pickel *et al.*, 2001; Maledi, 2017; Wagner *et al.*, 2018). These events are linked to detritus deposits in peat-forming swamps, amount of sediment weathering, temperature, pressure, pH, source rock and the migration of components within coal-bearing seams (Maledi, 2017).

Mineral matter in coal can be macroscopic or microscopic (Xiuyi, 2011). Macroscopic minerals occur in round pellets, lenticels, bands, nodules and sometimes in dispersed crystals. Microscopic minerals are seen as fractured crystalline fragments, isolated euhedral minerals, microscopic nodules and sub-microscopic crystal accumulates (Xiuyi, 2011). Furthermore, minerals tend to be hosted in cracks, fractures and cleats within the maceral matrices. It is important to note that some minerals occur in extremely fine grains of particles not exceeding several microns and are also dispersed in organic macerals, which can only be viewed under an electron microscope (Xiuyi, 2011). Minerals in coal arise from sedimentary rocks such as shales, siltstones and sandstones interbedded within fractures and between coal seams (Falcon and Ham, 1988). Understanding the properties and the characterisation of coal provide

information on the inherent size and distribution of minerals interbedded in coal for the beneficiation and recovery of REE from coal.

2.3.4.1 Formation of mineral matter in coal

The evolution regarding the incorporation of mineral matter in coal may be categorised into the following groups based on their origin (mineral matter) and mode of formation (Xiuyi, 2011; Wagner *et al.*, 2018):

I. Plant-derived minerals
II. Terrigenous detrital minerals
III. Chemical and biochemical minerals (authigenic minerals)
IV. Minerals created through diagenetic alteration

Minerals are accumulated in coal at different times, which define their genesis. The three significant roots (origin) of mineral matter in coal are epigenetic, syngenetic and detrital (Ward, 2002), which are discussed below.

The syngenetic formation of minerals occurred from plant-derived coal forming matter (Maledi, 2017; Wagner *et al.*, 2018). These minerals fall into two categories regarding the time of formation. Early syngenetic minerals are formed during the initial stages of peatification, soon after the burial of peat or other sediments, when major solidification has not taken place yet (Ward, 2002). The late syngenetic mineral formation occurs during the humidification-gelification of coal, associated with the deepened buried advanced peat formation stages of coalification (Ward, 2002). Late syngenetic mineral formation is because of chemical processes occurring between coal constituents and the environment. As a result, syngenetic minerals occur in ultra-dispersive forms and are closely distributed with the organic matter, thus presenting difficulties when beneficiating syngenetic minerals (Maledi, 2017). Important syngenetic minerals found in coal include siderite nodules, microcrystalline fragments of pyrite, and void filling compounds such as carbonates, quartz, kaolinite, sulphates, clays and phosphate minerals (Ward, 2002).

Epigenetic minerals are deposited into coal seams and fractures after coal compaction or after the coal source has reached its present rank (Xiuyi, 2011; Wagner *et al.*, 2018). Epigenetic minerals are also regarded as adventitious or excluded mineral matter found in void fillings and coal fissures. Typical mineral matter in coal via epigenetic mineralisation consists of silica,

clays, illite, dolomite, apatite, pyrite, ankerite, siderite, marcasite, dawsonite and chlorites (Ward, 2002). Epigenetic minerals tend to be large and are easily liberated during the milling of coal and beneficiation processes (Maledi, 2017).

Detrital mineralisation typically occurs when minerals were deposited into the peat by either moving water, wind or are introduced into the peat by epiclastic and pyroclastic processes (Ward, 2002). Epiclastic procedures involve lithic clasts and minerals liberated by ordinary weathering processes from pre-existing merged rocks (Xiuyi, 2011; Wagner *et al.*, 2018). Traditionally, epiclastic minerals are derived from the erosion of volcanoes or ancient volcanic terrains. Pyroclastic minerals are formed via the breakdown of magma, as gases are released from volcanic vents in the air or beneath water (Ward, 2002). Detrital minerals include sporadic bands of clay minerals, feldspar, tonsteins and quartz fragments, which are all thoroughly mixed matter (Ward, 2002). Nonetheless, it is typically difficult to determine the origin of each mineral, as many minerals of different origins can occur in the same coal seam (Wagner and Matiane, 2018).

A fraction of some of the mineral species occurring in coal reserves is presented in Table 2-4, and a portion of these minerals cannot be viewed by the naked eye (Maledi, 2017; Wagner *et al.*, 2018). Nonetheless, a few mineral groups and some individual minerals such as silicates, pyrite and calcite can be seen with the naked eye if granted the correct specimen (Ward, 2002). This is the core reason for the evolution of enhanced analytical techniques to view microscopic amounts of mineral matter in coal. Minerals in coal can be abundant, rare, common or frequently seen in most coals (Falcon and Ham, 1988; Ward, 2002; Xiuyi, 2011). Likewise, analytical techniques such as X-ray diffraction (XRD), SEM-EDX, petrographic analysis and X-ray fluorescence (XRF) assist in determining and viewing the minerals present in coal. Mineral matter can affect the grade of the coal as low-grade coals tend to have high amounts of mineral matter compared to their counterpart high-grade coals (Maledi, 2017). Although the geological occurrence of minerals in coal is regarded as having deleterious effects on coal operations as they release toxic elements and contribute largely to CFA and discard coal stockpiles, they do have beneficial features to the industry (Honaker and Groppo, 2016). CFA and discard contain REE and are future reserves for the recovery of CREE. Likewise, many of these minerals found in coal (Table 2-4) are known to bear REE such as apatite, illite, kaolinite, xenotime, monazite, muscovite, biotite, calcite and other clay minerals (Faure, 1993; Akinyemi *et al.*, 2012; Wagner and Matiane, 2018).

Table 2-4: Minerals in coal deposits (adapted from Saxby (2000) and Xiuyi (2011)).

Mineral groups	**Minerals**
Arsenide	Lollingite
Sulphides	Pyrite, marcasite, galena, sphalerite, melnikovite, cooperite, siegenite, pyrrhotite, chalcopyrite, bornite, tetrahedrite, tennantite, argentite, chalcocite, realgar, ferroselite, ullmannite, platarsite, arsenopyrite, glaucodot, stibnite, bismuthinite, millerite, cinnabar, orpiment, herzenbergite, covellite
Selenides	Penroseite, clausthalite, hakite
Oxides	Quartz, chalcedony, hematite, cristobalite, uraninite, ilmenite, corundum, spinel, chromite, magnetite, hetaerolite, anatase, rutile, brookite, cassiterite, columbite
Hydroxides	Limonite, bauxite, goethite, lepidocrocite, diaspore, boehmite, gibbsite, brucite, portlandite, chalcophanite
Silicates	Kaolinite, illite, sericite, montmorillonite, mixed-layer clay minerals, dickite, halloysite, chlorite, ferrihalloysite, muscovite, hydromuscovite, feldspar, zircon, leucite, zeolite, tourmaline, coffinite, andalusite, garnet, olivine, kyanite, topaz, staurolite, sphene, epidote, allanite, pyroxene, actinolite, hornblende, chloritoid, talc, serpentine, pyrophyllite, glauconite, biotite, gadolinite, barytolamprophyllite, fenaksite, canasite
Carbonates	Calcite, dolomite, siderite, ankerite (ferroan dolomite), dawsonite, strontianite, aragonite, magnesite, barytocalcite, azurite
Vanadate	Carnotite, tyuyamunite
Phosphates	Apatite, phosphorite, xenotime, monazite, svanbergite, berlinite, florencite, crandallite, gorceixite, autunite, torbernite, vivianite, goyazite
Tungstate	Scheelite
Sulphates	Barite, gypsum, anhydrite, celestite, linarite, alunite, natrojarosite, jarosite, alunogen, epsomite, kieserite, melanterite, szomolnokite, mirabilite, polyhalite
Nitrates	Nitronatrite
Halides	Halite, sylvine, bischofite, fluorite
Amorphous mineral	Opal, volcanic glass

2.3.5 Rank of coal

The rank is the degree of maturation or metamorphism of coal achieved by process variations such as temperature, time, pressure as a result of peat burial or vicinity to heat following peat accumulation (Falcon and Ham, 1988; Ward and Suárez-Ruiz, 2008). The transformation of peat into different coal ranks passes through progressive stages, i.e., peat → lignite (brown coal) → sub-bituminous → bituminous → semi-anthracite → anthracite → graphite (Falcon and Ham, 1988). Coal's position in these coalification levels is regarded as its rank. The maturity is enhanced or affected by significant deviations in the macerals' physical, chemical and technological properties, particularly in the vitrinite and liptinite groups (Falcon and Ham,

1988). The inertinite retains its original structure, chemistry, form and, for the most part, undergoes minimum change throughout coalification.

The quantitative determination of coal rank in reactive macerals (liptinite and vitrinite) can be achieved by determining its proportion of volatile matter, carbon content, moisture content and hydrogen (Falcon and Ham, 1988). However, using volatile matter as a parameter to determine coal rank is not reliable for establishing the rank of coals depleted in volatile matter. This is because the thermal dissociation of minerals accounts for up to 60% of volatile matter in coal (Falcon and Ham, 1988). Carbonate minerals such as calcite contribute to carbon dioxide, whilst clay minerals contribute to water vapour and basic oxides. In addition, the coal inertinite contributes significantly higher carbon content with lower volatile matter, thus indicating another source of carbon achieved by rank alone. Coincidently the presence of high proportions of liptinite indicates a low carbon content with increased amounts of volatile matter (Falcon and Ham, 1988). Thus, volatile matter and carbon content do not produce reliable indicators for coal rank (Falcon and Ham, 1988).

Hence a more uniform standard approach is used to determine the rank of coal by measuring the light reflected from a polished vitrinite particle surface under oil immersion (Falcon and Ham, 1988; Ward and Suárez-Ruiz, 2008). This reliable standard technique referred to as vitrinite reflectance (SANS 7404-5) is preferred because the optical reflectance of vitrinite increases with an increase in the rank of coal, as depicted in Figure 2-4 (Ward and Suárez-Ruiz, 2008). As the carbon content increases, the optical reflectance of vitrinite and the coal's C:H ratio increases, whereas the volatile matter decreases (Falcon and Ham, 1988). Low-rank coals (lignite, sub-bituminous and bituminous) are high in volatile matter, moisture content, porosity and reactivity and are thus more easily oxidisable than higher rank coals (semi-anthracite, anthracite and graphite). High-rank coals are more difficult to ignite and require higher temperatures for combustion. Due to rank being only measured by optical microscopy, the only requirement for determining the rank is the presence of vitrinite (Falcon and Ham, 1988).

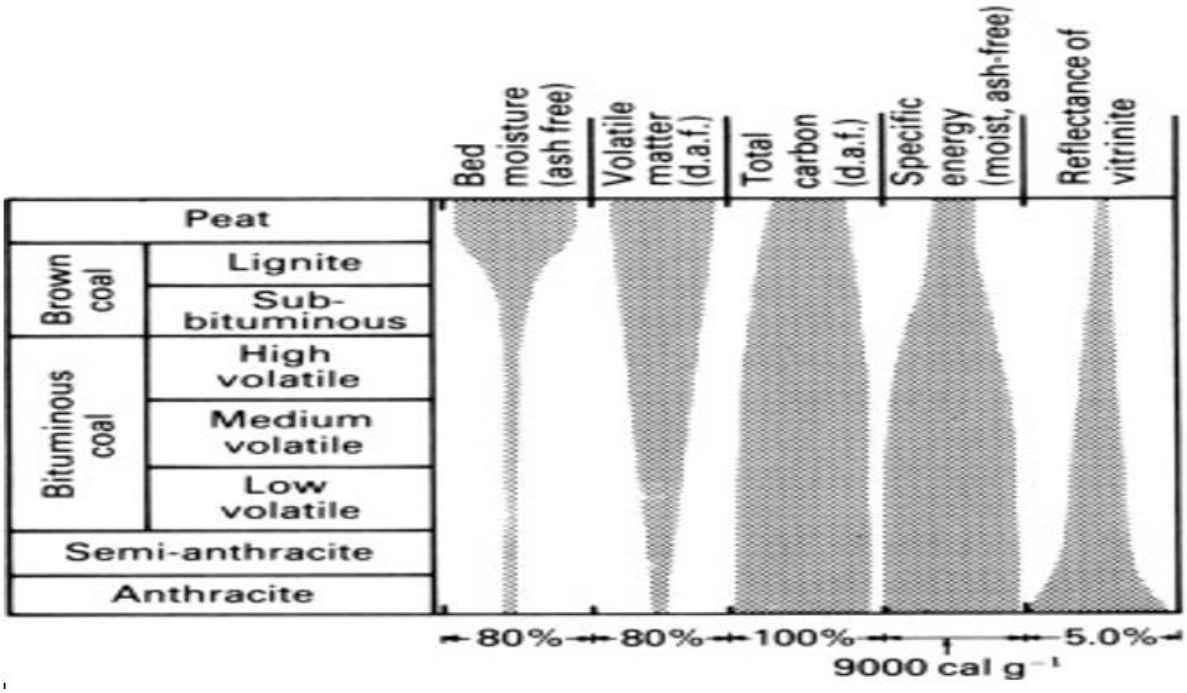


Figure 2-4: Variation in the key coal properties for rank advancement (from Ward and Suárez-Ruiz (2008)).

2.3.6 Coal grade

The grade of coal is an assessment of the amount of mineral matter and organic matter present in coal. Furthermore, it reflects the extent to which the accumulation of plant vegetation has been kept free of contamination by inorganic mineral matter during and after peat burial and during the coal's rank advancement (Ward and Suárez-Ruiz, 2008). High-grade coal consists of a low amount of mineral matter and an increased amount of organic matter (Suárez-Ruiz and Ward, 2008).

2.4 Overview of South African coals

2.4.1 South African coal reserves

South Africa's main source of energy generation is dominated by coal-powered stations, and the country is a major participant in the global coal market (Mills, 2010). South Africa exports about 25% (Wagner and Matiane, 2018) of the coal produced annually and is the dominant player in the African coal market as it holds 95% of Africa's coal reserves (Mills, 2010). The recoverable coal reserves in South Africa are estimated to be 58 billion tonnes (Mills, 2010). Coal exports generate more income than any other commodity in South Africa (Ratshomo, 2016).

Currently, the Witbank and Highveld coalfields are the main source of coal production in South Africa and represent 75% of the country's coal production (Ratshomo, 2016). The Waterberg coalfield is regarded as the most promising coalfield for future coal mining in the country (Faure *et al.*, 1996; Moumakwa, 2010) as the Witbank and Highveld coalfields are close to exhaustion (Jeffrey, 2005; Pooe and Mathu, 2011). South Africa hosts relatively shallow coal mines with thick coal seams close to the surface, thus reducing mining costs (Eberhard, 2011). More than 50% of the coal mining occurs in opencast mines, with the balance being mined underground (Eberhard, 2011).

Coal in the South African region generally contains a variable ash content and can reach up to 65% in ash content underground (Eberhard, 2011). Thus, export-grade coal and coal required for power generation in South Africa requires prior beneficiation (Eberhard, 2011). The beneficiation of the coal generates discard coal. The estimated discard coal available in stockpiles in South African is more than one billion tonnes, and more discard is constantly being added at a rate of approximately 60 million tonnes per annum (Eberhard, 2011; van Breugel *et al.*, 2019). Discard coal provides many environmental challenges but can also provide a potential source for economic gain if it can be recycled in other processes. As reported by Luttrell *et al.* (2016), the amount of discard coal available from coal preparation plants, as well as the fines generated during mining activities, provide a potential source for REE recovery.

2.4.2 Geological setting of coalfields in South Africa

South African coals were formed during the Permian Period to the mid-Triassic Period and are located in the Gondwana Karoo Basin (Falcon and Ham, 1988). The formation occurred under low cool-climatic temperatures to warmer climatic regimes (Falcon, 1986). South Africa hosts 19 coalfields, with 18 coalfields belonging to the Karoo Basin and the remaining coalfield lying in the Kalahari Basin (Jeffrey, 2005). These 18 coalfields are predominantly situated in Mpumalanga, KwaZulu-Natal, Limpopo and the Free State, with reduced amounts in Northwest, Gauteng and the Eastern Cape (Jeffrey, 2005). The stratigraphy of the Karoo Basin is composed of Dwyka, Ecca, Beaufort and Stormberg groups. The majority of coalbeds in South African occur in the Ecca Group of the Karoo Basin, with the Waterberg coalfield lying in the embayment of the Kalahari Basin (Faure *et al.*, 1996). Figure 2-5 represents the 19 coalfields situated in the country, which further emphasises the abundance of coal reserves in South Africa.

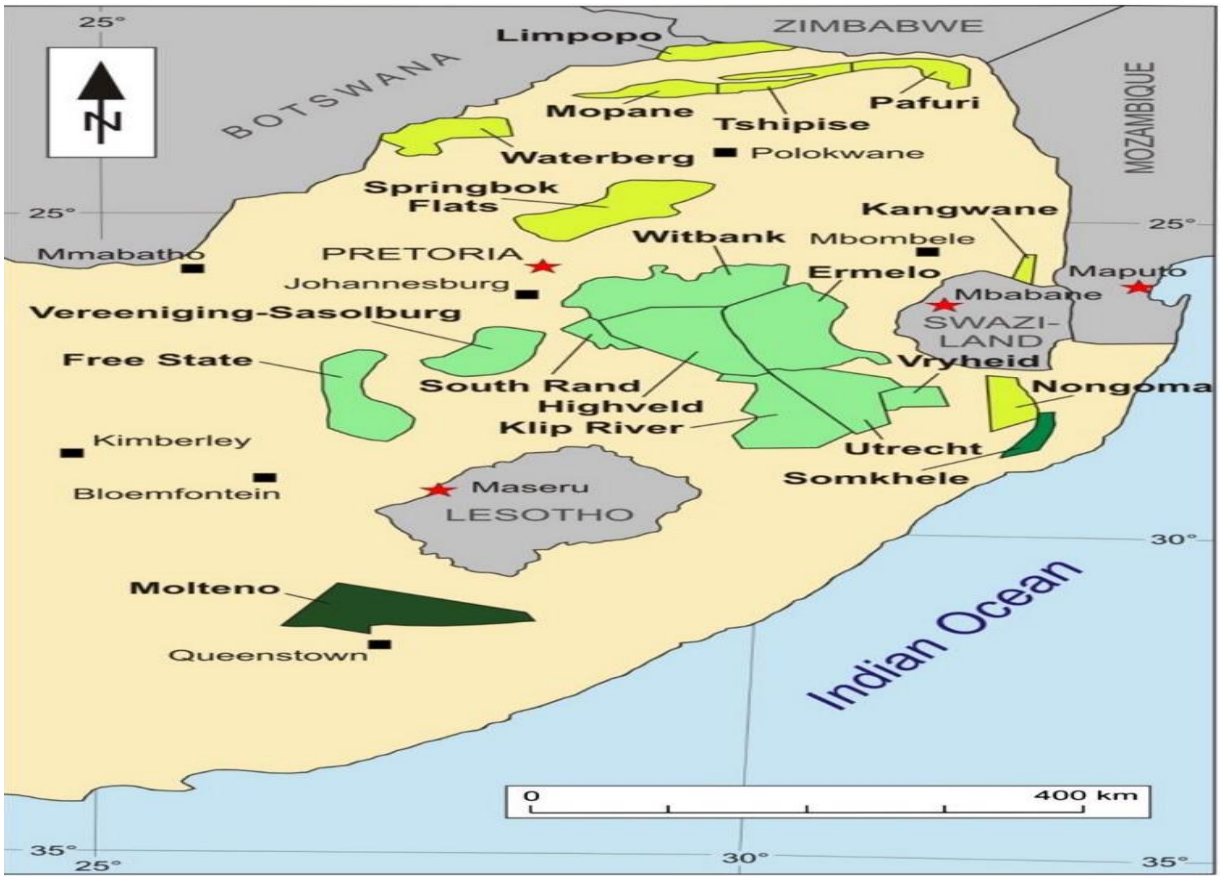


Figure 2-5: Illustration of the 19 coalfields situated in South Africa (adapted from Snyman (1998)).

2.5 Occurrence of REE and REE-bearing minerals in South African coal reserves

The major REE-bearing minerals reported in South African coals include kaolinite and illite Akinyemi *et al*. (2012). In 1980, Caigher used XRD analysis to determine the mass percentage of the dominant minerals in South African coals: 54.1% kaolinite, 29.2% illite and 16.7% of mixed layered clays. Akinyemi *et al*. (2012) conducted a mineralogy investigation on sub-bituminous coals from the Tutuka Power Station in Mpumalanga. The XRD analysis revealed a spectrum indicating a coal high in siliceous minerals such as quartz and kaolinite with low amounts of pyrite (Figure 2-6).

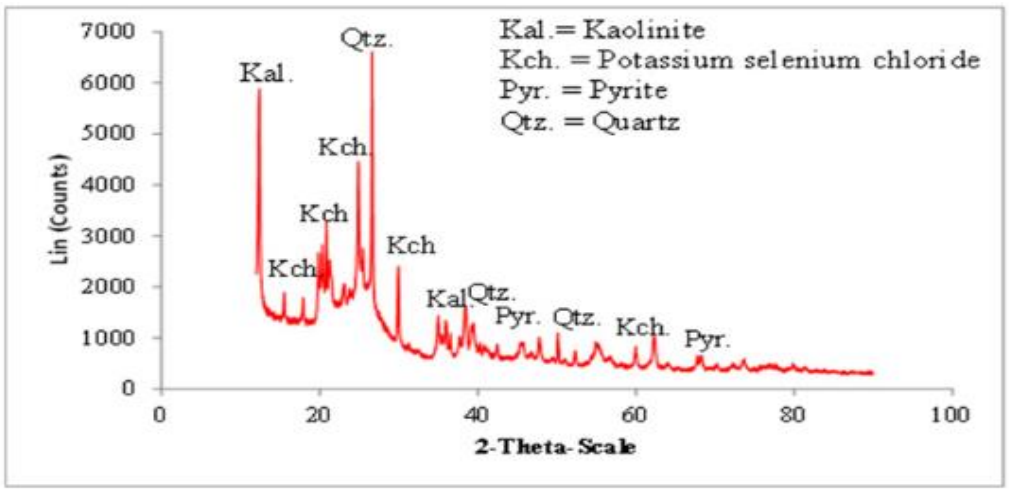


Figure 2-6: XRD spectrum for raw coal from the Tutuka Power Station (Akinyemi *et al*., 2012).

Numerous mineralogical and elemental investigations conducted on South African coal indicate the presence of REE (Faure *et al.*, 1996; Akinyemi *et al*., 2012; Wagner and Matiane, 2018). The study conducted by Wagner and Matiane (2018) on sub-bituminous grade C coal samples observed via XRD indicated that REE are associated with minerals such as kaolinite [$Al_2Si_2O_5(OH)_4$], quartz [SiO_2], calcite [$CaCO_3$] and muscovite [$KAl_2(Si_3Al)O_{10}(OH,F)_2$], with lesser amount associated with pyrite [FeS_2]. Furthermore, the investigation indicated the presence of REE in all raw coal samples tested with values exceeding 111 ppm, which is above the average concentration (69 ppm) of REE in world coals (Ketris and Yudovich, 2009). The ash samples analysed reflected an increase in REE concentration of four times that in raw coal, as expected, as CFA is rich in minerals and thus contains more REE (Wagner and Matiane, 2018). This proves the existence of REE in some South African sub-bituminous medium rank C coal.

REE recovery from coal deposits is costly, time-consuming and requires a combination of processes to generate native REE elements. Seredin and Dai (2012) stated that the initial step before subjecting coal to the beneficiation processes is to identify the suitable discard coal with an REE content exceeding 100 ppm. A study conducted by Faure (1993) on the Waterberg coalfield in Limpopo identified a two-metre-thick carbo-tonstein zone situated 64 metres below the topmost coal seam at the base of the Grootegeluk formation. This formation was found with mineral inclusion of kaolinite, apatite, calcite, zircon, siderite, xenotime and clay minerals belonging to the smectite and kandite group. According to Faure (1993), the carbo-tonstein layer contents of REE exceeded 250 ppm, thus depicting a potential source for REE recovery.

Furthermore, this two-metre-thick seam comprises carbonaceous mudstones with an organic content below 40% and is enriched in HREE, hence indicating a potentially viable source for REE recovery (Faure, 1993). Additionally, the carbo-tonstein layer was enriched with REE and is composed of more than 60% mineral matter. The base is composed of clay minerals such as kaolinite, apatite, siderite and calcite (Figure 2-7). This seam is likely to produce a significant quantity of coal discard after beneficiation due to its high inorganic mineral content.

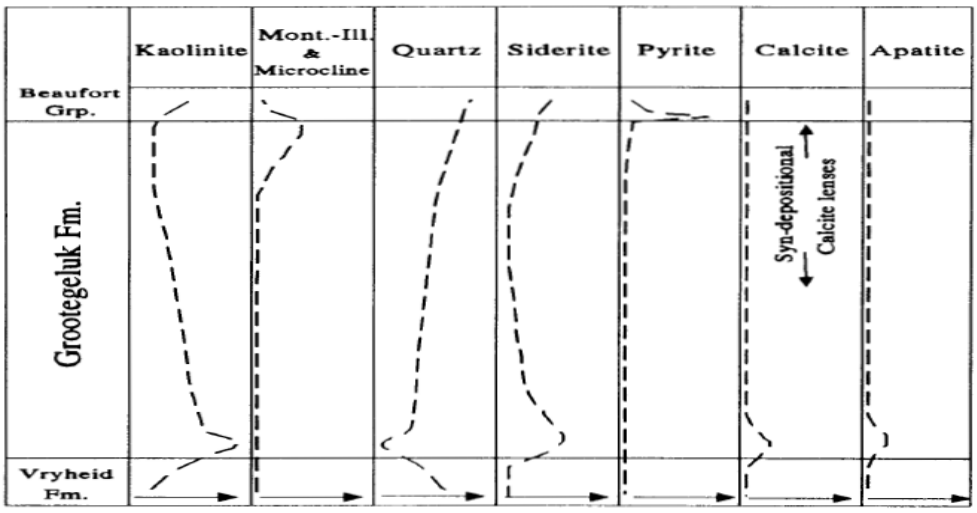


Figure 2-7: Variation of the minerals by depth in the Grootegeluk formation based on XRD and petrographic analysis (Faure, 1993).

2.5.1 Modes and formation of REE minerals present in coal

REE originate in the Earth's crust and coal naturally as trace phases in phosphate, carbonate and sulphide minerals and are not restricted to xenotime, monazite, bastnaesite and apatite minerals (Lin *et al.*, 2017). Many studies have investigated the potential of extracting REE from coal discard and the bonds or forms of REE present in coal (Honaker *et al*., 2016; Zhang and Honaker, 2019b; Honaker *et al.*, 2019; Yang *et al.*, 2019). Dai *et al.* (2012) summarised the forms or modes of REE minerals present in coal resources into three principal categories:

I. Syngenetic pyroclastic and clastic minerals consisting of monazite, lesser amounts of xenotime, zircon and apatite
II. Diagenetic and epigenetic minerals established of authigenic origin: associates of phosphates, oxides, carbonates, sulphates, water-bearing phosphates and silicate combined REE
III. Organic compounds: authigenic and organically bound REE

Furthermore, coals enriched in REE are formed under numerous geological conditions at various stages in the progressive growth of coal basins. Seredin and Dai (2012) categorised the REE accumulation in coal into four generic types:

I. Terrigenous type, REE input into coal via surface waters
II. Tuffaceous type associated with the sinking and leaching of acid and alkaline volcanic soot
III. Infiltration of the rapid movement of groundwater, which is well known in uranium geology
IV. Hydrothermal type related to the downwards flow of thermal mineral water and deep fluids

The first two generic classes of REE accumulation typically occur at the initial stage of coal formation, known as the peat bog stage (Seredin and Dai, 2012; Dai and Finkelman, 2018). In contrast, the infiltration type is largely epigenetic in origin. The hydrothermal type may be formed at any time during the maturity of the coal deposit. REE-rich coals may be of multistage and polygenetic origin. Beneficiation before processing the REE by different techniques has been proposed to extract or recover a high concentration of this valuable resource from coal. Henceforth, REE in coal may be associated with the organic or mineral fraction of coal. The following section outlines some of the techniques used to concentrate the coal and other conventional ores.

2.6 Physicochemical separation and physical separation of REE minerals

The beneficiation of REE primarily exploits the differences in surface chemistry, magnetic properties, electrical characteristics and specific gravities between different minerals and elements within the ore (Jordens *et al.*, 2013; Honaker *et al.*, 2016). The recovery of REE from conventional REE sources and coal deposits consists of physico-chemical separation, physical beneficiation, hydrometallurgical methods, or a hybrid of hydrometallurgical and pyrometallurgical techniques. A few investigations conducted regarding REE recovery or enrichment via chemical and physical separation techniques are discussed below.

2.6.1 Froth flotation

Froth flotation is a technique that relies on the difference in surface chemistry and wettability of the coal particles in separating coal organic from its inorganic minerals (Gupta and Li, 2016; Zhang *et al.*, 2017; Gupta *et al.*, 2019). During this process, air bubbles created attract and

combine with the ultrafine hydrophobic carbon matter in the coal whilst the inorganic matter remains in the solution (Gupta *et al.*, 2019). The carbon matter attracted to the air bubbles float as an aggregate called froth, whilst the inorganic matter sinks and is removed as tailings (Li and Yang, 2014).

Froth flotation has been used extensively to recover and enrich REE from xenotime, bastnaesite, monazite and other REE-bearing minerals (Li and Yang, 2014). It was also used to beneficiate the REE from the world's largest REE-bearing deposit, the Bayan Obo deposit in China (Li and Yang, 2014). Yang *et al.* (2015) combined froth flotation and high gradient magnetic separation (HGMS) to recover REE from a complexed ore that includes carbonates, silicates and oxides and other REE-bearing minerals (e.g., zircon and pyrochlore etc.). They used a hydroxamate reagent, a fatty acid type of reagent, a sulfosuccinamate type of reagent and sodium oleate powder as collectors, in addition to a high gradient magnetic separator. A 53% REE recovery was achieved, based on the froth flotation process, with sodium oleate as the most efficient collector and at an average particle size of 80 µm. The combined recovery circuit (froth flotation plus HGMS) recorded a recovery of 67.4%. The only benefit from integrating both techniques is the high recovery of REE, but at a low concentrate grade below 5%.

A study conducted by Honaker *et al.* (2016) on three coal strata, Fire Clay, Fire Clay Rider and Eagle seams, with sodium oleate, talon 9400 and oleic acid as collectors yielded a REE recovery above 60%. During this recovery procedure, the only limitation experienced was the low-grade concentration of 350 ppm, but with the combination of flotation techniques (rougher-cleaner-recleaner), a concentration of 1183 ppm was produced. Zhang *et al.* (2017) investigated the flotation of fine discard coal with diesel and methyl isobutyl carbinol as a collector and frother, respectively. The results obtained revealed that 38% of the feed, consisting of 10% ash forming minerals and 85% combustible material, were removed in the clean coal fraction. The low ash products primarily consisted of minute amounts of REE. Additionally, a continuous flotation column and a batch flotation cell were used with sodium oleate as a collector. A TREE recovery of 20% and concentration of 4700 ppm with an enrichment ratio of 10:1 at an optimum particle size of 2.76 µm was obtained from the continuous flotation column. Furthermore, with a TREE recovery above 30%, both flotation cells exhibited exceptionally low REE concentrations of less than 1000 ppm, which shows that large amounts of unwanted minerals and organic matter were also recovered. Nonetheless, the

continuous flotation column was more efficient as it achieved twice more REE than the batch flotation cell.

A recent investigation by Gupta *et al.* (2019) used a batch froth flotation approach on coal from Alaska. An Aerofroth-88 (2-Ethylhexanol, specific gravity (SG) = 0.83) and fuel oil (SG = 0.83) were used as a frother and collector, respectively. A TREE recovery of 77.3% at a concentration of 506 ppm for - 75 µm coal particle size was achieved. Gupta and Li (2016) also developed a novel froth flotation technique named hydrophobic hydrophilic separation (HHS), which enhanced and recovered extremely ultrafine particles. HHS generated an REE concentrate of 17428 ppm from the Fire Clay coal sourced from the decarbonised thickener underflow. An enrichment ratio of 53:1 was achieved in this study using octyl hydroxamate as a collector.

Froth flotation is a highly effective beneficiation technique for producing a pre-concentrate before REE leaching. The only limitation is that the coal or the ores used must be milled to a fine particle size to achieve a significant REE yield, which is energy-intensive and costly (Jordens *et al.*, 2013; Zhang *et al.*, 2015; Honaker *et al.*, 2016). Additionally, the process recovers large amounts of excess unwanted minerals, increasing the cost of downstream purification processes.

2.6.2 Magnetic separation

Magnetic separation techniques have been used extensively in the beneficiation of REE-bearing minerals as it assists in separating the highly magnetic gangue from the desired paramagnetic REE-bearing minerals (Jordens *et al*., 2013). A study conducted in the Yunnan province in China on a REE mineral ore utilised the Boxmag Rapid high gradient magnetic separator to recover scandium. The optimum grinding size used was 0.074 mm with 80% passing. At this particle size (74 µm) and with a magnetic field intensity of 1450 kA/m, 73.86% of scandium was recovered with a concentration of 251 ppm (Gao and Chen, 2010). HGMS is limited because it can only be applied to small particle sizes with a particle size limitation of less than 10 µm. Due to this limitation, a poor concentrate of 251 ppm scandium was achieved.

Honaker *et al.* (2016) used a wet high-intensity magnetic separator to beneficiate three coal samples. The coals were subjected to four different magnetic field strengths of 1.5 T, 0.4 T, 0.75 T and 1.1 T. The study concluded that wet high-intensity separation was significantly

effective in recovering paramagnetic REE such as monazite and xenotime at ultrafine particle sizes. However, REE recovery was low (< 2%), mainly due to small mass recoveries and the fine particle size limitation. Furthermore, wet high-intensity magnetic separators can only be used with small sample sizes that require a high degree of particle liberation (Gao and Chen, 2010; Honaker *et al.*, 2016). Another investigation was conducted on a roof sample derived from a coal seam using a cross-belt electromagnetic separator to separate the sample into magnetic and non-magnetic components. According to Soundarrajan *et al.* (2015), equal amounts of REE were found to be present in the magnetic and non-magnetic constituents of the sample, with the non-magnetic component manifesting a marginally higher enrichment of REE.

2.6.3 Spiral, shaking table and multi-gravity separators

Froth flotation and magnetic separation are classified as physical separators used in the mineral processing industry to pre-concentrate REE (Jordens *et al*., 2013). Gravity separation uses different densities or specific gravities for the separation and recovery of REE-bearing minerals, commonly monazite, as it has a high SG relative to the gangue minerals (Honaker *et al.*, 2016). Jordens *et al.* (2016) employed the Falcon and Knelson concentrator to concentrate REE-bearing minerals from the gangue minerals in a Canadian study. The authors reported a maximum REE recovery of 19%, with a grade not exceeding 90000 ppm. Another study conducted by Khanchi *et al.* (2014) on Iranian monazite ore using a Humphreys spiral concentrator obtained a concentrate grade of 6050 ppm REO and a recovery of 58% of REO.

Honaker *et al.* (2016) conducted a key density separation study using a float sink on coal and coal by-products. Lithium meta-tungstate with a SG of 2.95 was mixed with water to separate REE at different relative densities. The study indicated that most REE (> 60%) were present between the 2.4 to 2.68 density fraction. The authors noted that the maximum REE concentrations were found in the middle-density fraction, largely due to the presence of out of seam gangue minerals (high density) and low-density carbon matter. Another study using a float sink was conducted by Lin *et al.* (2017) to determine the density fraction containing the maximum concentration of REE within the coal seam. They found that REE tend to be enriched in the middle-density (high inorganic content fraction), with a maximum REE grade of 400 ppm achieved; thus, showing the association of REE with mineral matter.

A multi-gravity separator (MGS) was used to beneficiate three samples originating from the Eagle seam, Fire Clay seam and Fire Clay Rider seam in the USA (Kiser *et al.*, 2015). An MGS consists of a conventional shaking table placed inside a rotating drum. It uses water as a transport medium for the particles and operates at an incline position allowing the less dense material to move downhill and exit at the bottom of the drum. The results revealed an REE enrichment of 12% to 17% for all three samples examined in the medium to high SG fractions. This also supports the sink float technique observations that the enrichment of REE occurred in medium to high SG fractions since REE are mainly distributed within the mineral matter. Density separation is a relatively good technique for the pre-processing of REE minerals before leaching, but it could lead to low-grade REE with large amounts of unwanted gangue in the concentrate (Kiser *et al.*, 2015; Honaker *et al.*, 2016). Subsequently, it requires a significant amount of liberation for effective separation, with an energy-intensive liberation step for the fine processing of the coal source (Zhang *et al.*, 2015).

2.6.4 Electrostatic separation

Electrostatic separation is typically used when physical beneficiation techniques do not suffice, and it is a valuable technique for processing mineral sands (Zhang *et al.*, 2015). The separation of different matter or minerals is based on their conductivity. This technique assists in separating native conducting minerals from less conducting or non-conducting native minerals (Jordens *et al.*, 2013).

Moghise *et al.* (2016) used a combination of physical separation techniques, magnetic separation and a shaking table, and then electrostatic separation to recover REE from iron mine waste. The result obtained indicated that REE were concentrated in the non-conductivity stream in the electrostatic separator, with a recovery of 89.4% and a grade of 12114 ppm. Soundarrajan *et al.* (2015) also used the approach for the beneficiation of roof rocks originating from the parting of a coal seam. A rotating drum, together with high tension electrodes, were employed to create different currents and trajectories for separating conducting and non-conducting coal fractions. A very small, partially significant amount of REE enrichment (355 ppm) was achieved in the conducting fraction, whilst the insulating fraction still contained a reasonable amount of REE (312 ppm). The authors further used the separator to beneficiate a coal discard sample. The REE enriched in the conducting fraction with a concentration of 313 ppm. Nonetheless, substantial amounts of 142 ppm REE were still present in the insulation fraction's concentrate.

Electrostatic separation is highly beneficial when combined with other physical separation techniques, thus resulting in extra processing costs. The process requires a large degree of fine feeds (< 37 µm), which requires drying before being fed into the separator (Jordens *et al.*, 2013). Apart from heavy mineral sands (ion-adsorbed clays), all other REE ores must be pulverised. For this reason, the energy cost related to drying milled ores is non-feasible for implementing these techniques on a large scale (Jordens *et al.*, 2013).

In summary, the physical beneficiation of conventional and non-conventional REE-bearing ores integrating different techniques effectively enriches REE in a feed before leaching. Thus, the potential to develop a feasible physical beneficiation process for recovering REE from coal is minimal due to the high cost of liberation and the size limitation of physical separation equipment (such as electrostatic and magnetic techniques). For this reason, this study used a combination of pyrometallurgy and hydrometallurgy for the recovery of REE to produce a pre-concentrate rich in REE. These techniques are discussed in Section 2.7.

2.7 Chemical beneficiation and thermal pre-treatment of REE

This section discusses using hydrometallurgical procedures and pyrometallurgical techniques on various primary and secondary ores such as coal and other REE wastes for REE recovery.

2.7.1 Hydrometallurgical techniques for REE recovery

Hydrometallurgy refers to the treatment of ores involving an aqueous solution for extracting and recovering metals via techniques such as leaching and precipitation (Wadsworth and Miller, 1979). There are currently many leaching techniques used on REE-rich deposits for the recovery of these elements. Acid leaching, alkaline leaching and ion-exchange leaching are fundamental to hydrometallurgical techniques employed for REE recovery (Kuppusamy *et al.*, 2019). Leaching is the process whereby the coal feed comes into contact with an acid/alkaline solution at a specified temperature for a certain period (Wadsworth and Miller, 1979). The solution is complexed with REE to recover these elements from the feed. Once the extraction is completed, the slurry is filtered, and the solid residue and the extracted leachate are then analysed to determine the concentration of the elements recovered (Honaker *et al.*, 2019).

Numerous studies have employed sequential REE extraction procedures to determine REE association and occurrence in coal (Rozelle *et al.*, 2016; Finkelman *et al.*, 2018; Yang *et al.*,

2019; Zhang and Honaker, 2019b). Based on the results of these studies, REE in coal are classified into five types:

I. Water-soluble
II. Ion-exchangeable
III. Carbonates
IV. Metal oxides
V. Acid-soluble

2.7.1.1 Ion-exchange leaching of REE

Ion-exchange leaching of coal for the recovery of REE was conducted by Rozelle *et al.* (2016) using 1 M $(NH_4)_2SO_4$, at a solid:liquid ratio of 1:2 and conditioned for one hour. The study also tested the ion-exchange capability of an ionic liquid (1-butyl-3-methylimidazolium chloride) and deep eutectic solvent (mixture of urea and choline chloride) to recover REE. TREE recovery of 72% and 89% was achieved for the two coal samples under investigation using ammonium sulphate ($(NH_4)_2SO_4$). A TREE recovery of 80% and 60% was achieved using the ionic liquid, and a TREE recovery of 71% and 89% was achieved using the deep eutectic solvent. However, ionic liquids are extremely costly and, therefore, not a feasible option. The application of ion-exchange leaching with $(NH_4)_2SO_4$ was also conducted by Yang *et al*. (2019). They used 0.1 M $(NH_4)_2SO_4$ at 75 ^oC, together with nitric acid (HNO_3), as a pH controlling agent. Only 9% to 10% of the TREE were recovered at an initial pH of 5, and when the pH was reduced further, the TREE recovery reached 15%.

A recent investigation quantified the occurrence of REE in 20 coal samples using 1 M ammonium acetate (CH_3COONH_4) for the ion-exchange leaching tests (Finkelman *et al.*, 2018). Only small amounts (0% to 5%) of TREE were leached in their ion-exchange forms. Although Rozelle *et al.* (2016) produced a TREE recovery of 89%, more recent studies (Finkelman *et al.*, 2018; Yang *et al*., 2019) suggest that minimal amounts of REE occur in ion-exchangeable forms in coal.

2.7.1.2 Sequential digestion/leaching of REE

A significant study reported by Laudal *et al.* (2018) employed a sequential digestion procedure to understand and quantify the modes of occurrence of REE in coal. The study employed a water-soluble test, ion-exchange leaching test and an acid leaching test. Deionised water stirred for 24 hours was used in the water-soluble test, whilst the ion-exchange test subjected the coal

sample to 1 M ammonium acetate. The first two tests illustrated that minimal amounts of coal REE occur in water-soluble or ion-exchangeable forms. Furthermore, 1 M HCl and 1 M phosphoric acid (H_3PO_4) were compared to 0.5 M sulphuric acid (H_2SO_4). With 1 M HCl, 80% to 95% of REE were recovered, whilst with 0.5 M H_2SO_4, REE recovery of 22% to 32% was achieved compared to 5% to 15% recovery with 1 M H_3PO_4. The main limitation with H_3PO_4 lixiviate is the low solubility of REE in H_3PO_4 dissolution because H_3PO_4 has reduced acidic conditions as it is only partially deprotonated.

A recent investigation conducted by Montross *et al.* (2020) also used a sequential digestion procedure on the underclay rock of Central Appalachian coal seams. Ammonium sulphate, HCl and H_2SO_4 were used for the ion-exchange and acid-soluble experiments. For the $(NH_4)_2SO_4$ ion-exchange test, a small amount of REE (7.5%) were recovered, whilst 20% REE was recovered for both 1 M HCl and 1.2 M H_2SO_4. The authors also used a 0.1 M citrate solution consisting of citric acid, sodium chloride and sodium citrate and obtained a 33% REE recovery. Additionally, in the pH range of 3 to 6 for the citrate solution, REE were relatively leached out at all pHs, with impurity elements reduced at higher pHs.

An additional recent study by Zhang and Honaker (2019b) employed a sequential extraction procedure to determine the mode of occurrence of REE in coal. The details of the sequential extraction procedure are depicted in Figure 2-8. The results obtained from the study reveal that minimal amounts of REE were recovered in the ion-exchangeable and carbonate forms after calcination (Zhang and Honaker, 2019b). Consequently, increased amounts of approximately 54% of REE were extracted in their oxide forms, whilst about 40% of REE were recovered in their acid-soluble forms (Figure 2-9). Lastly, it was also noted that insoluble silicates correspond to a minor fraction of REE present in calcined coal compared to the initial non-calcined coal sample. This indicates that calcination improves the solubility of silicates and can thus improve REE recovery during acid leaching.

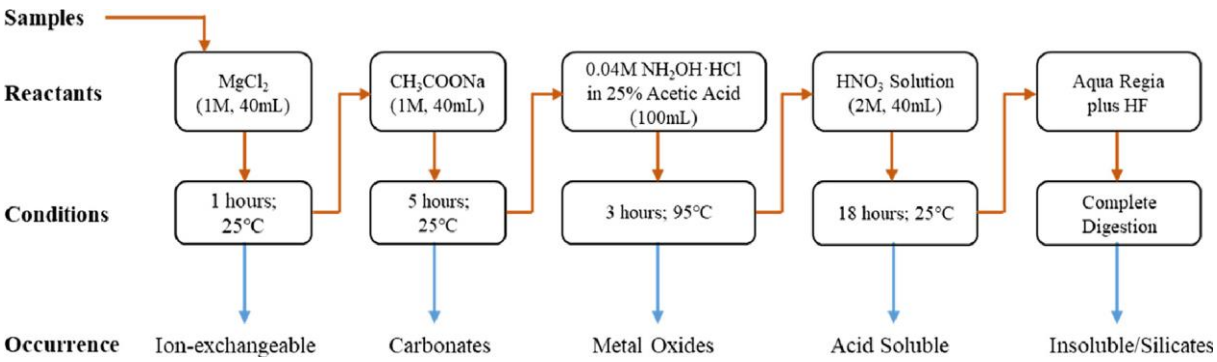


Figure 2-8: The sequential extraction procedure for REE recovery from coal (adapted from Zhang and Honaker, 2019b)

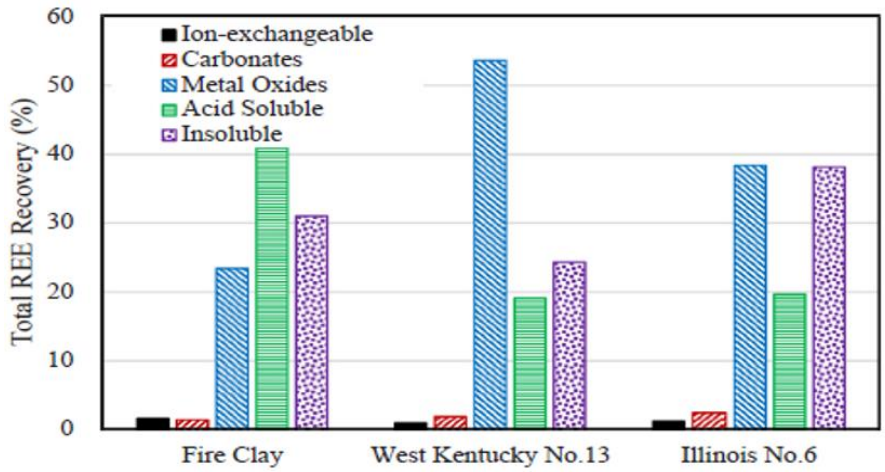


Figure 2-9: Representation of REE recovery based on their mode of occurrence in sequential extraction tests (Zhang and Honaker, 2019b)

2.7.1.3 Acid leaching of REE

The extraction of REE and phosphors from iron mine tailings and shredded Waste Electrical and Electronic Equipment (WEEE) using the acid leaching process was conducted by Peelman *et al.* (2018). Iron mine wastes typically contain elevated concentrations of REE ranging between 1200 to 1500 ppm, with monazite and apatite being the dominant REE (Peelman *et al.*, 2018). The iron mine tailings were subject to froth flotation to produce a REE-rich pre-concentrate for the leaching tests. The WEEE tailings are mainly composed of REE from the NdFeB and samarium-cobalt magnets and are initially exposed to roasting at 500 ^{o}C for one hour to demagnetise the wastes. The iron mine wastes (includes apatite and monazite) were subjected to HNO_3 (65% wt.) at 60 ^{o}C for one hour, with a liquid:solid ratio of 2:1, which resulted in a recovery of 43% of TREE. HREE had a higher recovery rate of 70% to 90% than

LREE (26% to 47%), as LREE were distributed in the monazite fraction, which resisted dissolution under the given conditions.

Peelman *et al.* (2018) noted that H_3PO_4 forms during the leaching of apatite and monazite (phosphate-containing ores). The PO_4^{3-} ions formed can chelate with REE to form an insoluble REE-phosphate product. The formation of such bonding can be prevented by adding excess HNO_3 to stop the dissociation of H_3PO_4 and maintain a low pH. The WEEE wastes consisted of abundant amounts of iron (58%), which was why it was oxidised under low temperature to reduce its iron reactivity. Acidic leaching using H_2SO_4 was added to the oxidised WEEE and 99% recovery of Nd was achieved, together with high recoveries of REE, which were originally in minimal amounts. Precipitation was performed with Na_2SO_4 to improve the grade. The linked-up process recovered 93% Nd (as the sample comprised mainly Nd) (Peelman *et al.*, 2018).

The leaching of the Illinois Basin coal was conducted by Yang *et al.* (2019) on coarse, middlings and fine refuse generated from the ROM, which primarily consisted of the floor and roof segments of the basin that contain amounts of fluorapatite. The samples were subjected to froth flotation to remove excess carbon. The acid leaching test employed 1.2 M H_2SO_4, at 75 ^oC, with solids:liquid ratio of 10 g/l. Leachate samples were drawn at 0.5, 1, 3, 5, 10 and 24 hrs and were analysed using ICP-optical emission spectrometry to determine REE recovery over time. The REE recovery increased rapidly within the first five hours for all the samples before reducing. From the middling sample, a maximum REE recovery of 50% was achieved. Additionally, more HREE were recovered in the larger size fraction (- 180 µm), whilst the recovery of the LREE improved as the coal was milled further to - 10 µm (Yang *et al.*, 2019).

The coarse refuse sample had a low REE recovery of 30%; thus, the authors blank roasted the coal at 750 ^oC to improve its subsequent leaching to 74%. The fine refuse sample exhibited a low recovery of 28% (which can be attributed to REE losses in the pre-flotation step due to extremely fine particle sizes), which was consequently improved by NaOH chemical activation, and, thereafter, the identical leaching test reflected a recovery exceeding 76%. The importance of thermal activation and chemical activation converts REE-bearing minerals such as phosphates and silicates into more readily leachable forms of REE oxides/chlorides (Yang *et al.*, 2019).

Acid leaching was used to extract REE from CFA in several studies (Park and Liang, 2019; Peiravi *et al.*, 2017; Kolker *et al.*, 2017). The average global approximation of REE in CFA is 445 ppm (Ketris and Yudovich, 2009); thus, CFA is a good source for REE recovery. Research conducted at Illinois University used coal initially burned in a furnace at 750 ^{o}C to produce ash that was subsequently leached with HNO_3 (Kolker *et al.*, 2017; Ried, 2018). The study achieved a REE recovery of 90% at a concentration of 6 M HNO_3. However, HNO_3 leaching at high concentrations can be extremely costly when developing a commercial plant, thus rendering this method unfeasible. REE are trapped in a silicate mullite form in CFA and thus, require an aggressive high molarity acidic solution for recovery.

Bioleaching of REE from CFA is another option available for the recovery of REE. An investigation conducted by Park and Liang (2019) using microbial strain *Candida bombicola* achieved a high REE recovery of 93%. This study demonstrated that it is feasible to recover REE and metals by bioleaching techniques, but developing large scale bioleaching plants will not be feasible as it can be a time-consuming process; thus, more thorough research is required in the bioleaching field.

A recent investigation by Middleton *et al.* (2020) on the leaching of coal residue from a power plant in the USA using 1 M of HCl resulted in a REE recovery of 80%. The study also revealed that at low pHs, REE-bearing minerals manifest a positive charge, thus preventing the sorption or complexing of REE onto clay minerals during leaching. However, at pHs above 4.5, deprotonation of the mineral surface results in negatively charged hydroxyl mineral groups, causing REE cations to adsorb and complex with these mineral groups. Therefore, this results in reduced amounts of REE being recovered by the lixiviate. Another investigation was conducted by Yang and Honaker (2020) on a Fire Clay coal sample of 1.4 to 1.6 SG. Both coal samples were subjected to flotation (rougher stage to three cleaner stages) prior to leaching. The first tailings obtained were subjected to a second froth flotation using octanohydroxamic acid ($C_8H_{17}NO_2$), whilst the tailings from the second flotation stage were used as the feedstock for the acid leaching tests. A 11 µm particle size exhibited the highest TREE recovery of 84%. When lixiviates HCl, HNO_3 and H_2SO_4 at 1 M were employed to leach REE from the same coal samples tailings, it resulted in a TREE recovery of 80%, 76% and 74%, respectively (Yang and Honaker, 2020). In the first 10-15 minutes of leaching, HCl and HNO_3 displayed extremely fast leaching rates, whereas H_2SO_4 was least effective due to its slow leaching rates.

Computer monitors and tubes of colour television are typically coated with a powder rich in sulphides and oxides that constitute REE, primarily europium and yttrium. Resende and Morais (2010) used the scraped powder coatings from a computer monitor. The sample was characterised via XRD and atomic absorption spectrometry. XRD results revealed that the dominant minerals present in the sample were zinc sulphide and yttrium oxide sulphide. Lixiviated H_2SO_4 and HCl were used in the experiments, where leaching variables such as temperature, acid:solid ratio and leaching time were investigated. The result indicated that H_2SO_4 is more selective than HCl when leaching yttrium and europium from the scrapped powder coatings from a computer monitor with the optimal acid:solid ratio of 1500 g/kg. Sulphuric acid leaching reflected a maximum recovery of 97% REE (Y + Eu), and this optimal recovery significantly occurred between 0.5 hours and 1.5 hours and at an optimal leaching temperature of 60 ^oC.

A fluorescent lamp waste was likewise used by Tunsu *et al.* (2016) as a feedstock for REE recovery, using a two-stage leaching process employing HNO_3 lixiviate. 1 M of HNO_3 was used in the first leaching stage, at a leaching time of ten minutes to remove impurities such as calcium, barium, antimony, silicon, strontium, etc., with a REE loss between 2% to 3%. The residue left from the first stage was leached in 2 M HNO_3, resulting in a REE recovery exceeding 88 % for yttrium and europium.

With a large emphasis placed on extracting REE from coal, an integral study was conducted by Zhang and Honaker (2018). Natural leachate generated in coarse coal refuse piles, which occurs via pyrite oxidation in the presence of water, was used as a source for REE recovery. Staged precipitation of the leachate using NaOH indicated that REE precipitate and are enriched in the pH range of 4.8 to 6.1 due to REE adsorption on iron hydroxy-sulphate complexes. This investigation proposed using HNO_3 to leach (re-dissolve) the REE from the precipitates, resulting in more than 95% REE recovery. Thereafter, oxalic acid was added to precipitate the REE-oxide products.

2.7.1.4 Alkaline pre-treatment before leaching

Alkaline pre-treatment of coal and coal residue improves and enhances REE recovery from coal before acid leaching (Kuppusamy *et al.*, 2019). The pre-treatment process converts the REE-bearing minerals, i.e., phosphates and silicate crystals, into REE hydroxides (reaction 2-2), which are subsequently more soluble during acid leaching (Kuppusamy *et al.*, 2019).

Furthermore, acid leaching enhances REE recovery as the crystal structure of the dominant clay minerals are destroyed, resulting in the release of the encapsulated REE (Zhang *et al.*, 2020). Additionally, mineral matter such as quartz and clays react with NaOH to form more soluble sodium silicates and sodium aluminate (as seen in reactions 2-3 and 2-4), which typically increases in solubility within the alkali leaching solution (Kuppusamy *et al.*, 2019). Therefore, the REE remain behind with the solid residue and are leached out in the subsequent acid leaching stage.

$$REEPO_{4(s)} + 3NaOH_{(aq)} \rightarrow 3REE(OH)_3 + Na_3PO_4 \quad (2\text{-}2)$$

$$SiO_{2(s)} + 2NaOH \rightarrow Na2SiO_{3(aq)} + H_2O_{(aq)} \quad (2\text{-}3)$$

$$Al_2O_32SiO_2{:}2H_2O_{(aq)} + 6NaOH_{(aq)} \rightarrow 2Na_2SiO_{3(aq)} + 2NaAlO_{2(aq)} + 5H_2O_{(aq)} \quad (2\text{-}4)$$

Yang *et al.* (2019) conducted alkaline pre-treatment of fine coal residue using 8 M NaOH, with a pulp density of 10 g/l for two hours at 75 ^oC. The remaining solid residue was then leached in 1.2 M H_2SO_4 for five hours. The TREE recovery significantly improved (via alkaline pre-treatment) from a mere 22% to 75%. In another recent study, alkali pre-treatment was applied to coal tailings from the flotation cell (Kuppusamy *et al.*, 2019). The coal was leached with a high alkali concentration of 20% NaOH at 190 ^oC for one hour. The residue after leaching was subjected to 7.5 wt.% HCl at 50 ^oC for 30 minutes. Significantly higher amounts of REE were leached in the acid solution than the initial alkali (NaOH) leaching (97% LREE recovery and 76% HREE recovery).

A combination of thermal and alkaline treatment, also known as alkaline baking, was used to decompose monazite ores for the recovery of REE. The REE-phosphate mineral baked at 120 ^oC in concentrated NaOH (75%), resulted in the mineral forming a $RE(OH)_3$ precipitate (Yang, 2019), with thulium hydroxide precipitates also generated. The reaction mechanism is illustrated by reactions 2-5 and 2-6. The precipitates produced were dissolved in acid to recover the REE, using 6 M of HCl acid for two hours, leading to 93% of REE being recovered. The thulium was removed when the REE were re-bleached, as the REE were dissolved in the solution and thulium remained in its solid state.

$$REEPO_{4(s)} + 3NaOH \rightarrow REE(OH)_{3(s)} + 3Na^+ + PO_4^{3-} \quad (2\text{-}5)$$

$$Th_3PO_{4(s)} + 12NaOH \rightarrow 3Th(OH)_{4(s)} + 12Na^+ + 4PO_4^{3-} \quad (2\text{-}6)$$

2.7.2 Thermal pre-treatment and leaching of REE (pyrometallurgy)

Thermal pre-treatment method has been applied on many REE-bearing minerals and coal to increase the acid leaching efficiency of REE (Zhang and Honaker, 2019b; Zhang and Honaker, 2020). Thermal pre-treatment, also known as pyrometallurgy, engages the pre-treatment of an ore via roasting, calcining or heating before leaching (Wadsworth and Miller, 1979). The process promotes the degradation and decomposition of REE-bearing minerals, thereby increasing the surface area available for the lixiviate to react with the targeted minerals or elements (Zhang and Honaker, 2019a). An increased amount of REE recovered in milder acidic concentrations, in turn, means a reduction in the amount of acid consumption during leaching (Zhang and Honaker, 2019a; Zhang *et al*., 2020). Roasting and calcination eliminates unwanted volatiles and reduces the volume and concentration of acid required in leaching. Moreover, it also converts contaminant mineral elements such as iron sulphide into hematite, which is more difficult to leach (Honaker *et al.*, 2019). As such, acid leaching might be an economically feasible process route for REE recovery. Thermal pre-treatment without any additives at 400 ^{o}C to 600 ^{o}C converts REE-bearing minerals (REE carbonate minerals) in coal into REE oxides as depicted in reaction 2-7.

$$REE_2(CO_3)_3 \rightarrow REE_2CO_3 + 3CO_2 \quad (2\text{-}7)$$

In a study conducted on the coal-rich segment originating from the Western Kentucky No. 13 coal seam (Yang *et al.*, 2019), the coal middling of - 180 µm was subjected to blank roasting at 750 ^{o}C for two hours to oxidise the REE before leaching with 1.2 M H_2SO_4 at 75 ^{o}C for five hours. The REE recovery via acid leaching considerably improved from 31% (non-roasted coal) to 74% (roasted coal). Furthermore, the blank roasting assisted in converting REE-bearing minerals into readily leachable forms of REE oxides. The authors reported that roasting resulted in the degradation and breaking down of the coal particles into thin flakes, leading to an increase in the surface area and exposure of ion-exchangeable REE, REE oxides and the micro-dispersed mineral matter in the organic matrices during leaching.

Honaker *et al.* (2019) also used the Western Kentucky No. 13, Fire Clay and Illinois No. 6 seams, all calcined at 600 °C, 750 °C and 900 °C for 10, 60 and 120 minutes. Following calcination, acid leaching was conducted using 1.2 M HCl at 75 °C. From the XRD analysis, the main minerals present in the non-calcined coal samples were kaolinite, quartz, illite, pyrite and anatase, whilst for the calcined coal samples, kaolinite was found to be diminished due to

dehydroxylation of the crystal structure of kaolinite. At a temperature of 900 °C, the structure of illite was partially destroyed compared to the coal calcined at 600 °C, which illustrates fully developed peaks of illite. Pyrite was transformed into hematite in the calcined coal sample at 600 °C and above, which is a less acid leachable form, resulting in less Fe ions being leached (Honaker *et al.,* 2019). However, it is important to note that the minerals present in the calcined coal sample or fluidised bed boiler at 600 °C to 900 °C are distinctively different from those present in conventional power plant ash (Honaker *et al.,* 2019). Conventional power plant boilers function at elevated temperatures of 1480 °C to 1590 °C and typically consist of minerals in an amorphous glassy structure, crystalline quartz, and different mineral phases such as mullites that resist acid leaching (Honaker *et al.,* 2019). Additionally, South African coals typically combust at 1549 °C to 1793 °C, contributing to the formation of minerals in a crystalline form within the ash left behind (Taole *et al.*, 2015).

The leaching tests illustrate that TREE recovery improved from a mere 25% (non-calcined coal) to a significantly enhanced 80% for the calcined coal at 600 °C (Honaker *et al.*, 2019). TREE recovery decreased at calcination temperatures greater than 750 °C, owing to the pozzolanic nature of clays that leads to a decreased surface area and encapsulation of REE minerals. In this case, more aggressive acid conditions will be required, significantly increasing the cost of acid leachates.

Honaker *et al.* (2019) concluded that two essential aspects improved REE recovery from calcined coal via leaching. The organic and inorganic association and distribution of REE in coal are liberated and released when undergoing calcination, enhancing REE leaching. REE associated with clays like kaolinite become dehydrated, resulting in an increased surface area, increasing REE exposure available to the leachate. Secondly, calcination at increased temperatures of 600 °C assists in eliminating the organic-volatile matter whilst leaving behind the non-volatile REE that are converted into REE oxides. Therefore, resulting in an improved REE solubility in the lixiviate and an enhanced REE recovery (Honaker *et al.*, 2019).

Another study also used calcination before leaching coarse coal discard and middlings originating from the Pocahontas No. 3 coal seam in the USA (Zhang and Honaker, 2019a). A dense medium bath was employed to obtain the 2.2 SG coal fraction used in the experiments. Ammonium sulphate and 1.2 M HCl at 75 °C were used for the ion-exchange and acid leaching tests, respectively. Calcination was done at five different temperatures (400 °C, 500 °C, 600

°C, 750 °C and 900 °C) on the coarse discard/refuse coal and middlings. The XRD analysis indicated that pyrite undergoes thermal decomposition at 400 °C and transforms to hematite. At higher calcination temperatures, dehydroxylation of kaolinite, muscovite and illite occurred, resulting in the Al-OH bonds breaking and the subsequent degradation of the crystal structure of kaolinite. The samples calcinated at 400 °C had the maximum surface area, pore size and volume, whilst samples calcinated at temperatures exceeding 600 °C had reduced pore size and surface area. The ion-exchange test produced REE (< 20%) for both calcined and non-calcined coal, whilst the acid leaching tests at 1.2 M HCl produced REE of about 80% within the first 15 minutes (Figure 2-10). After 15 minutes of rapid acid leaching, the REE recovery remained reasonably constant, showing that the REE are extremely soluble in the leachate after calcination of the coal source. At calcination temperatures above 750 °C, TREE recovery decreased due to the clay minerals sintering at temperatures > 600 °C.

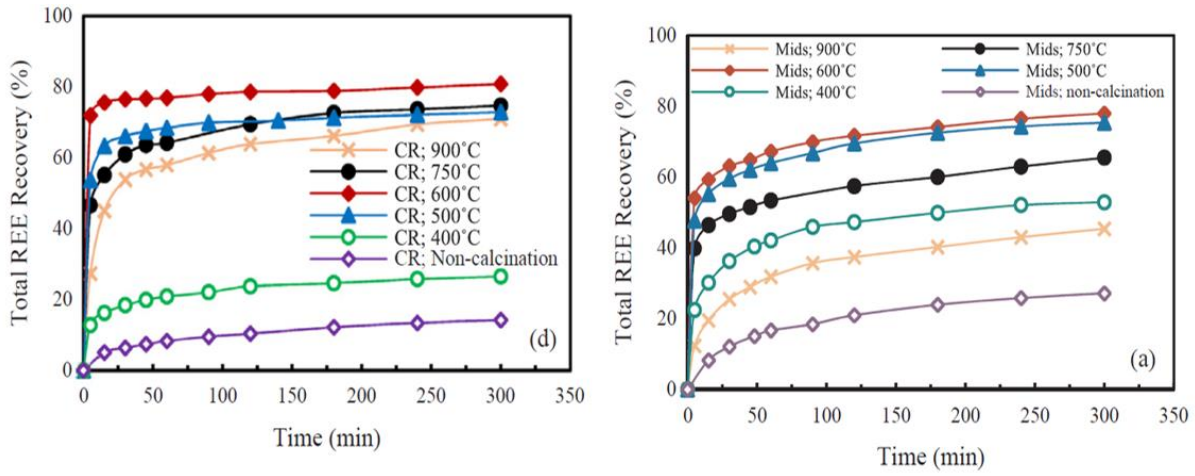


Figure 2-10: Acid leaching of coarse refuse coal and middlings coal at different calcination temperatures (Zhang and Honaker, 2019a).

Another investigation of calcination before leaching used coals from the Fire Clay, West Kentucky No. 13 and Illinois No. 6 seams (Zhang and Honaker, 2019b). All the samples were calcined at 600 °C based on previous leaching-calcination studies. The leaching tests employed dilute HNO_3 and $(NH_4)_2SO_4$. At a pH of 4 and 1 M $(NH_4)_2SO_4$, 45% of REE were recovered.

Monazite, another significant REO-containing mineral, is known as a REE-phosphate mineral. Monazite does not decompose below 1950 ^oC but can react with CaO at 700 ^oC as a solid-phase reaction. In a study conducted by Wenyuan *et al.* (2006), NaCl and $CaCl_2$ were added to the reaction to improve decomposition efficiency and increase the mass transfer rate. Many of the

older processes required roasting and baking the mineral, followed by leaching in HCl or H_2SO_4. The reactions between monazite CaO and NaCl is presented in reaction 2-8, where the major REE product comes in the form of a REO and is leached with hot water or HCl. This process achieves an ore decomposition of 90%.

$$15CaO + 3NaCl + 10REEPO_4 \rightarrow 3Ca_5Cl(PO_4)_3 + Na_3PO_4 + 5REO_2O_3 \quad (2\text{-}8)$$

Guo *et al.* (2018) studied the concentrated H_2SO_4 roasting of monazite ores to convert the REE-phosphates to REE-sulphates (reactions 2-9 and 2-10). The REE-sulphates were leached and recovered by filtration and then neutralised with an alkaline source to obtain $RE(OH)_3$ precipitates. This acid baking process reaches high recovery rates of 95% but has an extremely poor selectivity and leaves behind large amounts of hazardous, radioactive thorium slag.

$$2REEPO_4 + 3H_2SO_4 \rightarrow REE_2(SO_4)_3 + 2H_3PO_4 \quad (2\text{-}9)$$

$$Th_3(PO_4) + 6H_2SO_4 \rightarrow 3Th(SO_4)_2 + 4H_3PO_4 \quad (2\text{-}10)$$

Sodium carbonate roasting was used on fluorine-carbonate ores by the Changchun Institute of Applied Chemistry in China with the addition of Na_2CO_3 to the ore at temperatures above 350 ^oC (reactions 2-11 and 2-12). This allowed the release of REE into their oxide form. The REE oxides were then leached using 2 M HNO_3 (reactions 2-13 and 2-14), resulting in a leaching recovery of up to 93% (Kumari *et al.*, 2015).

$$2REEFCO_3 + Na_2CO_3 \rightarrow REE_2O_3 + 2NaF + 3CO_{2(g)} \quad (2\text{-}11)$$

$$4CeFCO_3 + 2Na_2CO_3 + O_2 \rightarrow 4CeO_2 + 4NaF + 6CO_{2(g)} \quad (2\text{-}12)$$

$$REE_2O_3 + 6HNO_3 \rightarrow 2REE(NO_3)_3 + 3H_2O \quad (2\text{-}13)$$

$$CeO_2 + 4HNO_3 \rightarrow Ce(NO_3)_4 + 2H_2O \quad (2\text{-}14)$$

2.8 Chapter Summary

In this chapter, REE have been described with special focus on the techniques that have been optimised for enhancing their recovery. The review included those studies aimed at optimising REE recovery from CFA, which is costly because fine liberation is required as REE are encapsulated in a crystalline mullite form that resists acid leaching. Many researchers have also applied physical beneficiation techniques on coal and discard coal, with the main drawback being particle size, liberation/grinding cost, low recovery and low concentrations. However,

many researchers have achieved improved REE recovery from coal by employing hydrometallurgy techniques. Calcination before leaching was conducted on high SG fraction discard coal in the USA. The current study incorporated a calcination step prior to an optimised leaching for REE recovery from discard and ROM coal originating from the Waterberg coalfield in South Africa. To my knowledge, this is the first study in South Africa employing calcination and acid leaching to recover REE from South African discard coal without prior physical beneficiation.

CHAPTER 3: METHODOLOGY

3.1 Introduction

This chapter outlines the analytical techniques used to characterise and determine the REE present in the discard and ROM coal samples used in this study. These analytical techniques provided a deeper understanding and insight into the distribution of the organic and inorganic components (minerals) and their association with the REE in the coals. The detailed description of the calcination and leaching tests, along with the experimental equipment utilised are outlined and explained in this chapter.

3.1.1 Origin and collection of samples

One ROM sample, denoted by RC1 and one discard coal sample referred to as DC1 (discard coal sample) were supplied from a Waterberg coalfield processing plant. The discard coal (DC1) sample was a result of the beneficiation of the ROM coal, and both samples originated from the same coal seam.

3.1.2 Sample preparation

The as-received coal samples, DC1 and RC1, were sun-dried to remove excess moisture before taking representative samples by utilising the coning and quartering technique. Thereafter, the sub-samples were crushed, milled and screened to -1 mm, with a representative split removed, and the remaining sample was milled to -212 µm. Resulting in another representative split removed and the remainder was milled to -106 µm. The - 1 mm particle size split was subjected to petrographic analysis and the - 212 µm to proximate, total sulphur, forms of sulphur, ultimate, XRD and FTIR (Fourier transform infrared) analyses. The leaching and calcination tests were conducted on both coal samples at 90% passing - 106 µm, with the same particle size subjected to the Tescan Integrated Mineral Analyzer (TIMA).

3.1.3 Sample relative densities

The RC1 and DC1 samples were subjected to float and sink tests in a zinc chloride solution at different relative densities (RD) of 1.4, 1.5, 1.6, 1.7 and 1.8. This was done to have a general overview of the samples' relative density. At a relative density of 1.7 about 90% of the RC1 reported to the float. Thus, approximately 95% of DC1 reported to the sink of RD 1.8, indicating DC1 had an overall relative density greater than 1.8.

3.2 Analytical techniques

The particle size distribution (PSD), proximate, ultimate, total sulphur and forms of sulphur, petrography, XRD, FTIR and ICP-MS analyses were conducted to ascertain the extent of REE available for extraction in the as-received samples prior to hydrometallurgy beneficiation. In addition, TIMA analysis was conducted to determine the particle size of REE in the -106 μm fraction of the coal and their association with the inorganic minerals and organic matter within the coal.

3.2.1 Particle size distribution analysis

The PSD on the -106 μm was determined for RC1 and DC1 using the Malvern Mastersizer 2000 with the Hydro 2000MU dispersion unit in the GENMIN laboratories at the University of the Witwatersrand. The analysis was conducted by adding the coal sample into 800 ml of distilled water at a pump speed of 3000 rpm, with the ultrasonic probe set for three minutes to assist in dispersing the sample when agglomerates formed.

3.2.2 Proximate analysis

The proximate analysis was carried out to determine the inherent moisture, volatile matter, ash content and fixed carbon content (calculated by subtracting the total moisture volatile matter and the ash content from a 100%) of DC1 and RC1. The proximate analysis was conducted according to ASTM D-5142. An in-house LECO Corp TGA701 Thermogravimetric Analyzer was used for the analysis at the University of the Witwatersrand. One gram of each coal sample was stage-wise placed in a crucible. The coal's inherent moisture content was determined under a nitrogen atmosphere at a flow rate of 10 L/min and a temperature of 107 ^{o}C. The volatile matter was determined at a temperature within a 107 °C and 950 °C range and at a heating rate of 43 °C/min in an atmosphere of nitrogen and held at this temperature for seven minutes. For the ash content determination, the remaining sample in the crucible was heated in an atmosphere of oxygen from 650 °C to 750 °C, and the remaining residue gave the total ash content of the sample.

3.2.3 Ultimate and total sulphur analysis

The ultimate and total sulphur analyses for DC1 and RC1 were conducted at the Bureau Veritas Testing and Inspections South Africa (Pty) Ltd. The samples were prepared according to the ACT-TPM-001 method based on the ISO 13909-4: 2001 standard. The ultimate analysis was executed according to the ISO 12902: 2001 method for carbon, hydrogen and nitrogen. The

total sulphur analysis was carried out according to the ISO 19579: 2006 standard. Roughly 0.25 g of the samples were subjected to the analyses at 1450 ^{o}C, with the analysing time ranging between 60 and 300 seconds.

3.2.4 Forms of sulphur analysis

The forms of sulphur analysis (organic sulphur, pyritic sulphur and other non-pyritic sulphide minerals), was undertaken at the Bureau Veritas Testing and Inspections South Africa (Pty) Ltd. The samples were prepared according to the BV-TPM-001 method based on ISO 13909-4: 2001, with the total sulphur determined according to the ISO 19579: 2006 and the forms of sulphur conducted according to the ISO 157 methods.

3.2.5 Petrography

DC1 and RC1 were milled to - 1 mm and then submitted to the University of Johannesburg for the petrography analysis. The milled coal particles were set in epoxy resin under a vacuum for 24 hours to produce an ore block. Subsequently, the ore block was subjected to polishing as per the ISO 7404-part 2 standard and a final polishing step to 0.05 µm with OPS lubricant using a Struers Tegraforce polisher. After placing a drop of immersion oil on the polished blocks, the samples were then examined under a Zeiss Axio Imager M2M petrographic microscope. The microscope is attached to a Hilgers Diskus-FOSSIL system for vitrinite reflectance determination based on the ISO 7404-part 3 standard. In addition, a partial-automated point counting step was applied for maceral and microlithotype evaluation (conducted according to ISO 7404-3 and 4) at a magnification of 500x under oil immersion. The major petrographically observable mineral groups, the organic matter present, their distribution and their association were determined.

3.2.6 X-ray diffraction analysis

XRD was conducted according to the ASTM D-3682-13 method, using the Bruker D2 Diffractometer to identify the mineral phases present in DC1 and RC1. The XRD analysis deployed a Cu-Kα radiation [= 1.54184] in the 2-theta range of 10 to 50 °C at 0.02° with a counting time of 31.4 seconds for each step. The generated XRD patterns were matched with the Bruker D2 database of diffractograms to identify the dominant mineral phases and their peaks in the samples.

3.2.7 Fourier transform infrared spectroscopy

The FTIR spectrometer was applied to determine the functional groups and bonding characteristics between the carbon and mineral fractions of DC1 and RC1. A PerkinElmer Spectrum FTIR Spectrometer with attenuated total reflectance was used to analyse 0.05 g of DC1 and RC1 (- 212 µm particle size). The FTIR spectra were obtained between 4500 and 400 cm^{-1} with a resolution of 4 cm^{-1}.

3.2.8 Tescan Integrated Mineral Analyzer analysis

TIMA is one of the latest, state-of-the-art, multifaceted automated mineralogical techniques that provides a particle-by-particle measurement of mineral phases, grind size, liberation, elemental composition and detects minimal amounts of REE (Gottlieb and Dosbaba, 2015). It incorporates Energy Dispersive X-ray (EDX) with Backscattered Electron (BSE) signals to identify and compare minerals to the TIMA mineral library entries. The TIMA analysis was conducted at the University of the Witwatersrand, School of Geosciences.

The milled DC1 and RC1 of - 106 µm, were subjected to TIMA analysis dot mapping (overall view of the large sample area, for REE and mineral quantities determination) and high-resolution mapping (a higher resolution view for a specific small area of interest in the sample to determine the REE associations/distributions with the mineral or organic matter). The advantage of TIMA over SEM-EDX is that it provides enhanced imaging, with better detection limits and faster processing times. Two grams of RC1 and DC1 were pulverised to - 106 µm and then placed into a 25 mm (diameter) mould. Thereafter, 5 ml of the mixture (epoxy resin & hardener) was added to the pulverised coal mould and left for six hours to cure the epoxy resin mould. The 25 mm (diameter) block was then removed from the mould and polished using a Struers Rotopol polisher. Thereafter the block was carbon-coated before being analysed on the TIMA.

3.2.9 Inductively coupled plasma mass spectrometry

DC1 and RC1, - 106 µm fraction, were subjected to ICP-MS analysis (at the University of Johannesburg) to quantify the REE and impurity elements present in the samples. Prior to analysis, four steps were required to digest the raw coal samples:

1) 500 mg of the raw sample was placed in a microwave vessel with 6 ml HCl and 2 ml HNO_3 and 0.2 ml HF

2) The samples were heated to approximately 180 ^{o}C and incubated at this temperature for ten minutes in a microwave digestion system.
3) The samples were filtered and diluted to 50 ml with deionised water.
4) An additional ten times dilution factor (1 ml to 10 ml of 2 % HNO_3) was added.

The leachate samples extracted from the experiments in Section 3.4 were directly analysed via the ICP-MS instrument.

3.3 Experimental procedure

The experimental procedure followed in this study is depicted in Figure 3-1. The samples (non-calcined) were analysed to observe and determine their properties, the REE concentration, associations, distributions and the extent of REE. Subsequently, as-received RC1 and DC1 and their respective calcined samples were subjected to leaching tests as outlined in Figure 3-1 before determining their REE concentration and recovery. During the leaching tests, the concentration, solid (g):liquid (l) ratio, leaching temperature and calcination temperature were investigated and varied to determine the influence on REE recovery. From the data attained, the study established an enhanced calcination, optimised leaching process, which aided the improvement in the % leaching recovery of REE.

3.3.1 Summary of Experimental Procedures

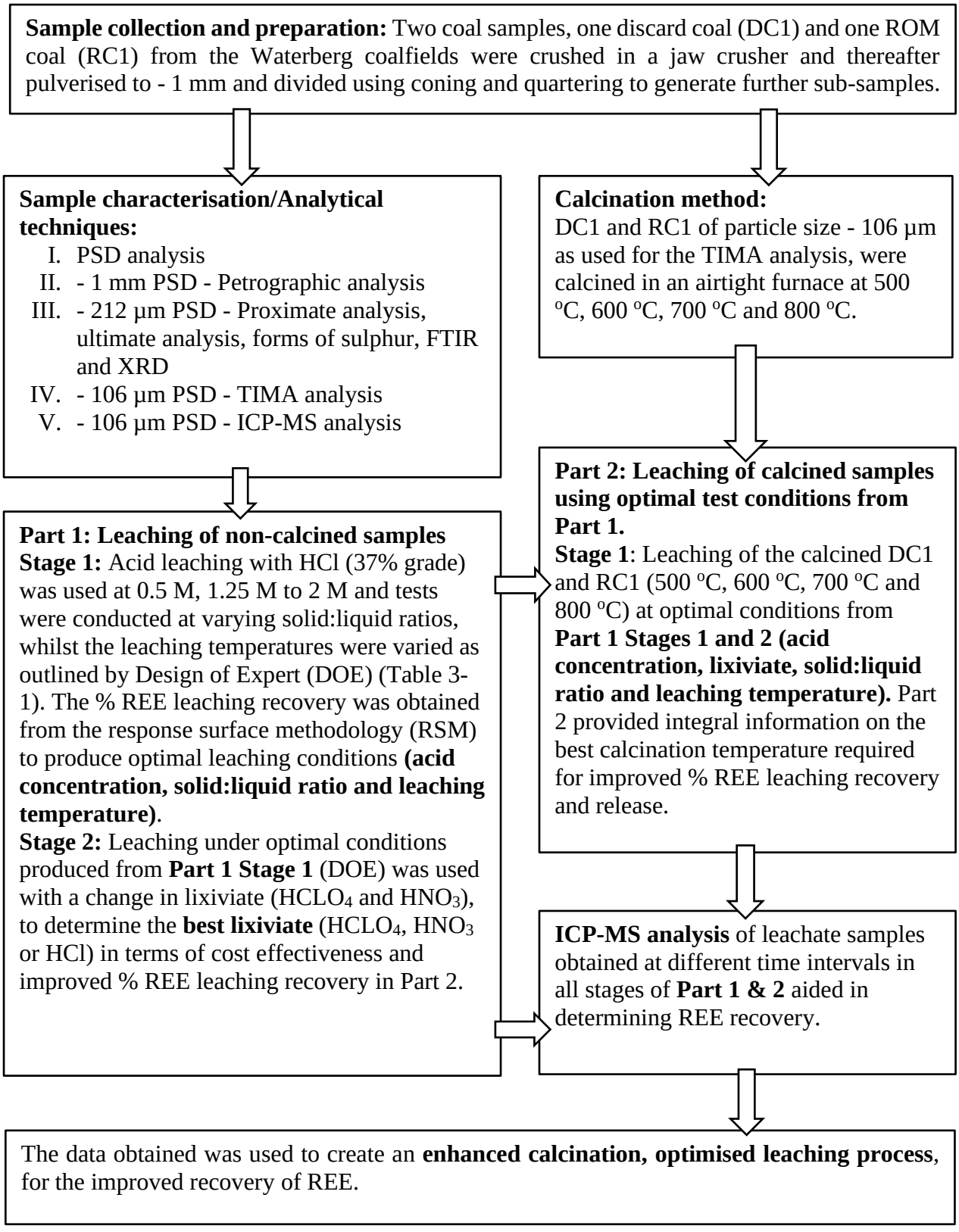


Figure 3-1: Overview of the calcination and leaching methodology applied in the study.

3.4 Beneficiation and recovery of REE

3.4.1 Part 1: Leaching of the non-calcined samples

3.4.1.1 Stage 1: varying concentration, solid:liquid ratio and temperature

In Part 1 of the experiments, HCl was used as the leaching agent. The response surface methodology (RSM) Box-Behnken design was used on the DOE software. Fifteen leaching runs (Table 3-1 and Table 3-2) of varying acid concentrations, changing pulp density (solid:liquid ratio) and varying leaching temperatures were generated. The fifteen leaching runs were applied to RC1 and DC1 of a PSD of - 106 µm. The PSD was determined by an analogy in a study conducted Zhang and Honaker (2019).

The acid leachate was prepared by mixing deionised distilled water with the designated volumes of lixiviates in a triple neck round bottom flask, placed on top of a stirring-heating plate (Figure 3-2) to achieve the concentrations of 0.5 M, 1.25 M and 2 M. Equation 3-1 and 3-2 were used to determine the designated volumes of acid required to achieve the stipulated concentrations (0.5 M, 1.25 M and 2 M) in a one-litre leaching slurry.

$$C_A \times V_A = C_L \times V_L \tag{3-1}$$

Rearranging equation 3-1 to produce equation 3-2:

$$V_A = \frac{C_L \times V_L}{C_A} \tag{3-2}$$

Where V_A represented the volume of the acid required for mixing with deionised distilled water, C_L illustrated the stipulated concentrations (0.5 M, 1.25 M and 2 M) of the 1-litre leachate slurry, V_L indicated the volume of the leachate slurry (1-litre in this case), and C_A represented the original concentrations (before mixing) of the leaching acids employed in the study.



Figure 3-2: Image of the experimental leaching set-up.

For the leaching test, 10 to 40 grams of RC1 or DC1 was mixed with the prepared leachate solution to obtain a 1-litre leaching slurry, stirred at 530 rpm (Figure 3-2), according to the test procedure outlined by Yang (2019). Thereafter, 15 ml of the slurry was drawn with a 0.45 µm microfilter plunger syringe (Figure 3-3) at time intervals of 1, 15, 30, 60, 120 and 180 minutes. A 0.45 µm microfilter syringe was used to separate and filter out the suspended solids from the leachate. The leachate samples removed at each time interval in Part 1 and Part 2 (leaching of calcined samples, Figure 3-1) were then subjected to ICP-MS analysis to determine the REE recovery from each sample.

The leaching recovery was determined by using equation (3-3):

$$\%\ REE\ leaching\ recovery = \frac{mREE_{leachate}}{mREE_{concentrate}} \times 100 \quad (3\text{-}3)$$

Where $mREE_{leachate}$ signified the mass of REE in the lixiviate and $mREE_{concentrate}$ represented the mass of REE in the original sample. Further manipulation of equation (3-3) resulted in equation (3-4):

$$\%\ REE\ leaching\ recovery = \frac{C_L \times V_L}{C_{RS} \times M_{RS}} \times 100 \quad (3\text{-}4)$$

Where C_L represented the TREE/elemental concentration in the leachate in µg/ml and V_L depicted the volume of leachate in ml. C_{RS} illustrated the REE/elemental concentration in µg/g of the initial raw sample and M_{RS} signified the weight of the coal sample added to the leachate

in grams. Equation 3-3 was used in developing the % REE leaching recovery models over time for the varied factors.



Figure 3-3: Image of the microfilter-syringe employed for leachate extractions.

Table 3-1: Experimental design matrix (from DOE) for the leaching of non-calcined RC1.

Run	Factor 1 A: HCl concentration (M)	Factor 2 B: Solid:liquid ratio (g/l)	Factor 3 C: Temperature (°C)
1	0.5	25	30
2	1.25	40	50
3	1.25	40	30
4	1.25	10	30
5	1.25	25	40
6	0.5	10	40
7	1.25	25	40
8	2	40	40
9	1.25	10	50
10	0.5	40	40
11	2	25	30
12	2	10	40
13	0.5	25	50
14	2	25	50
15	1.25	25	40

Table 3-2: Experimental design matrix (from DOE) for the leaching of non-calcined DC1.

Run	Factor 1 A: HCl concentration (M)	Factor 2 B: Solid:liquid ratio (g/l)	Factor 3 C: Temperature (°C)
1	0.5	25	30
2	1.25	40	50
3	1.25	40	30
4	1.25	10	30
5	1.25	25	40
6	0.5	10	40
7	1.25	25	40
8	2	40	40
9	1.25	10	50
10	0.5	40	40
11	2	25	30
12	2	10	40
13	0.5	25	50
14	2	25	50
15	1.25	25	40

The optimal leaching conditions attained from DOE (RSM) based on the % REE leaching recovery were implemented for the optimisation tests on non-calcined RC1 and DC1. The optimal leaching conditions were also used in Part 1 Stage 2 and Part 2 of the leaching experiments (Table 4-11).

3.4.1.2 Stage 2: leaching of non-calcined samples under DOE optimal conditions

The $HClO_4$ and HNO_3 leaching experiments were conducted on RC1 and DC1 based on the optimal % REE leaching recovery conditions from Part 1 Stage 1 (DOE). $HClO_4$ and HNO_3 of grades 70% and 69%, respectively, were used in Stage 2 of the leaching experiments. The data from this stage provided an insight into the acid with the highest % REE leaching recovery and most cost effective and thereby was the acid of choice utilised in Part 2 (calcined leaching test) (Figure 3-2).

3.4.2 Calcination method and apparatus

RC1 and DC1 were subjected to calcination at 500 °C, 600 °C, 700 °C and 800 °C under a static environment in an airtight furnace. Each coal sample was calcined for two hours at the respective target temperatures and at a heating rate of 10 °C/min.

3.4.3 Part 2: Leaching of the calcined samples at optimal parameters

The calcined DC1 and RC1 were leached under the optimal parameters (ideal acid concentration, optimum solid:liquid ratio, and best leaching temperature) attained from Part 1 Stage 1 and the best acid lixiviate obtained from Part 1 Stage 2 (Table 4-11). Part 2 of the leaching experiment provided critical information regarding the optimal calcination temperature required for an improved % of REE leaching recovery and release.

The data obtained was used to create an enhanced calcination optimal leaching process to improve the recovery of REE.

3.5 List of apparatus and equipment required for the leaching tests

List of inventories and equipment:

- Thermometer
- pH meter
- TGA furnace
- 1 litre triple neck round bottom flasks/beaker
- Heating plate
- Ceramic weighing crucibles
- TGA crucibles
- Magnetic stirrer/agitator
- 15 ml centrifuge tubes (leachate sample storage)
- 80 ml glass beaker
- Syringes
- Microfilters 0.45µm (to attach to the syringe)
- Stopwatches

CHAPTER 4: RESULTS AND DISCUSSION

4.1 Introduction

This chapter presents the results achieved by characterising the two coal samples, RC1 and DC1, used in this study. The characterisation techniques that were used are proximate, petrography, XRD, ultimate, total sulphur, forms of sulphur, FTIR, TIMA and ICP-MS analyses. Furthermore, the chapter provides a thorough discussion of the concentration of REE before and after calcination, and the data obtained after leaching. Detailed information on the influence of different leaching parameters on REE recovery performance is also presented.

4.2 Coal characterisation results

4.2.1 Physico-chemical properties and petrography results

According to the proximate analyses both the RC1 and DC1 samples contained a high ash and low carbon content, similar to the data obtained by Faure *et al.* (1996) from the same coalfield. DC1 was significantly enriched (68.26%) in ash content and had a very low fixed carbon content (15%), as indicated in Table 4-1. RC1 had a lower ash content of 50% and a higher carbon content of 27% than DC1. The higher ash content noted in DC1 was expected as this is the coarse discard fraction of RC1 after beneficiation. The higher ash content in DC1 correlates well with the higher mineral content indicated by the petrographic analysis data (Table 4-1). The XRD analysis (Figure 4-2) also depicted a sample with higher inorganic mineral intensities relative to RC1.

The ultimate and petrographic analyses further validated the low quality and reactivity of the coal shale as per ISO 11760 definition, in terms of its low total carbon content and high inertinite content (Table 4-1). Both samples are "***Coal shale***" but will be referred to as coal throughout the thesis for ease of reference. The total sulphur content in RC1 was greater than that of DC1. This supports the increased quantity of the carbominerite pyrite and sulphur present in RC1 relative to DC1, as illustrated by the petrographic (microlithotypes) (Table 4-1). In this manner, it may be noted that pyrite and other sulphur minerals were intimately interlinked or packed into cracks and fissures within the organic maceral matrices. Upgraded clean coal shale products associated with some organic and pyritic sulphur are associated with the beneficiation of RC1, whilst the discard coal (DC1) had lower amounts of sulphur and was predominantly "rock", which implies the source coal rock, ROM source coal is highly contaminated with roof and floor rocks as well as high ash coally bands.

Table 4-1: Summary of the characteristics of the ROM coal (RC1) and coal discard (DC1).

Parameters/Samples	**RC1**	**DC1**
Proximate analysis; air-dried (%)		
Inherent moisture content	2.98	2.71
Volatile matter	19.00	14.02
Ash content	50.85	68.26
Fixed carbon (calculation)	27.18	15.01
Ultimate analysis (vol %)		
Total sulphur (S)	1.83	0.41
Total carbon (C)	34.30	18.8
Hydrogen (H)	1.89	0.97
Nitrogen (N)	0.74	0.41
Forms of sulphur analysis (vol %)		
Total sulphur	2.09	0.415
Pyritical sulphur	1.37	0.29
Sulphatic sulphur	0.11	0.02
Organic sulphur	0.61	0.11
Petrography analysis		
Maceral groups (vol %)		
Vitrinite	4.55	2.39
Liptinite	5.43	1.39
Reactive inertinite	1.20	0.40
Total reactive macerals	11.18	4.18
Total inertinite	39.05	17.89
Inert inertinite	37.85	17.49
Total macerals/organics	**49.04**	**21.67**
Mineral groups (vol %)		
Clays	12.4	10.9
Quartz	36.3	64.6
Pyrite	1.6	2.6
Carbonates	0.7	0.2
Total mineral matter	**50.96**	**78.33**
Microlithotypes (vol %)		
Monomaceral	12.6	2.9
Bimaceral	1.4	0.2
Tricameral	7.4	0.0
Total carbominerite	29.2	6.1
Carbominerite silicate (quartz)	26.8	0.2
Carbominerite pyrite	1	0.4
Rock	48.2	90.8

From the petrographic analysis (Table 4-1), both coal shale samples were low in organic matter content and the macerals present fell predominantly in the inertinite group. RC1 contained marginally higher organic matter (37.85%) compared to DC1 (21.67%). In conjunction with the petrographic analysis, the volatile matter content from the proximate analysis was found to range between 19% (RC1) and 14% (DC1). The coals can be classified as low-volatile matter

coals (on SA grading) and medium C bituminous coals (on vitrinite reflectance). Both values relate well with the study by Faure (1993) on the same coal strata. According to another study conducted by Faure *et al.* (1996), the coals in this zone are enriched in inertinite, which is an outcome of a poorly drained proximal floodplain setting.

4.2.2 Mineralogical composition of the coals

The minerals in coal differ significantly from location to location, in the same seam, in different seams and from coalfield to coalfield (Faure, 1993). Hence, in this study, RC1 and DC1 were subjected to XRD, for qualitative analysis of the mineral phases, and petrography and TIMA modal liberation analyses to determine the quantitative composition of the minerals present. Additionally, the TIMA image analysis provided an insight into the association and distribution of the REE with the inorganic (mineral) and organic fractions of the coal.

From the petrographic analyses, quartz and kaolinite were the major mineral species in RC1 and DC1, with smaller amounts of pyrite and trace quantities of carbonate minerals present (Table 4-1). Carbominerite (a mixture of minerals and macerals) was the dominant microlithotype group in RC1, accounting for almost 29.2 vol % of the sample, whereas DC1 was composed of 90% rock (mineral matter representing 50-100% of the particle). RC1 coal had microlithotype particles rich in various organic macerals (21.4%), whereas DC1 had only 3.1 % of the same types of particles (Table 4-1).

RC1 had more pyrite (4.86%) than DC1 (2.36%), according to the TIMA modal liberation analysis (Table 4-2). This difference was confirmed by the petrographic analysis (Table 4-1). The high sulphur content of RC1 appears to be the result of the presence of pyrite and other sulphur bearing elements (organic sulphur) as well as a larger quantity of carbominerite pyrite. However, pyrite was the only sulphur bearing form in DC1 and was in minimal quantities.

The petrographic analysis, forms of sulphur and TIMA image analysis correlate well with sulphur and pyrite contents. The TIMA image analysis (Table 4-2), XRD (Figure 4-2) and petrographic analyses (Table 4-1) also indicated a high mineral matter content in DC1 as per Figure 4-3. These results were validated by the corresponding high rock percentage (“rock”) of 90.8% (Table 4-1). This, in turn, corresponds well to the high ash content in the proximate analysis for DC1.

The micrographs captured from petrography are depicted in Figure 4-1a to 4-1h. In RC1, a certain amount of vitrinite and liptinite was evident, whilst elevated amounts of inertinite were captured (Figure 4-1a to 4-1d). This corresponds well with South African coals from this coalfield, typically inertinite rich in the lower coal seams (Faure, 1993; Faure *et al.*, 1996). RC1 comprised significant quantities of quartz, pyrite, clay minerals and small amounts of calcite and siderite mixed within the clay minerals (Figures 4-1b to 4-1c). The pyrite and the clay minerals (kaolinite) typically fill in cracks and cleats of the organic matrices. Quartz minerals are seen as rounded circular mineral grains (Figure 4-1b and 4-1c) embedded in the organic and inorganic matrix. Such forms could have formed from droplet solutions within the organic peat (Wagner *et al.*, 2018). The fine brown grainy-textured worm-like shapes in Figures 4-1a to 4-1h are specific forms of clay minerals (kaolinite) well known in Southern African coals. These were present in both RC1 and DC1. Furthermore, the grainy oval worm-like shapes indicative of kaolinite in Figure 4-1g correlating with the intense kaolinite peaks exhibited in Figure 4-2 for the DC1 sample.

Minimal amounts of organic macerals were observed in DC1 (Figures 4-1e to 4-1h). The images indicated that DC1 was composed of large amounts of quartz, illustrated by the well-rounded particles embedded in the coaly matrix (Figure 4-1e and 4-1h). DC1 was also highly enriched in clay minerals, exhibiting various colours of bright grey to brownish particles (Figure 4-1g and 4-1h), with smaller amounts of pyrite present in bands and fissures attached to the inertinite macerals.

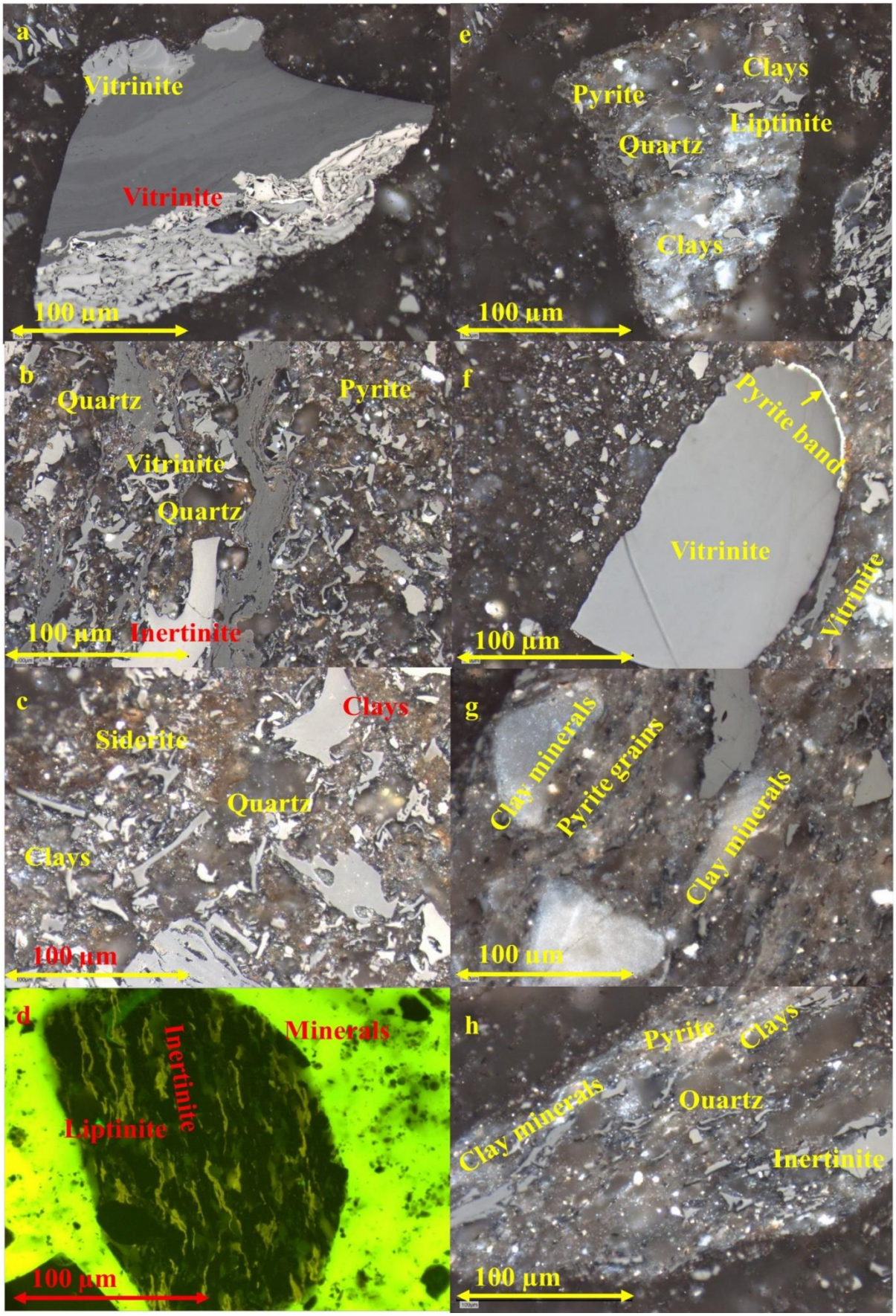
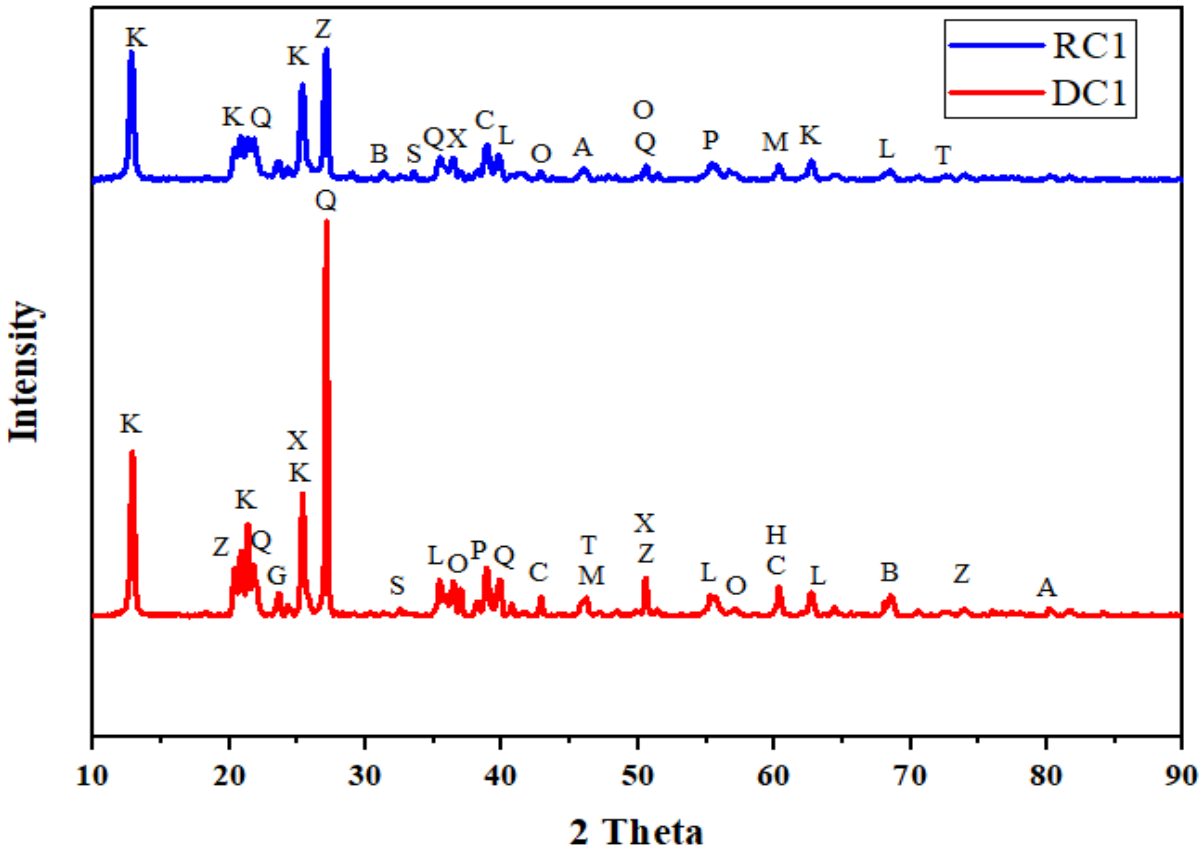


Figure 4-1: Petrography images 1a, b, c, d (RC1) and 1e, f, g, h (DC1).

There were many petrographically unidentifiable mineral forms filling the cracks and cleats within the organic macerals of the RC1 and DC1 (Figure 4-1a to 4-1h). These are accessory minerals that tend to contain significant amounts of ultrafine bright particles, which may be REE bearing minerals. Therefore, these results were further investigated with the TIMA image analysis.

The XRD analysis indicated a high abundance of clay minerals, particularly kaolinite and the silicate mineral quartz, in RC1 and DC1 (Figure 4-2). This correlates with the petrography results (Table 4-1 and Figure 4-1). RC1 was predominantly composed of kaolinite ($Al_2Si_2O_5(OH)_4$), quartz (SiO_2), substantial amounts of zircon ($ZrSiO_4$), lower amounts of pyrite (FeS_2) and minor amounts of apatite ($Ca_5(PO_4)_3(OH, F, Cl)$) and calcite ($CaCO_3$) (Figure 4-2). Trace amounts of the REE-bearing minerals monazite ($(Ce, La, Nd, Th)PO_4$) and xenotime (YPO_4) were detected. The same minerals were also observed in the DC1 sample (Figure 4-2), only in increased volumes and masses, noted by their greater peak intensities. This is expected, as the DC1 origin coal is the tailings (discard) of the RC1 origin ROM pre-processed coal. The small amounts of monazite and xenotime indicate the potential occurrences of REE in these coal sources.



K: Kaolinite, Q: Quartz, S: Siderite, A: Ankerite, C: Calcite, P: Pyrite, M: Muscovite, L: Chlorite, Z: Zircon, T: Apatite, **O: Monazite**, B: Beryl, G: Plagioclase, **X: Xenotime**, H: Schorl.

Figure 4-2: XRD diffractograms for RC1 and DC1.

From the TIMA modal liberation results presented in Table 4-2, the major minerals in both samples were kaolinite, quartz and Al_2SiO_5 polymorphs. The Al_2SiO_5 polymorphs are the reason why higher quantities of quartz and silicates were observed in the petrographic analysis (Table 4-1 and Figure 4-1). Nonetheless, kaolinite was evidently the more dominant mineral in both samples, as observed by the TIMA modal liberation and image analysis (Table 4-2 and Figure 4-3). This was also reinforced by the XRD peak intensities (Figure 4-2) of kaolinite in relation to quartz for the two samples (RC1 and DC1). DC1 was found to contain more kaolinite and quartz but less pyrite than RC1. Trace amounts (< 1%) of minerals such as calcite, apatite, muscovite and ankerite were observed in both samples.

Table 4-2: TIMA modal liberation analysis results for the quantities of the various mineral species present in RC1 and DC1.

Parameters/Samples	**RC1**	**DC1**	**Parameters/Samples**	**RC1**	**DC1**
TIMA analysis/mass % of mineral phases			**TIMA analysis/mass % of mineral phases**		
Kaolinite	57.66	59.25	Biotite	0.04	0.03
Quartz	15.97	17.13	Chlorite - Clinochlore	0.00	0.00
Al_2SiO_5 polymorphs	18.47	13.63	Chlorite - Chamosite	0.01	0.00
Pyrite	4.86	2.73	Plagioclase	0.07	0.87
Hematite/Magnetite	0.06	0.06	Chromite	0.03	0.00
Ankerite	0.72	0.38	Apatite	0.02	0.01
Beryl	0.38	0.47	Olivine	0.00	0.00
Schorl	0.45	0.53	Goethite	0.02	0.01
Muscovite	0.25	0.22	Pyrrhotite	0.01	0.01
Calcite	0.19	0.04	The rest (identified		
Almandine spessartine	0.04	0.10	minerals in very minimal		
Grossular	0.00	0.02	detection quantities)	0.02	0.03
Pyrope	0.00	0.00	**Total % of minerals**		
Orthoclase	0.00	0.05	**recognised**	**97.26**	**95.57**

The BSE (backscattered electron) images achieved from the bright particle search of the TIMA image analysis (Figure 4-3) provided critically important results with respect to the REE-bearing minerals, their associations and distribution in origin coal. The major REE-bearing minerals identified from the TIMA software were pyrite, kaolinite, hematite/magnetite and zircon, as seen in Figure 4-3a to 4-3h.

In DC1 (Figure 4-3e to 4-3h), scandium was largely distributed with kaolinite and quartz dispersed in the organic matrices. Yttrium, holmium and ytterbium were associated with zircon and kaolinite (Figure 4-3e to 4-3h). Hematite/magnetite and pyrite were the predominant REE-bearing minerals, which were associated with specific REE notably samarium, neodymium, europium, terbium, erbium and dysprosium (Figure 4-3e to 4-3h). Many HREE (Y, Gd, Dy, Yb) were distributed in the organic matrices dispersed with kaolinite (Figure 4-3f and 4-3h). This suggests that these REE may be weakly ion-adsorbed on the organic fraction and clay minerals of the DC1 origin coal (Laudal, 2017).

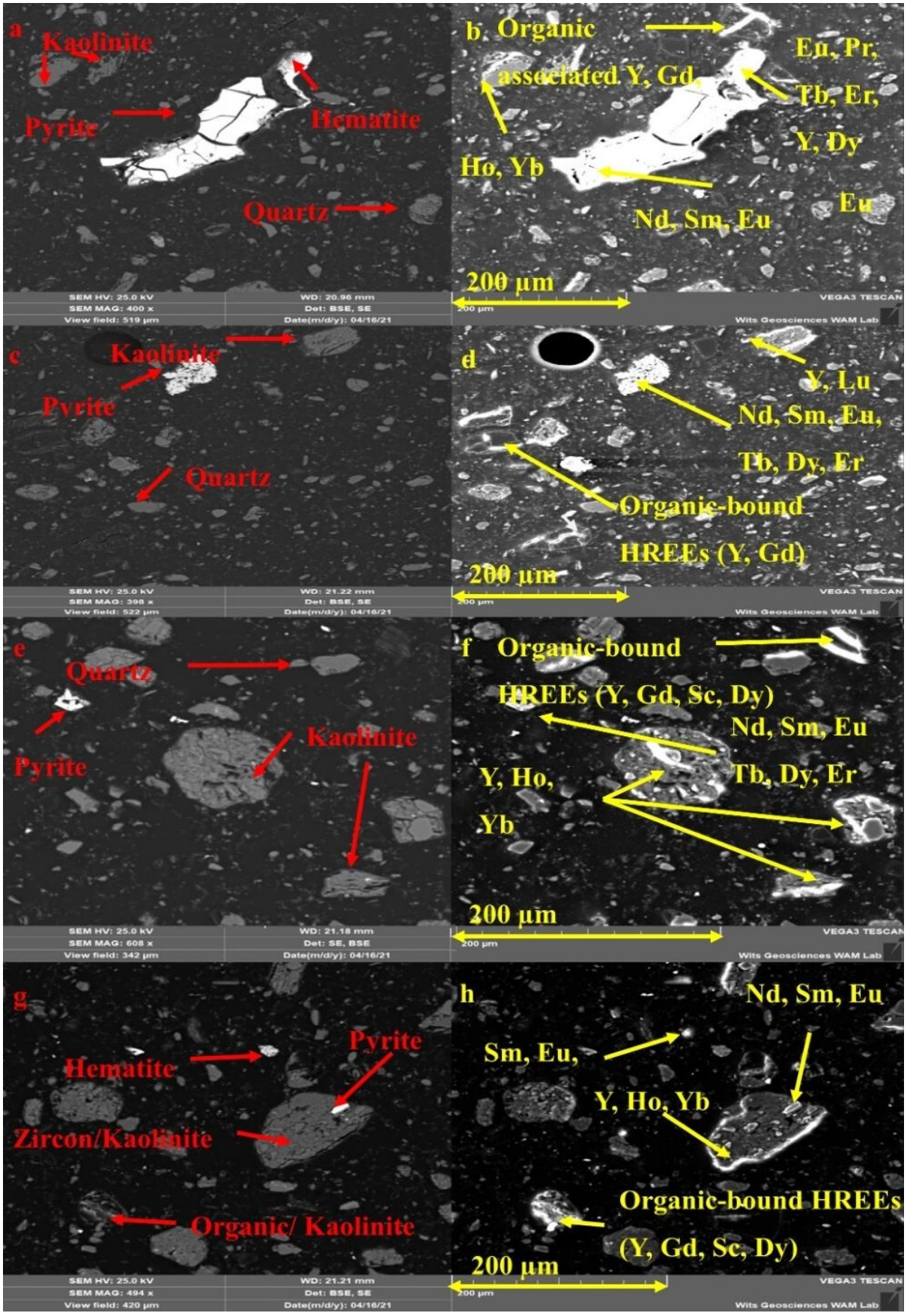


Figure 4-3: TIMA image results of REE-bearing minerals for RC1 (BSE image a and c, and SE image b and d) and DC1 (BSE image e and g, and SE image f and h).

With regards to RC1, yttrium, europium and minor amounts of scandium and gadolinium were associated with kaolinite dispersed in the organic matrices (Figure 4-3a to 4-3d). Furthermore, as seen in Figures 4-3a and 4-3b, samarium, praseodymium, terbium, erbium and dysprosium were distributed within the magnetite/hematite minerals. The BSE images of RC1 depicted bright pyrite particles with kaolinite and quartz grains in the surroundings (Figure 4-3a and 4-3c). The BSE bright particle image (Figure 4-3a) together with the SE image (Figure 4-3b) are evidence that the bright REE (Nd, Sm, Eu, Tb, Dy, Y and Er) are significantly associated with pyrite, magnetite/hematite and kaolinite. Some HREE such as Ho, Yb and Y are bonded with kaolinite (Figure 4-3b). However, some bright phases of HREE and particularly Y, Ho, Gd, Dy, were attached to the carbon fraction (Figure 4-3d). These results illustrate that a substantial amount of the HREE was associated with the organic matrices in RC1.

Notably, some of the REE were within the cracks and cleats of the organics, whilst some REE were attached to the grain boundary of the kaolinite and quartz minerals dispersed in the organic matrices (Figure 4-3b and 4-3h). This suggests that these REE may have been weakly ion-adsorbed onto the organic fraction and clay minerals of DC1 (Laudal, 2017). It should be noted that minimal amounts of REE were associated with quartz, with quartz rather observed as an REE diluting mineral. The size and PSD of the bright particles known to be REE hosts ranges from 5 µm to 106 µm (in the -106 µm milled samples fraction), as shown in Figure 4-3b, 4-3d, 4-3f and 4-3h. These REE particles were either fully liberated or attached to the carbon or mineral fractions of the samples, indicating the tiny sizes of the single native REE.

From the parts analysed for RC1 and DC1 and considering the fine liberation of the elements, it is difficult to conclude that the REE are only found in or associated with organic macerals or inorganic mineral fractions in coal. However, it may be deduced that REE are associated with both the inorganic mineral as well as the organic maceral fractions of the coals. Additionally, this research has demonstrated that REE occur in cracks, cleats and fissures of organic matrices and need to be considered as such when REE extraction and recovery are under consideration.

4.2.3 Fourier transform infrared spectroscopy results.

Coal is a conventional example of a chemically heterogenous substance in nature, constituting of a sophisticated macromolecular network of organic (carbon, hydrogen) structural units, connected by covalent and non-covalent bonds (He *et al.*, 2017). The FTIR spectra obtained

was construed based on previous literature (Güler *et al.*, 2010; Equeenuddin *et al.*, 2016; He *et al.*, 2017; Yin *et al.*, 2019; Mabuza *et al.*, 2020).

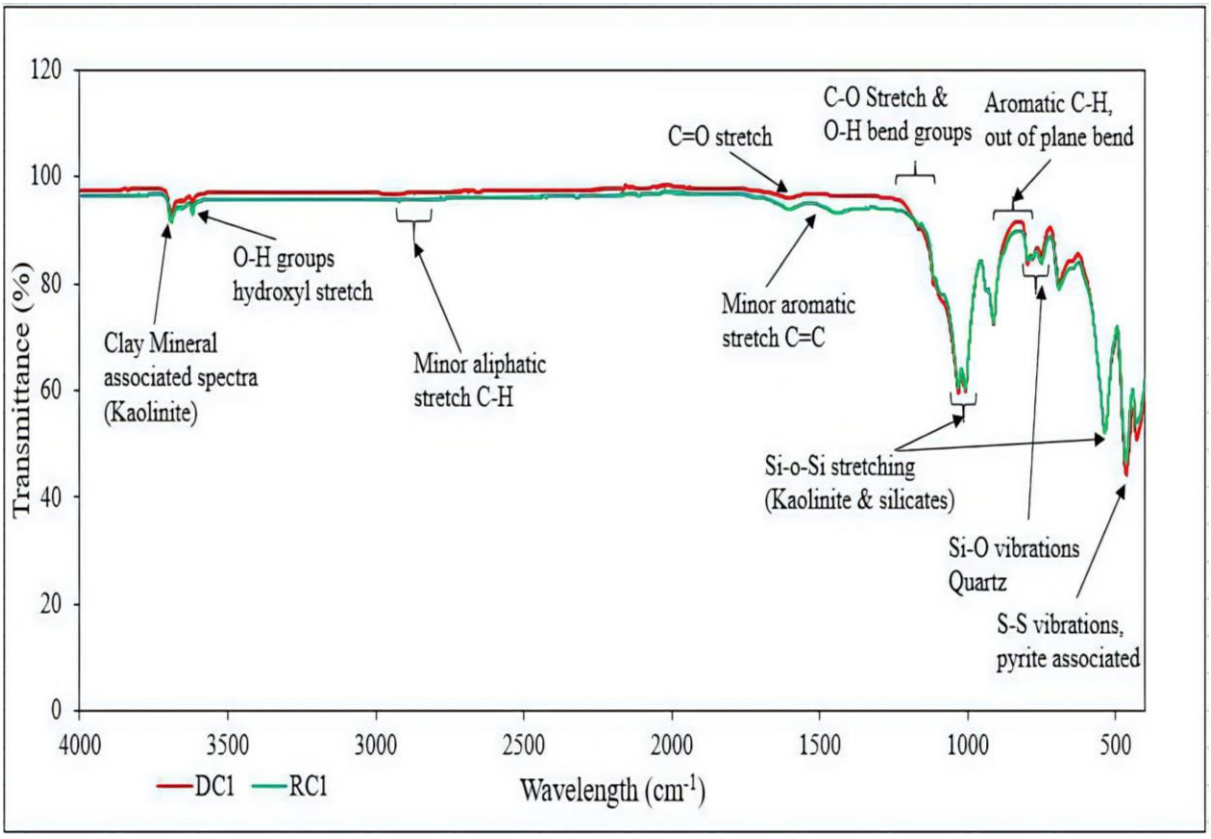


Figure 4-4: FTIR spectrum for the ROM (RC1) and discard coals (DC1).

RC1 and DC1 manifested near-identical FTIR spectra, with stronger peaks observed for the mineral matter than the carbon matter, confirming the rich mineral content of both samples (Figure 4-4). The presence of minor straight-chain aliphatic carbon structures was observed at wavelengths between 2950 cm^{-1} and 2800 cm^{-1}. At a band of 1600 cm^{-1}, representing the aromatic C=C nature (cyclic, ring-like) of carbon, RC1 had a stronger absorption peak relative to DC1. A stronger absorption peak at 1600 cm^{-1} correlates well with an increase in carbon content. Thus, the carbon content of the ROM coal (based on the RC1 result) relative to the discard coal (based on the DC1 result) is significantly higher, correlating with the petrography and proximate analysis. The aromatic C-H out of plane bend was assigned at a wavelength of 902 cm^{-1} to 750 cm^{-1} (Figure 4-4), concluding that the ROM and discard coals exhibit a slightly weaker aliphatic structure and a considerably greater aromatic structure. Furthermore, small amounts of oxygen-containing functional groups (C=O) were indicated by the peak at around 1700 cm^{-1}, implying that the coal samples contain carbonyls such as carboxylic acids. At an IR

band of 1200 cm^{-1} to 1050 cm^{-1}, the presence of the C-O stretch and O-H groups re-highlights the presence of carboxylic acid or alcohols in both coal samples.

The peak appearing at 3650 cm^{-1} was attributed to O-H stretching vibration (Figure 4-4), with these hydroxyl groups being attributed to the clay minerals (kaolinite) (Georgakopoulos *et al.*, 2003; Equeenuddin *et al.*, 2016; Behera *et al.*, 2017). The absorption peak at 3698 cm^{-1} indicates the abundance of kaolinite and other trace minerals within the two coal samples (Georgakopoulos *et al.*, 2003; Behera *et al.*, 2017). Prominent peaks present at 1000 cm^{-1} to 650 cm^{-1} (Figure 4-4) indicate Si-O-Si vibrations and reflected the abundance of kaolinite and silicates in the ROM and discard coals (Equeenuddin *et al.*, 2016; Behera *et al.*, 2017). The bands near 760 cm^{-1} and 696 cm^{-1} (Figure 4-4) were associated with Si-O vibrations, thereby displaying the significant presence of the quartz mineral in the ROM and discard coals (Equeenuddin *et al.*, 2016; Behera *et al.*, 2017). Characteristic IR S-S bands in the spectra region of 500 cm^{-1} (Figure 4-4) confirm the presence of sulphur in the form of carbominerite (C-S) and pyrite in the ROM and discard coals (Equeenuddin *et al.*, 2016).

The FTIR analysis (Figure 4-4) clearly shows that the mineral matter content is larger than the organic matter in both coals. Evidently, the presence of the hydroxyl groups and carbonyl groups may be significant as these anionic groups provide bonding sites for REE cations.

4.3 REE contents

4.3.1 Comparative quantitative results of REE

ICP-MS was used to determine the quantity and extent of REE in RC1 and DC1. The ICP-MS results (Table 4-3) are of a confidence level greater than 95 %. The TREE content in RC1 and DC1 was more than 225 ppm (Table 4-3). This exceeds the average TREE values of the Earth's upper continental crust (UCC; 146 ppm), the world average TREE in coals (72 ppm), and the average TREE in Chinese and USA coals of < 138.47 ppm, according to Taylor and McLennan (1985) and Ketris and Yudovich (2009). Furthermore, the TREE contents of 225 ppm and 245 ppm for RC1 and DC1, respectively (Table 4-3), is well above the cut-off grade of 130 ppm for REE in coal as stipulated by Zhang *et al.* (2015) (Dai and Finkelman, 2018). This is significantly greater than the REE contents of 121 ppm, for coals reported from the Witbank and Highveld coalfields by Wagner and Matiane (2018).

Table 4-3: ICP-MS results for individual REE contents and TREE, outlook coefficient ($C_{outlook}$), together with important REE ratios.

REE native elements (concentration in ppm)/Samples	RC1	DC1
La	41.99	47.20
Ce	88.05	100.86
Pr	9.32	10.52
Nd	35.93	39.18
Sm	6.53	7.16
Eu	1.19	1.11
Gd	5.29	5.10
Tb	0.73	0.69
Dy	3.81	3.71
Ho	0.67	0.66
Er	1.73	1.72
Tm	0.20	0.23
Yb	1.24	1.50
Lu	0.20	0.16
Sc	11.08	10.27
Y	17.49	15.43
∑TREE	225.45	245.42
∑HREE	42.44	39.39
∑LREE	183.00	206.04
∑CREE	117.21	119.28
∑UCREE	63.13	69.90
$C_{outlook}$	0.96	0.88
LREE:HREE	4.31	5.23
% CREE	27.00	25.20
% UCREE	28.00	28.48

It has also been established that the HREE in the two South African ROM and discard coals tend to show a greater affinity for coals with higher organic contents. This explains why the RC1 coal sample was slightly more enriched in HREE than DC1, as it constituted greater quantities of fixed carbon and organic macerals, as seen in Table 4-1. The LREE:HREE ratio for RC1 (4.3) was lower than that of DC1 (5.2), denoting that the increase in LREE contents is associated with an increase in the ash and mineral content of the coal. Thus, HREE quantities increase with an increase in maceral contents, as exhibited by RC1.

4.3.2 Comparative quantitative REE results for the two calcined coal samples

RC1 and DC1 were calcined at 500 ^{o}C, 600 ^{o}C, 700 ^{o}C and 800 ^{o}C. Table 4-4 shows that the TREE content increased significantly as the calcination temperature increased from 500 ^{o}C to

800 ^{o}C. This occurs due to the degradation and removal of the coal's volatile matter and carbon structure (Zhang and Honaker, 2019a), subsequently increasing the REE concentrations in calcined RC1 and DC1. The highest concentration of TREE was at a calcination temperature of 800 ^{o}C, with RC1 and DC1 concentrations of 362.29 ppm and 390.70 ppm, respectively. At these four temperatures, the calcined DC1 subsequently had a higher TREE concentration than the calcined RC1. The outlook coefficient ($C_{outlook}$) for all calcined samples exceeded the $C_{outlook}$ for raw samples. However, this cannot be used to assess the economic potential of calcined samples as primary or secondary raw ore because it has been enriched. As seen in Table 4-3 and Table 4-4, the % CREE in the calcined RC1 and DC1 were more than that of the raw RC1 and DC1, indicating that calcined coals are significantly more economically valuable.

Table 4-4: ICP-MS results for individual REE contents and the TREE, outlook coefficient ($C_{outlook}$) and REE ratios for the calcined coal samples.

REE native elements (concentration in ppm)	**RC1 500 ºC**	**DC1 500 ºC**	**RC1 600 ºC**	**DC1 600 ºC**	**RC1 700 ºC**	**DC1 700 ºC**	**RC1 800 ºC**	**DC1 800 ºC**
La	55.93	60.88	59.70	66.55	64.66	69.85	67.47	75.14
Ce	117.28	130.10	125.20	142.21	135.59	149.27	141.49	160.56
Pr	12.41	13.57	13.25	14.83	14.35	15.56	14.97	16.74
Nd	47.85	50.54	51.09	55.24	55.33	57.98	57.73	62.37
Sm	8.69	9.23	9.28	10.09	10.05	10.59	10.49	11.39
Eu	1.58	1.43	1.69	1.56	1.83	1.64	1.91	1.76
Gd	7.04	6.57	7.52	7.19	8.14	7.54	8.50	8.11
Tb	0.97	0.89	1.03	0.97	1.12	1.02	1.17	1.09
Dy	5.07	4.78	5.41	5.23	5.86	5.49	6.12	5.90
Ho	0.89	0.85	0.95	0.93	1.03	0.97	1.07	1.05
Er	2.30	2.21	2.46	2.42	2.66	2.54	2.78	2.73
Tm	0.26	0.29	0.28	0.32	0.30	0.34	0.32	0.36
Yb	1.65	1.93	1.76	2.11	1.90	2.22	1.99	2.38
Lu	0.26	0.20	0.28	0.22	0.30	0.23	0.32	0.25
Sc	14.75	13.24	15.75	14.48	17.06	15.19	17.80	16.34
Y	23.29	19.90	24.87	21.75	26.93	22.83	28.10	24.56
∑TREE	300.29	316.59	320.58	346.04	347.19	363.22	362.29	390.70
∑HREE	56.53	50.91	60.34	55.65	65.35	58.41	68.20	62.83
∑LREE	243.76	265.77	260.24	290.50	281.83	304.92	294.09	327.99
∑CREE	156.12	153.87	169.01	168.18	180.50	176.53	188.35	189.89
∑UCREE	78.57	90.17	89.77	98.55	97.22	103.45	101.44	111.28
$C_{outlook}$	1.98	1.70	1.88	1.70	1.85	1.70	1.85	1.70
LREE:HREE	4.31	5.21	4.31	5.21	4.31	5.21	4.31	5.21
% CREE	35.96	32.50	38.39	35.53	41.58	37.29	43.38	40.11
% UCREE	37.29	36.73	39.81	40.15	43.12	42.15	44.99	45.34

4.3.3 Estimation of the quality of RC1 and DC1 as an REE source

An important criterion proposed by Seredin (2010) was employed in this study to evaluate the potential of the ROM (from RC1 evaluation) and discard coals (from DC1 evaluation) as a source of REE. This approach classifies an ideal ore as containing as many CREE (Nd, Eu, Tb, Dy, Er, Y) as possible relative to the UCREE (Ce, Ho, Tm, Yb, Lu). The standard is known as the $C_{outlook}$ (Seredin and Dai, 2012). The proposed criterion uses a ratio of the sum of the CREE divided by the sum of the UCREE as depicted in Equation 4-1 (Seredin, 2010).

$$C_{outlook} = (^{(\sum CREE)}/_{\sum REE}) / (^{(\sum UCREE)}/_{\sum REE}) \quad (4\text{-}1)$$

Where $\sum CREE$ denotes the sum of CREE for demand (Nd, Eu, Tb, Dy, Er, Y), $\sum REE$ signifies the sum or total contents of all 17 REE and $\sum UCREE$ symbolises the UCREE (Ce, Ho, Tm, Yb, Lu).

The $C_{outlook}$ values obtained for RC1 and DC1 were plotted on the $REY_{def,\ rel}$ % (% CREE) graph (Figure 4-5) developed by Seredin (2010). The plot provides an insight into the economic viability and extraction of the ore. As shown in Figure 4-5, category I depicts an unpromising source, II indicates a promising source, whilst III indicates a highly promising source for economic engineering development (Seredin, 2010; Seredin and Dai, 2012).

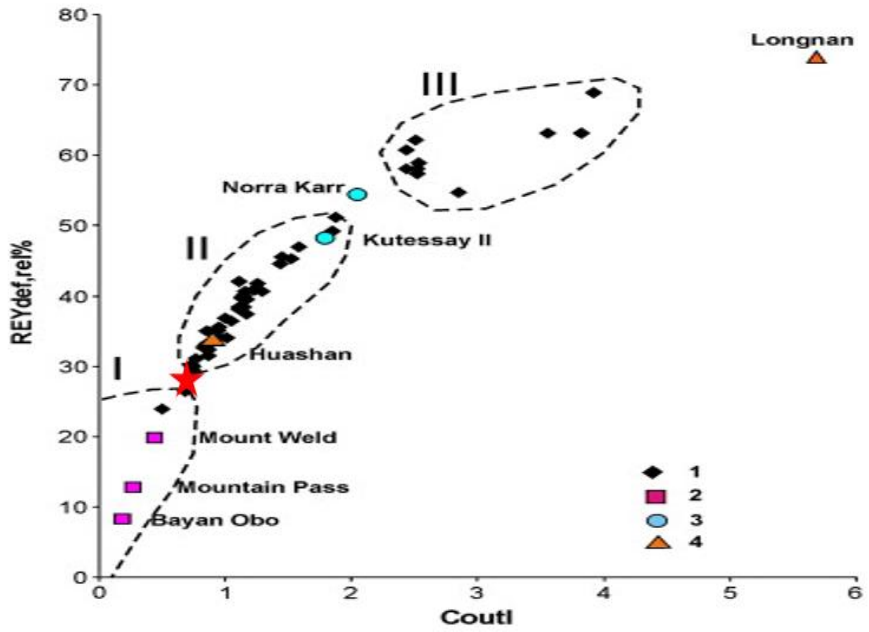


Figure 4-5: Categorisation of the RC1 (representing the ROM coal) (denoted by the **red star**) and DC1 (representing the discard coal) (denoted by the **red star as well, similar position on chart**) by employing the $C_{outlook}$ in conjunction with the $REY_{def,\ rel}$ % (Seredin and Dai, 2012).

RC1 had a $C_{outlook}$ of 0.96 compared to 0.88 of DC1, with a $REY_{def,\ rel}$ % (% CREE) of 27% and 25%, respectively. Both $C_{outlook}$ values are well above that of 0.64 for world coals, as determined by Ketris and Yudovich (2009). This higher $C_{outlook}$ is owed to the high concentrations of CREE, most notably yttrium and neodymium. RC1 and DC1 are positioned on the borderline of category I and II (Figure 4-5). Nevertheless, due to the substantially high

$C_{outlook}$ and exceedingly high concentrations of TREE in these samples, this coal seam may be regarded as a promising source for REE recovery.

Seredin and Dai (2012) proposed a classification of REE into three groups notably HREE (Ho, Er, Tm, Yb, and Lu), MREE (Eu, Gd, Tb, Dy and Y) and LREE (La, Ce, Pr, Nd, and Sm) by employing the ratios of La_n:Lu_n, La_n:Sm_n, Gd_n:Lu_n. These ratios provide REE enrichment anomalies and information on the accumulation of REE during the coal formation stages. The anomalies are deduced based on the REE:UCC normalised values (Figure 4-6) and the ratios of the important REE (La_n:Lu_n, La_n:Sm_n, Gd_n:Lu_n) in each sample. The normalised values achieved for RC1 and DC1 resulted in ratios of La_n:Lu_n > 1, La_n:Sm_n < 1, Gd_n:Lu_n > 1 (Table 4-5), implying that the coals (ROM and discard) from which the samples were obtained are enriched in L-type and M-type distribution due to their high concentration of LREE and MREE (Seredin and Dai, 2012).

Table 4-5: Enrichment patterns and anomalies for individual REE of RC1 and DC1(Seredin and Dai, 2012).

Samples/ REE ratios	La_n:Lu_n	La_n:Sm_n	Gd_n:Lu_n	Ce_n:Ce_n	Eu_n:Eu_n	Gd_n:Gd_n	$REE_{def.\ rel}$ %	Y_n:Ho_n
RC1	2.24	0.96	2.23	1.01	1.00	1.12	27.00	0.94
DC1	3.08	0.99	2.59	1.03	0.89	1.06	25.20	0.85

Subscript $_n$ signifies the REE:UCC normalised values.

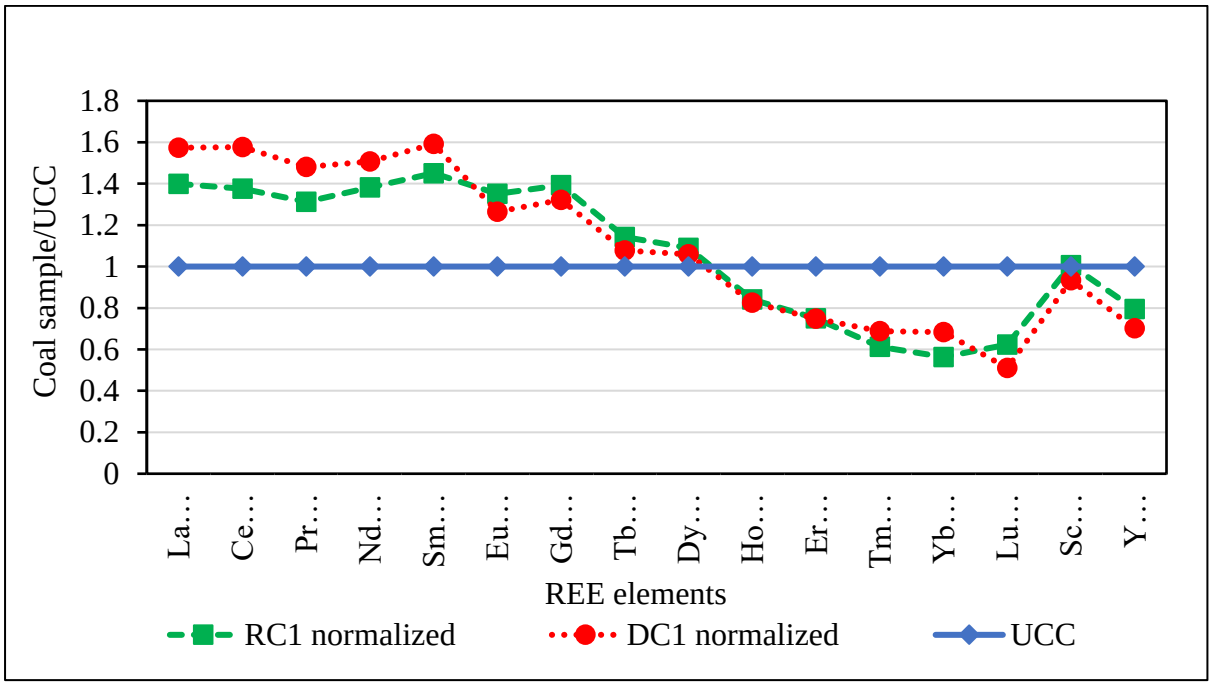


Figure 4-6: Normalised REE:UCC for RC1 and DC1.

4.4 Depositional environment of REE

The ratios presented in Table 4-5 form an integral part of understanding the type of REE deposition environment in the two coal sources. A La_n:Lu_n ratio larger than 2.2 for both RC1 and DC1 depicts coal of terrigenous or tuffaceous origin with REE accumulation occurring at the peat bog stage (Seredin and Dai, 2012). Secondly, due to the low amount of carbonate minerals present in RC1 and DC1, it is proposed that the REE arrived in the peat bog stage with pyroclastic acids enriched in LREE (Seredin and Dai, 2012). The ratios of La_n:$Sm_n < 1$ and Gd_n:$Lu_n > 1$ for RC1 and DC1 (m-type enrichment) manifest a slightly negative europium anomaly (Figure 4-6). This infers that the REE in the two coal sources may be of alkali mafic tuffaceous origin that formed on horizons (Seredin and Dai, 2012). Subsequently, the REE accumulation may have occurred due to hydrothermal (fresh water lakes) acid mixtures or may have occurred due to a higher sorption of MREE by humic matter relative to the LREE and HREE (Faure, 1993; Seredin and Dai, 2012).

It is integral to note that some REE are redox-sensitive such as Ce and Eu, whilst Y, Gd and La are non-redox-sensitive; hence occurrences of these REE may be anomalous or deviating (Dai *et al.*, 2016; Wagner and Matiane, 2018). Therefore, in addition to the above ratios, the ratios Ce_n:Ce_n, Eu_n:Eu_n, Gd_n:Gd_n and Y_n:Ho_n were developed by Dai *et al.* (2016) and applied by Dai *et al.* (2017) and Munir *et al.* (2018). These ratios refer to Eu, Ce, Gd and Y concentration anomalies, separating them from other REE. Equations 4-2, 4-3 and 4-4 were employed to determine the ratios (Ce_n:Ce_n, Eu_n:Eu_n and Gd_n:Gd_n), presented in Table 4-5:

$$Ce_n{:}\,Ce_n = Ce_n/(0.5La_n + 0.5Pr_n) \quad (4\text{-}2)$$

$$Eu_n{:}\,Eu_n = Eu_n/[(Sm_n \times 0.67) + (Tb_n \times 0.33)] \quad (4\text{-}3)$$

$$Gd_n{:}\,Gd_n = Gd_n/[(Sm_n \times 0.33) + (Tb_n \times 0.67)] \quad (4\text{-}4)$$

The Ce_n:Ce_n ratio (Table 4-5) of RC1 and DC1 exhibits a weakly negative anomaly to no significant anomaly (Figure 4-6). Secondly, the Ce_n:Ce_n ratio of approximately 1 (RC1 and DC1) may be due to REE deposition occurring due to an anoxic hydrothermal water environment (Chen *et al.*, 2015; Dai *et al.*, 2016). This further emphasises that the source coals may be of tuffaceous origin (Aubert *et al.*, 2001; Dai *et al.*, 2016). Furthermore, both samples manifested slightly negative Eu anomalies. The Eu_n:Eu_n ratio was 1 and 0.89 for RC1 and DC1,

respectively (Table 4-5). This slight negative anomaly implies that tonsteins are mixed with terrigenous material, and the TREE accumulation may be because of volcanogenic hydrothermal leaching input (Goodarzi *et al.*, 2006; Dai *et al.*, 2016). According to Faure *et al*. (1996), tonstein-rich layers result from the deposition of original volcanic ashes. With both coals containing elevated amounts of kaolinite and tonstein-originated elements, the formation of REE are most likely to have occurred via volcanogenic origin with hydrothermal water inputs, as is further supported by Dai *et al.* (2016).

The Gd_n:Gd_n ratio was between 1.12 and 1.06 for RC1 and DC1, demonstrating a weak positive anomaly (Figure 4-6). This infers that those hydrothermal injections may have been the source for Gd input into the coal strata (Dai *et al.*, 2016). Additionally, the Y_n:Ho_n ratio result represents the decoupling of geochemical twins Y and Ho, with RC1 and DC1 manifesting a ratio between 0.85 and 0.95 (Table 4-5). This, in turn, indicated a weak negative yttrium anomaly for the UCC. Therefore, the ratio indicated that Y accretion might be due to hydro-genetic or volcanogenic hydrothermal injections (Dai *et al.*, 2016). It may be concluded that the REE accumulation within the Waterberg coalfields may have occurred due to volcanogenic hydrothermal water inputs.

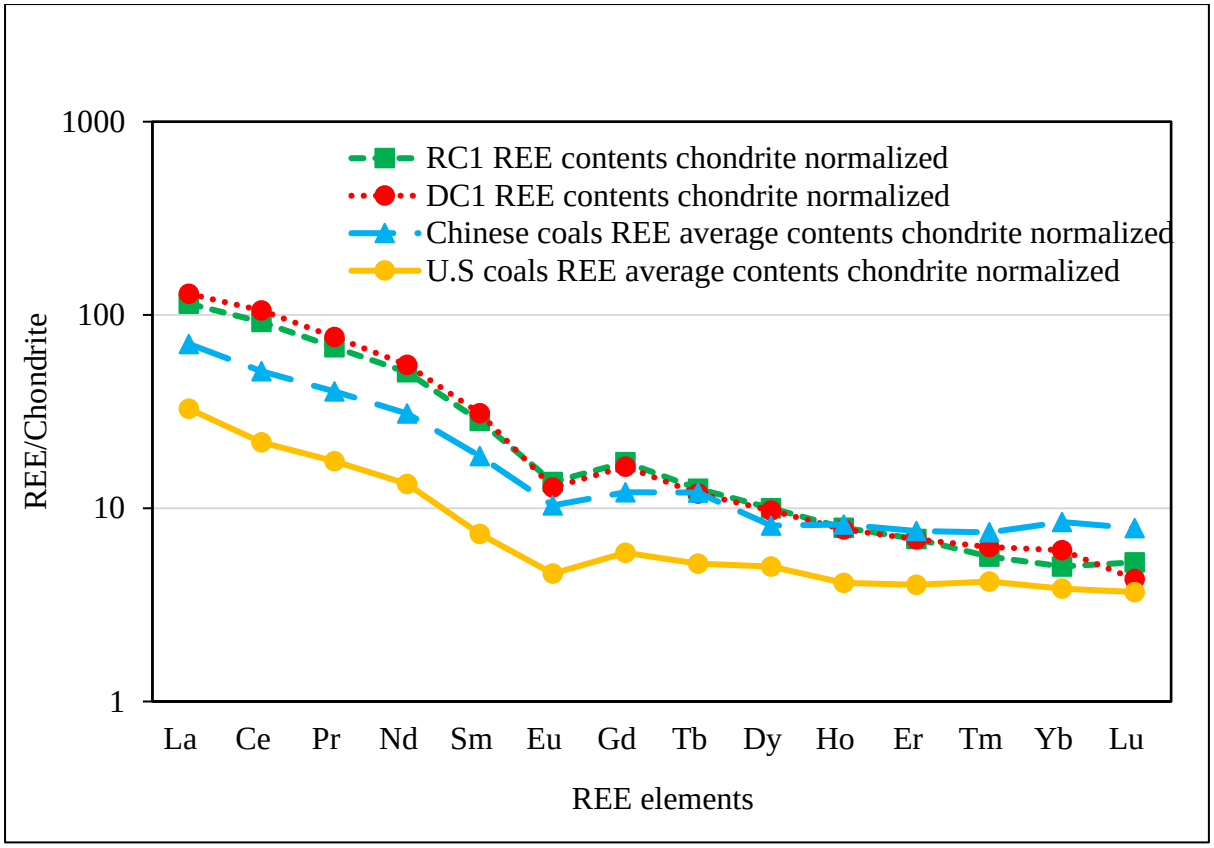


Figure 4-7: REE chondrite (Schmitt *et al.*, 1963) normalised plot for ROM coal (represented by RC1), discard coal (represented by DC1), USA coals (Finkelman, 1993) and Chinese coals (Dai *et al.*, 2008).

The chondrite normalised REE plot (Figure 4-7) depicts that the coal source from which RC1 and DC1 were obtained is significantly more enriched in LREE than the Chinese and USA coals used by Finkelman (1993) and Dai et *al.* (2008), respectively. Additionally, RC1 and DC1 were found to contain larger quantities of HREE relative to the USA coals (Finkelman, 1993) and similar quantities to the Chinese coals (Dai *et al.*, 2008). The comparisons in Figure 4-7 depict slightly weak negative Eu anomalies, further implying that REE accumulation in the RC1 and DC1 coal source was from hydrothermal water acid inputs.

The dominant minerals in the USA coals, according to Finkelman (1993), were typically quartz, with lesser amounts of illite, clay minerals, zircon and monazite. The coal samples used in this study were significantly enriched in kaolinite (clay minerals), in which elevated quantities of LREE reside. Correspondingly, the chondrite normalised REE plots for aluminosilicate (similar to kaolinite minerals) fly ashes were also represented by negative Eu anomalies correlating to the high LREE contents, as described by Kolker *et al.* (2017). A recent study by Baioumy *et al.* (2021) on kaolin ore also exhibited a partially negative Eu anomaly,

owing to an elevated concentration of LREE. Thus, these negative Eu anomalies observed in RC1 and DC1 confirms the elevated amounts of LREE. More so, the normalised REE chondrite plot is more granitic than basaltic, as indicated by Faure *et al.* (1996). This further emphasises that the REE in the ROM and discard coals reside largely within the clay minerals.

4.5 Hydrometallurgical treatment of RC1 and DC1 for REE recovery

4.5.1 Particle size distribution of samples used in the leaching tests

The size fraction of - 106 µm, as recommended by an anomaly deduced from Zhang and Honaker (2020), obtained from pulverisation of RC1 and DC1 were used for the leaching tests. Both samples were analysed using a Malvern Mastersizer 2000 with the Hydro 2000MU dispersion. REE recovery during acid leaching is significantly higher when employing a particle size of < 40 µm, and the cost of milling to this fine size can render a leaching process non-feasible (Jordens *et al.*, 2013). However, using a particle size of - 106 µm reduces the milling cost and may reduce the REE recovery. With calcination of this size fraction prior to leaching, REE recovery is expected to increase. RC1 manifested a 91% passing - 106 µm, DC1 achieved a 94% passing - 106 µm size fraction (Figure 4-8).

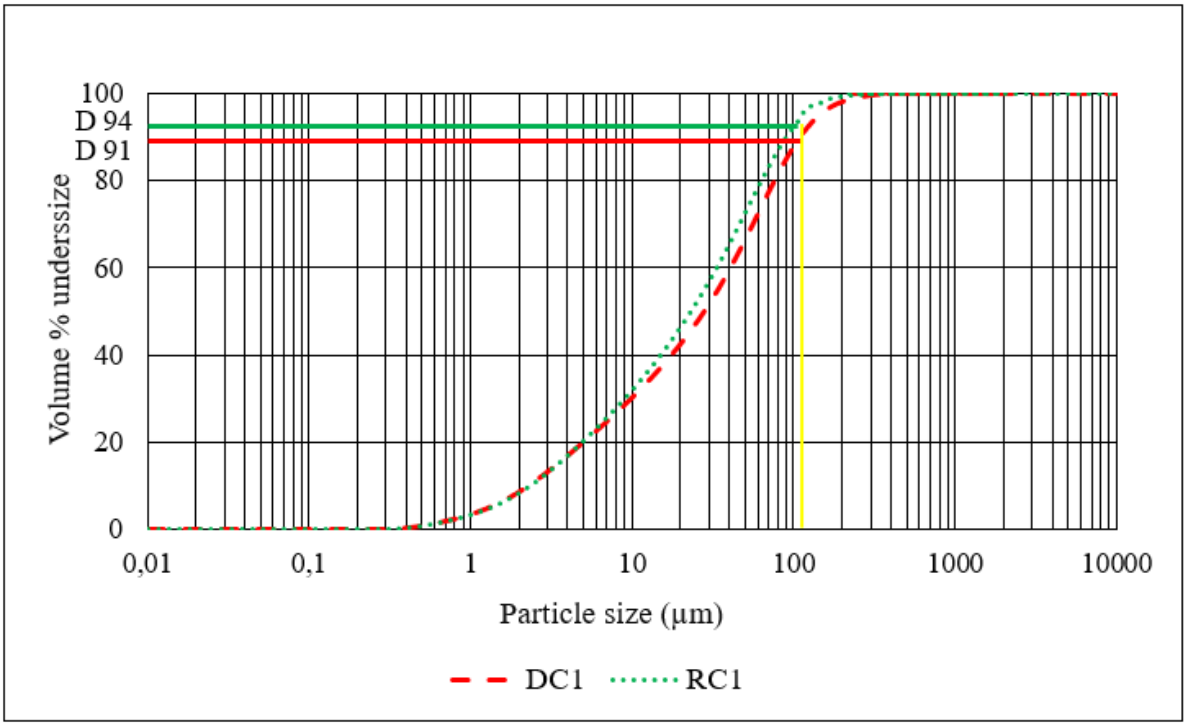


Figure 4-8: PSD analysis curve for RC1 and DC1.

4.5.2 Part 1 and stage 1 of the leaching results from non-calcined RC1 and DC1

RC1 and DC1 were subjected to 15 leaching runs each (30 runs in total) as per Tables 3-1 and 3-2. Three leaching factors generated using DOE were varied simultaneously in the 15 runs. The HCl concentration was varied between 0.5 M and 2 M, the temperature between 30 ^{o}C and 50 ^{o}C, and the solid:liquid ratio from 10 g/l to 40 g/l. The simultaneous variations in concentration, temperature and solid:liquid ratio enabled DOE to produce optimal leaching conditions. The percentage REE recovery per time as observed for the 15 lixiviate experimental runs on RC1 and DC1 are shown in Figure 4-9.

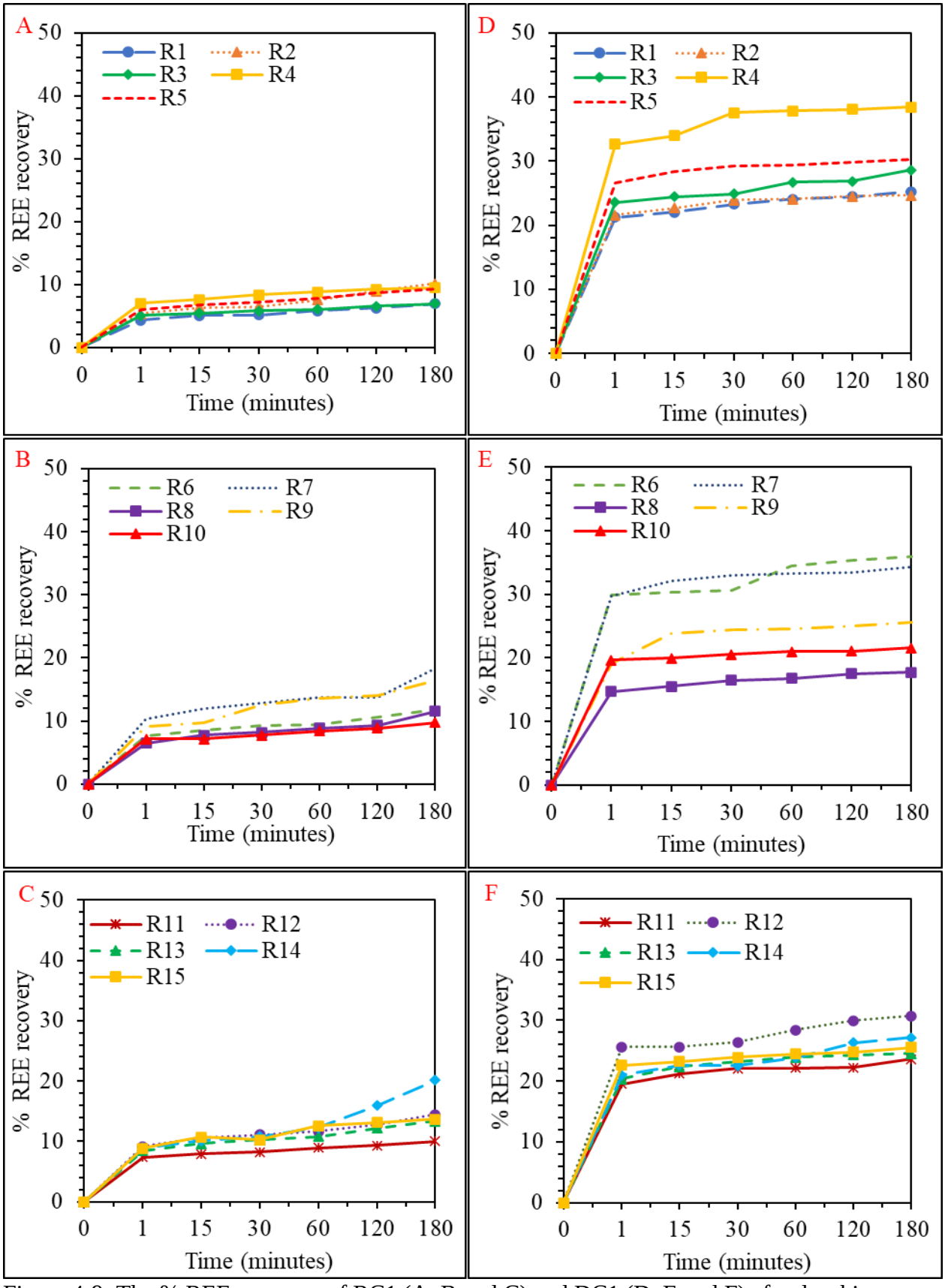


Figure 4-9: The % REE recovery of RC1 (A, B and C) and DC1 (D, E and F) after leaching.

R14 (REE recovery 21%), R7 (REE recovery 18.4%) and R9 (REE recovery 16.4%) reflected a promising REE recovery potential for RC1 (Figure 4-9 A to C). It was observed that the REE recovery occurs instantaneously at one min and, thereafter, gradually increases minimally until the end of the test (Figure 4-9 A to C). There was an increase in the percentage REE recovery for R7 and R9 between 120 and 180 minutes (Figure 4-9B). Furthermore, R14 had the highest REE recovery of 21%, followed by R7 (18.4%) and R9 (16.4%) from the 15 DOE runs carried out on RC1 (Figure 4-9 A to C). The high recovery noted for these three runs is because of the higher concentration (≥ 1.25 M) and high leaching temperature (> 40 ^{o}C) in which the leaching test was conducted.

The results from the 15 leaching runs carried out on DC1 are presented in Figure 4-9 D to F. At leaching run R4, R6 and R7, an overall percentage REE recovery of 38.4%, 35.9%, and 34.3%, was achieved respectively (Figure 4-9 D to F). These runs were operated at a low solid:liquid ratio (> 25 g/l), high leaching temperature (> 40 ^{o}C) and concentration ≥ 1.25 M. The maximum REE recovery from DC1 was higher than that from RC1. This was similar to the result obtained by Yang *et al.* (2019) where 50% REE was recovered from a coal middling.

The lower REE recovery noted in RC1 (higher carbon content) could be due to its interaction with HCl, leading to an induced chemical activation of the carbon molecules. With this interaction, the porosity of the carbon fraction could be increased (Toledo *et al*., 2020), leading to more reactive re-adsorption sites for REE (Budi *et al*., 2016). The increase in the REE leaching efficiency of the discard coal, based on the DC1 results, might be because of its lower physical carbon encapsulated REE-bearing minerals (Laudal *et al*., 2018). Consequently, allowing for more interaction between the REE-bearing minerals and the leachate, leading to a higher REE recovery. This trend corresponds with the observation made by Kim *et al.* (2016), Chen *et al.* (2020) and Yang and Honaker (2020).

4.5.3 Leaching mechanisms of the REE-bearing minerals

From the TIMA modal liberation, image analysis (Figure 4-3 and Table 4-2) and the XRD analysis (Figure 4-2), it is evident that kaolinite, pyrite/hematite, apatite, lesser amounts of xenotime and monazite were present in the coal samples. The above-mentioned minerals are the minerals that are associated with REE (Yang, 2019). For leaching of coals with HCl, the following reactions occur, as indicated in Equations 4-5 through to 4-11. The REE of the REE-bearing minerals move into the acidic solution. The REE cations form a complex with the

chlorine anions as outlined in reactions 4-5 to 4-11. The leaching reaction between REE from apatite (contained in the coal) and HCl result in soluble calcium phosphates, calcium chloride and soluble REE-bearing chlorides, as outlined in reactions 4-5 and 4-6 (Kim *et al.*, 2016; Soltani *et al.*, 2017). Pyrite, which was shown to associate with REE (Figure 4-3), does not completely dissociate under the mild acidic leaching condition (Kanungo, 1999). The incomplete dissolution reaction that may occur between pyrite associated REE and HCl is represented by Equations 4-7 and 4-8.

Numerous studies have indicated that REE are associated with monazite and xenotime minerals (Jordens *et al.*, 2013; Mudd and Jowitt, 2016; Guo *et al.*, 2018). According to Figure 4-2, the XRD analysis shows a minor amount of xenotime and monazite in RC1 and DC1. The reaction between HCl and monazite, as well as xenotime (Vijayalakshmi *et al.*, 2001; Amine *et al.*, 2019), is shown in Equation 4-11. Monazite and xenotime are known not to digest at very low leaching temperatures (Jordens *et al.*, 2013). However, at leaching temperatures above 50 ^{o}C, these minerals begin to dissolve, increasing the recovery of REE at higher leachate temperatures. This was demonstrated by the high percentage of REE achieved by R7 from both coal samples (Figure 4-9).

The leaching of REE-bearing zircon with HCl is almost impossible at a low acid concentration of 2 M as used in this study. The leaching of this mineral will require smelting and aggressive leaching conditions to solubilise the mineral (Blumenthal, 1973). Kaolinite, subjected to HCl leaching, does not completely dissociate under the mild acidic conditions of 2 M and 75^{o}C (Colina *et al.*, 2013). However, due to the fine liberation of - 106 µm, the surface area of the kaolinite increases (Laudal, 2017). Subsequently, the weakly ion-adsorbed REE are exposed and may detach from the clay mineral surface and, thereafter, form REE-bearing chloride bonds in an aqueous solution (Laudal, 2017; Kuppusamy *et al.*, 2019). Hence, not all the REE from the kaolinite minerals were released, albeit a fraction of REE on the surfaces of kaolinite were released according to Equations 4-9 and 4-10. Thus, illustrating the reason for the low REE obtained from the raw RC1 and DC1, as both coal samples were dominated by REE dispersed in the kaolinite matrices (Figures 4-9 and 4-3).

$$Ca(PO_4)_{2(s)} + 2HCl_{(aq)} \rightarrow 2CaCl_{2(aq)} + CaH_4(PO_4)_{2(aq)} \quad (4\text{-}5)$$

$$REE(PO_4)_{(s)} + 3HCl_{(aq)} \rightarrow REECl_{3(aq)} + H_3PO_{4(aq)} \quad (4\text{-}6)$$

$$FeS_{2(s)} + 2HCl_{(aq)} \rightarrow FeCl_{2(aq)} + 2HS_{(aq)} \quad (4\text{-}7)$$

$$REES_{3(s)} + 3HCl_{(aq)} \rightarrow REECl_{3(aq)} + 3HS_{(aq)} \quad (4\text{-}8)$$

$$(Al_2Si_2O_5(OH)_4)_{(s)} + 6HCl_{(aq)} \rightarrow 2AlCl_{3(aq)} + Si_2O_5(OH)_4.6H_{(aq)} \quad (4\text{-}9)$$

$$(REE_2Si_2O_5(OH)_4)_{(s)} + 6HCl_{(aq)} \rightarrow 2REECl_{3(aq)} + Si_2O_5(OH)_4.6H_{(aq)} \quad (4\text{-}10)$$

$$REE(PO_4)_{(s)} + 3HCl_{(aq)} \rightarrow REECl_{3(aq)} + H_3PO_{4(aq)} \quad (4\text{-}11)$$

4.6 Experimental design and statistical analysis results from DOE

This section outlines the results obtained from the REE leaching recovery after using the experimental Box-Behnken design on DOE. The results attained were displayed via the RSM. The RSM gathers mathematical, experimental and statistical data to model hydrometallurgical engineering problems (Alaoui *et al.*, 2015). This approach was applied to analyse the effect of the independent variables (HCl concentration, solid:liquid ratio and leaching temperature) on the response (% REE recovery). The analysis of variance (ANOVA) was used to verify and determine the significance and suitability (Abdulsalam *et al.*, 2019) of the three leaching factors. A linear model was developed by DOE to determine the impact of the relationships between the three factors and their direct effect on the percentage REE recovery. The desirability function was employed to deduce the optimal leaching parameters for increasing REE recovery from ROM coal (based on RC1 results) and discard coal (based on DC1 results).

4.6.1 Optimisation of the REE leaching recovery from DC1 and RC1

The actual experimental responses (Figure 4-9) and predicted responses of the REE recovered with respect to the simultaneous variation of the three leaching factors are displayed in Tables 4-6 (RC1) and 4-7 (DC1). The % REE leaching recovery after three hours was recorded in DOE to create a confined area for the RSM and to develop empirical equations (Teimouri, 2020). The development of the Empirical Equations 4-12 to 4-15 (Section 4.6.1.2) provided the predicted % of REE recovery.

The combined effect of the acid concentration, solid: liquid ratio and lixiviate temperature on the % REE recovery are presented in Table 4-6 and 4-7 for RC1 and DC1, respectively. It was observed that the REE recovery improved with an increase in temperature and HCl concentration. This is consistent with a study conducted by Yang (2019) which demonstrated an increase in REE recovery due to an increase in acid concentration and temperature. Furthermore, DC1 had a higher % REE recovery relative to RC1. This was attributed to the fact that the discard coal minerals are less encapsulated by the carbon matrices allowing for increased interactions between the REE-bearing minerals and the leachate (Laudal, 2017). In

the case of RC1, which was richer in carbon, the REE recovery was very low, and this might be due to the presence of carbon encapsulated REE-bearing minerals in the sample.

Table 4-6: Experimental vs predicted % REE leaching recovery from RC1.

Run	Factor 1 A: HCl concentration (M)	Factor 2 B: S:L (g/l)	Factor 3 C: Temperature (ºC)	Experimental REE recovery %	Predicted REE recovery %
1	0.5	25	30	6.92	6.71
2	1.25	40	50	10.1	13.78
3	1.25	40	30	6.91	6.87
4	1.25	10	30	8.59	10.12
5	1.25	25	40	7.18	11.95
6	0.5	10	40	11.84	11.79
7	1.25	25	40	18.34	11.95
8	2	40	40	11.56	12.11
9	1.25	10	50	16.46	17.03
10	0.5	40	40	9.76	8.54
11	2	25	30	9.99	10.28
12	2	10	40	14.44	15.36
13	0.5	25	50	13.33	13.62
14	2	25	50	20.16	17.19
15	1.25	25	40	13.66	11.95

S:L: solid:liquid ratio

Table 4-7: Experimental vs predicted % REE leaching recovery from DC1.

Run	Factor 1 A: HCl Concentration (M)	Factor 2 B: S/L (g/l)	Factor 3 C: Temperature (ºC)	Experimental REE recovery %	Predicted REE recovery %
1	0.5	25	30	24.55	25.99
2	1.25	40	50	32.10	30.44
3	1.25	40	30	26.43	23.93
4	1.25	10	30	34.32	32.49
5	1.25	25	40	30.32	31.47
6	0.5	10	40	35.24	33.52
7	1.25	25	40	34.33	31.47
8	2	40	40	28.39	29.41
9	1.25	10	50	38.32	39.00
10	0.5	40	40	24.31	24.96
11	2	25	30	28.14	30.44
12	2	10	40	37.23	37.97
13	0.5	25	50	30.39	32.50
14	2	25	50	38.59	36.95
15	1.25	25	40	32.04	31.47

S:L: solid:liquid ratio

4.6.1.1 Suitability and adequacy of the model (ANOVA)

The appropriateness of the linear fitted model (Equations 4-14 and 4-15) was studied by analysing the results of the ANOVA and fit summary presented in Tables 4-8 and 4-9. The model's suitability was assessed on DOE by the F-value, P-value (ANOVA) and R^2 values (Table 4-8 and 4-9). The significance of the linear model was examined using the probability (P-value) (Abdulsalam, 2019). The P-value indicates whether the model terms (concentration, solid:liquid ratio and temperature) are significant or not significant in terms of their influence on the REE leaching recovery (Amine *et al.*, 2019). A P-value < 0.0500 illustrates the model terms are significant, whilst values > 0.1000 displays the model terms as insignificant (Kraber, 2013; Whitcomb, 2018). The three leaching factors of A for HCl concentration, B for solid:liquid ratio and C for temperature were significant in the linear models for both coal samples (Equations 4-14 and 4-15), as presented in Table 4-8 and 4-9, since A, B and C had a P-value of 0.0453, 0.0261 and 0.0066, respectively for RC1 (Table 4-8). A, B and C reflected P-values of 0.009, 0.0001 and 0.0007 (Table 4-9) for DC1, respectively. Correspondingly, the linear models (Equation 4-14 and 4-15) were derived from DOE to predict the % REE leaching recovery. The model exhibited a P-value of 0.0147 and 0.0001 for RC1 and DC1. Consequently, the linear model for the % REE recovery and their factors are significant and suitable for the experimental data (Abdulsalam, 2019).

The F-value of 22.81 (DC1) and 5.52 (RC1) indicates that the linear model is significant, with only a 0.01% (DC1) and 1.47% (RC1) chance that an F-value this large could have occurred due to noise (Kraber, 2013; Alaoui *et al.*, 2015; Ji and Zhang, 2021). The P-value and F-value for the "lack of fit" RC1 coal was 0.99 and 0.11, respectively, whilst DC1 had a P-value and F-value of 0.9714 and 0.6043. Hence, this indicated an insignificant lack of fit (Teimouri, 2020). An insignificant lack of fit is essential and important for a linear model which fits experimental data (Teimouri, 2020).

Table 4-8: ANOVA table of the % REE recovery for RC1 with respect to the various leaching factors.

Source	Sum of Squares	df	Mean Square	F-value	P-value	Remark
Model (% REE recovery)	142.18	3	47.39	5.52	0.0147	Significant
A-Concentration	25.56	1	25.56	2.98	0.0453	Significant
B-Solid:liquid ratio	21.13	1	21.13	2.46	0.0261	Significant
C-Temperature	95.50	1	95.50	11.13	0.0066	Significant
Residual	94.39	11	8.58			
Lack of Fit	31.58	9	3.51	0.11	0.9928	Not Significant
Pure Error	62.81	2	31.41			
Cor Total	236.57	14				
R^2	0.8910					
Adjusted R^2	0.8822					
Predicted R^2	0.8749					
Adequate Precision	6.9313					

Table 4-9: ANOVA table of the % REE recovery for DC1 with respect to the various leaching factors.

Source	Sum of Squares	df	Mean Square	F-value	P-value	Remark
Model (% REE recovery)	270.95	3	90.32	22.81	0.0001	Significant
A-Concentration	39.60	1	39.60	10.00	0.0090	Significant
B-Solid:liquid ratio	146.57	1	146.57	37.02	0.0001	Significant
C-Temperature	84.77	1	84.77	21.41	0.0007	Significant
Residual	43.56	11	3.96			
Lack of Fit	35.45	9	3.94	0.97	0.6043	Not significant
Pure Error	8.11	2	4.05			
Cor Total	314.50	14				
R^2	0.9133					
Adjusted R^2	0.8937					
Predicted R^2	0.8744					
Adequate Precision	14.6668					

The fit summary factors (R^2, Adjusted R^2, Predicted R^2, Adequate Precision) for RC1 and DC1 are presented in Table 4-8 and 4-9, respectively. The R^2 value for the RC1 and DC1 linear models of % REE recovery are 0.8910 and 0.9133, respectively. This confirms a very good linear equation model (Equation 4-14 and 4-15) (Kraber, 2013; Abdulsalam *et al.*, 2019). The Adjusted R^2 of 0.88 (RC1) and 0.89 (DC1) are within a satisfactory range with the predicted R^2 values of 0.87 (RC1) and 0.87 (DC1). The difference between the adjusted and predicted R^2

values are less than 0.02 for both samples and are within a reasonable agreement limit (Kraber, 2013; Abdulsalam, 2019). The "Adequate Precision" is a value used for the measurement of the signal to noise ratio. A ratio greater than four is desirable for the model to navigate within the design space (Kraber, 2013). Hence, the "Adequate Precision" values of 6.93 (RC1) and 14.67 (DC1) show that the model attained is satisfactory and suitable for predicting the % REE recovery.

Table 4-6 and 4-7 further indicated the closeness of the experimental and predicted % REE leaching recovery. The relative similarities between the data further verifies the model's suitability (Abdulsalam, 2019; Teimouri, 2020) of the model. The predicted % REE leaching recovery is based on the actual linear model equations as discussed in Section 4.6.1.2.

4.6.1.2 Linear model equations for predicting % REE leaching recovery

The real linear model represented by Equations 4-14 and 4-15 contributed to creating various response surfaces in the design space to predict the % REE leaching recovery for both coal samples. DOE used equations 4-14 and 4-15 to provide the predicted % REE recovery displayed in Table 4-6 and 4-7. A coded and actual equation was deduced from DOE for a confined design space (Equations 4-12 to 4-15) (Teimouri, 2020). The Coded Equations (Equations 4-12 and 4-13) were used to indicate which leaching coefficient factors, A (HCl concentration), B (solid:liquid ratio) or C (leaching temperature), have the greatest impact on % REE leaching recovery (Kraber, 2013). A coefficient factor with a high impact has a coefficient > 1, whilst a low impact factor is reflected by < 1 (Kraber, 2013). The order of impact of each factor on the % REE recovery was derived from the coefficients of the Coded Equations (Equations 4-12 and 4-13) (Teimouri, 2020). The leaching temperature (C) had the highest impact, followed by factors A, then B (Equations 4-12 and 4-13). This is similar with the REE leachate study conducted by Ji and Zhang (2021) who also noted that the leaching temperature has the greatest effect on REE recovery.

Coded Equations:

$$\%\ \text{REE leaching recovery (RC1)} = 11.95 + 1.79A - 1.63B + 3.46C \quad (4\text{-}12)$$

$$\%\ \text{REE leaching recovery (DC1)} = 31.47 + 2.22A - 4.28B + 3.26C \quad (4\text{-}13)$$

Actual Equations:

$$\%\ \text{REE leaching recovery (RC1)} = -2.14 + 2.38A - 1.08B + 0.35C \quad (4\text{-}14)$$

$$\%\ \text{REE leaching recovery (DC1)} = 21.87 + 2.97A - 0.28B + 0.33C \quad (4\text{-}15)$$

The normal probability plots for residuals of the % REE leaching recovery for RC1 and DC1 are depicted in Figures 4-10 A and B, respectively. The data points on these plots are on the straight line, whilst some data points are a in close proximity to the straight line. Thus, the residuals, deviations of the predicted % REE recovery values from the observed experimental values, follow a normal distribution pattern (Figure 4-10, A and B). Hence, confirming the suitability and validity of the model.

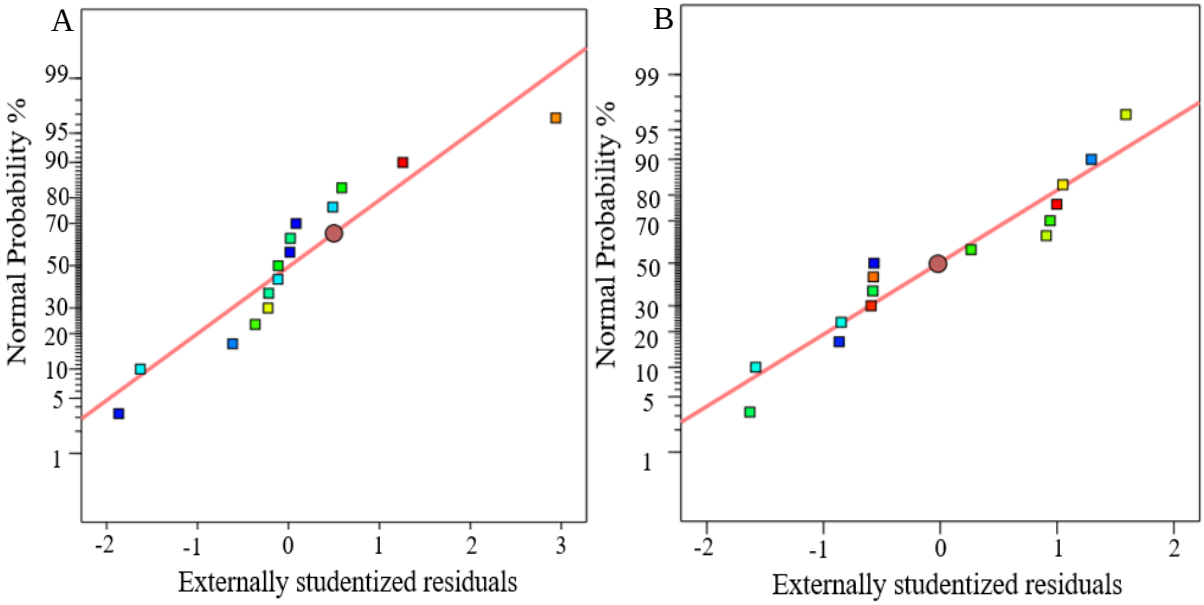


Figure 4-10: Normal probability plots of the % REE leaching recovery for RC1 (A) and DC1 (B).

Figures 4-11 A and B are the plots of residuals vs the predicted % REE leaching recovery from RC1 and DC1. The two plots indicate the verification and validity of the ANOVA analysis assumptions. Since all the data points for both coal samples are within a certain expected limit and do not deviate from 3.8 (Figure 4-11 A and B), confirming the suitability of the Model Equations 4-14 and 4-15.

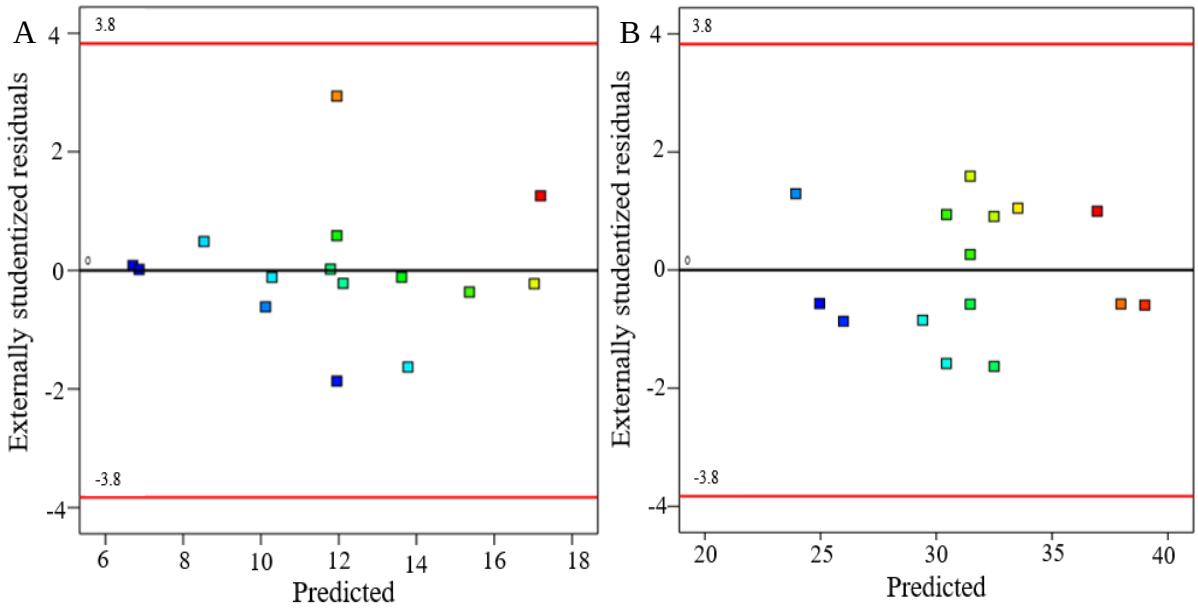


Figure 4-11: Residuals vs predicted plot for % REE leaching recovery for RC1 (A) and DC1 (B).

Figure 4-12 A and B were plotted using the experimental % REE leaching recovery (actual/observed) values and the predicted % REE leaching recovery values for RC1 and DC1 (Table 4-6 and 4-7). The experimental % REE leaching recovery values do not deviate or fluctuate vastly from the predicted % REE leaching recovery values because all data points are as close as expected to the straight line (Abdulsalam, 2019). The outlier for RC1 (Figure 4-12 A) could be caused by experimental errors. There were no significant outliers in DC1, as illustrated in Figure 4-12 B. However, the adjusted R^2 values of 0.8822 and 0.8937 for RC1 and DC1 indicate that the model is significant as the values are close to 1 (Kraber, 2013). Figures 4-12 A and B clearly indicated that the model fits well with the experimental data. Therefore, confirming the validity of the model (Equations 4-14 (RC1) and 4-15 (DC1)) as the data points were positioned as expected.

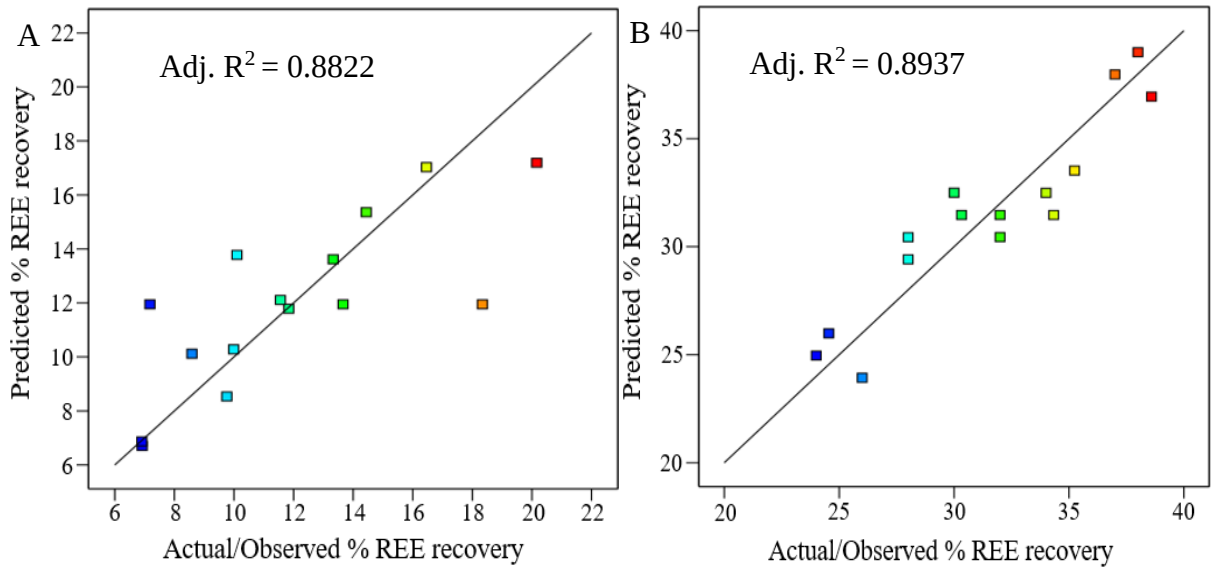


Figure 4-12: Linear regression plots for the predicted vs actual % of REE leaching recovery for RC1 (A) and DC1 (B).

4.6.1.3 Response plots for determining the effect of HCl concentration on the % REE leaching recovery

The effect of HCl concentration on the % REE leaching recovery was examined at 0.5 M, 1.25 M and 2 M. It must be noted that the solid:liquid ratio and temperature were also varied simultaneously. However, to investigate the effect of the single factor A (HCl concentration), the solid:liquid ratio and temperature were kept constant (10 g/l and 50 ^{o}C) whilst the stirring speed at 530 rpm was constant throughout the experiments. The effect of the single factor A (HCl concentration) indicated that % REE leaching recovery increased from 15.3% at 0.5 M to 18.8% at 2 M for RC1 (Figure 4-13 A). For DC1, the % REE leaching recovery increased from 36% to 41% (Figure 4-13 B) under the same conditions. Furthermore, at a higher acid concentration, there is an increase in hydronium ions in solution, leading to a decrease in the pH to almost zero (Bandara and Senanayake, 2015; Yang, 2019). At low pH values, REE form cations that are easily dissolved in the lixiviate solutions by attaching to the chlorine anions (Bandara and Senanayake, 2015). For both coal samples, an increase in concentration increased the % REE leaching recovery. Several investigations have also confirmed that the REE recovery increases with increased acid concentration (Laudal *et al.*, 2018; Yang, 2019; Yang *et al.*, 2019; Ji and Zhang, 2021). The two graphs were found to be in the 95% confidence range (Figure 4-13 A and B).

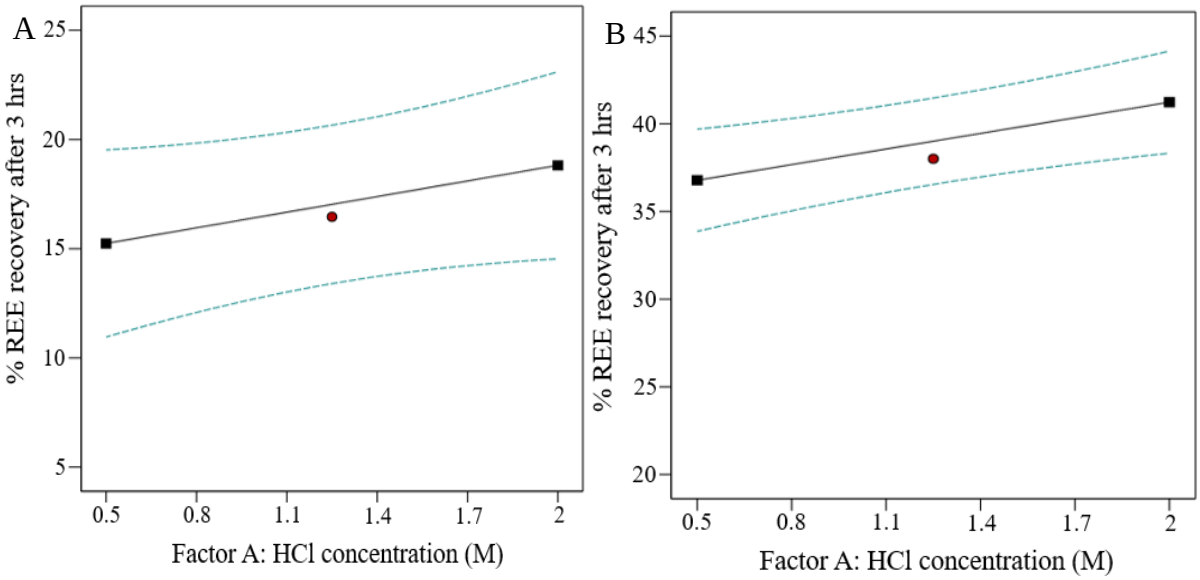


Figure 4-13: % REE leaching recovery vs HCl concentration for RC1 (A) and DC1 (B).

4.6.1.4 Response plots for determining the effect of solid:liquid ratio on the % REE leaching recovery

The effect of solid:liquid ratio (pulp density), ranging from 10 g/l to 40 g/l, on the % REE leaching recovery was assessed. The leaching temperature and HCl concentration were maintained at 50 ^{o}C and 2 M. The % REE leaching recovery increased from 32% at 40 g/l to 41% at 10 g/l for DC1. Thus, % REE leaching recovery is inversely proportional to the solid:liquid ratio (Figure 4-14 B). The % REE leaching recovery for RC1 was 15.5% at an elevated solid:liquid ratio of 40 g/l, whilst at a low ratio of 10 g/l, the % REE leaching recovery increased to 18.8% (Figure 4-14 A). Therefore, it can be deduced that the % REE leaching recovery is improved when the solid:liquid ratio is reduced to 10 g/l. This concurs with other studies on coal and REE-bearing minerals showing that the % REE leaching recovery increases with a decrease in solid:liquid ratio (Yang, 2019; Ji and Zhang, 2021). However, in a study conducted by Li *et al.* (2013) on bastnaesite, the % REE leaching recovery increased when the liquid to solid ratio increased. In addition, a recent study conducted by Amine *et al.* (2019) showed an increase in % REE leaching recovery to 43% for a phosphate-based REE ore when the solid:liquid ratio was increased. Seemingly, the optimal pulp density for REE recovery may vary from source to source and for different coals.

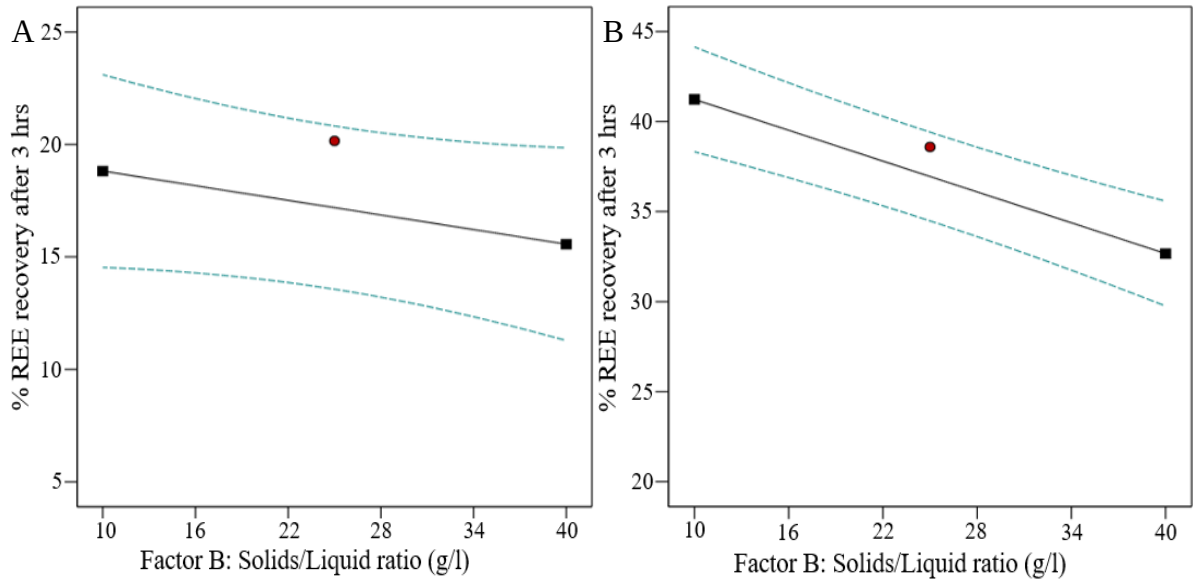


Figure 4-14: % REE recovery leaching vs solid:liquid ratio for RC1 (A) and DC1 (B).

4.6.1.5 Response plots for determining the effect of leaching temperature on the % REE leaching recovery

The effect of the leachate temperature on % REE leaching recovery was examined at leaching temperatures in the range of 30 ^{o}C to 50 ^{o}C using DOE whilst the acid concentration and pulp density were maintained at 2 M and 10 g/l. The % REE leaching recovery improved from 34% at 30 ^{o}C to a maximum of 41% at 50 ^{o}C for DC1 (Figure 4-15 B). Likewise, RC1 showed an increase in % REE leaching recovery from 12% at 30 ^{o}C to 18.9% at 50 ^{o}C (Figure 4-15 A). Hence, the % REE leaching recovery is directly proportional to the leaching temperature. According to Ji and Zhang (2021), REE associated with kaolinite typically require increased temperatures to be released from their hydroxyl bonding with kaolinite. In other words, an increase in leaching temperature promotes the partial dissolution or solubility of kaolinite and release of REE, therefore increasing REE recovery. REE recovery is temperature-sensitive, with several studies indicating the % REE recovery increases with an increase in leaching temperature (Li *et al.*, 2013; Amine *et al.*, 2019; Yang, 2019; Ji and Zhang, 2021). Almost all the REE in this coal seam are found within the REE-bearing minerals such as pyrite, magnetite, monazite, xenotime and kaolinite (Figure 4-2 and 4-3).

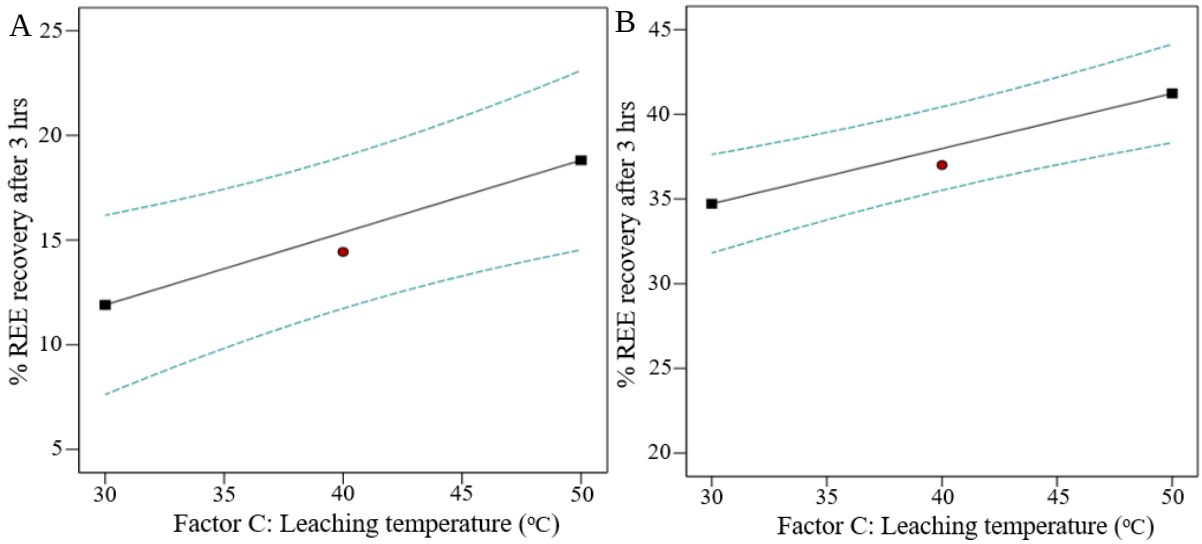


Figure 4-15: % REE leaching recovery vs leaching temperature for RC1 (A) and DC1 (B).

4.6.1.6 Response surface methodology plots for the interactions between the leaching factors and the % REE leaching recovery

The interactions between HCl concentration (factor A), solid:liquid ratio (factor B) and leaching temperature (factor C) were studied to understand the simultaneous relationships between them. The present investigation has established the influence of these factors on the percentage of REE leaching recovery. This was performed by engaging the RSM on DOE to attain 3D response surfaces and 2D contour plots. Figure 4-16 A and B represent the % REE leaching recovery with respect to changes in HCl concentration (0.5 M to 2 M), varying leaching temperatures (30 ^{o}C to 50 ^{o}C) and at a constant solid:liquid ratio of 10 g/l. The lines on the contour plots (Figure 4-16 A and B) indicate % REE leaching recovery after three hours with respect to a change in temperature and HCl concentration. Optimal and best conditions are indicated in the dark red converging area representing the highest % REE leaching recovery (Teimouri, 2020). Therefore, a HCl concentration of 2 M, 50 ^{o}C and a low pulp density (10 g/l) are noted as the best operating parameters to enhance REE recovery. It is apparent that the % REE leaching recovery was above 40% for DC1, whilst it was 18% for RC1 (Figure 4-16 A and B), signified by the red shaded region.

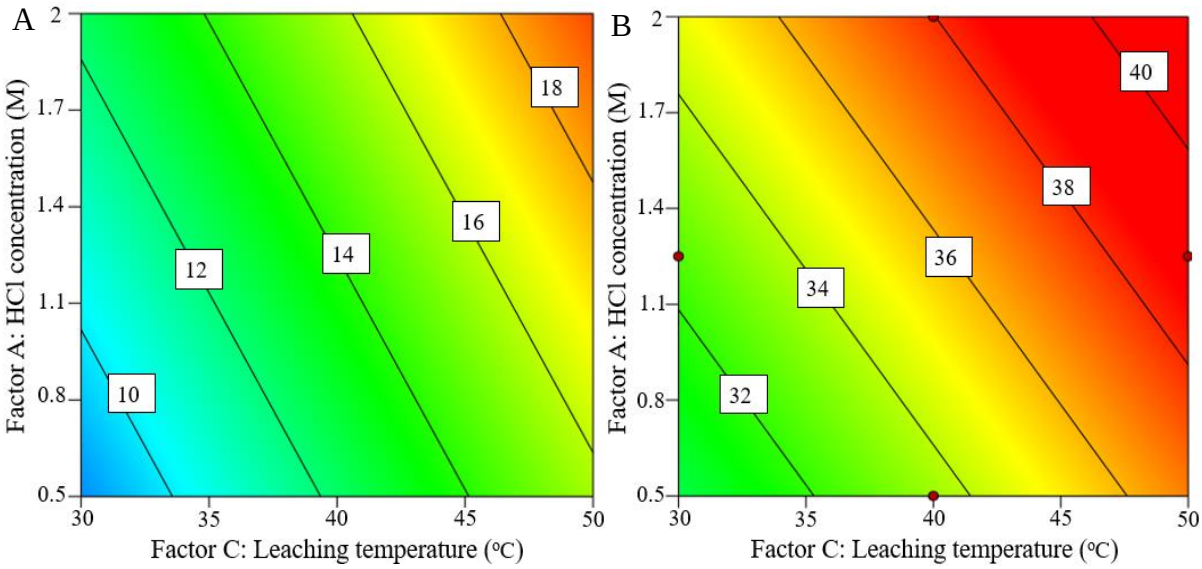


Figure 4-16: Contour plots for the relationship between HCl concentration and leaching temperature with respect to % REE leaching recovery for RC1 (A) and DC1 (B).

The RSM 3D plots for RC1 and DC1 (Figure 4-17 A and B) were designed based on the Actual Equations of 4-14 and 4-15 for the % REE leaching recovery. The % REE leaching recovery improved with an increased temperature and HCl concentration (Figure 4-17 A and B), as highlighted by the contour plots (Figure 4-16). Several studies have also shown that the REE recovery increases with increased temperature and acid concentration (Li *et al.*, 2013; Amine *et al.*, 2019; Yang, 2019; Ji and Zhang, 2021). The 3D plots assisted in visualising the best simultaneous temperature and acid concentration conditions required to increase REE recovery. For both coal samples (RC1 and DC1), it is evident that REE recovery was at its maximum at 2 M HCl and 50 ^{o}C (Figure 4-17 A and B).

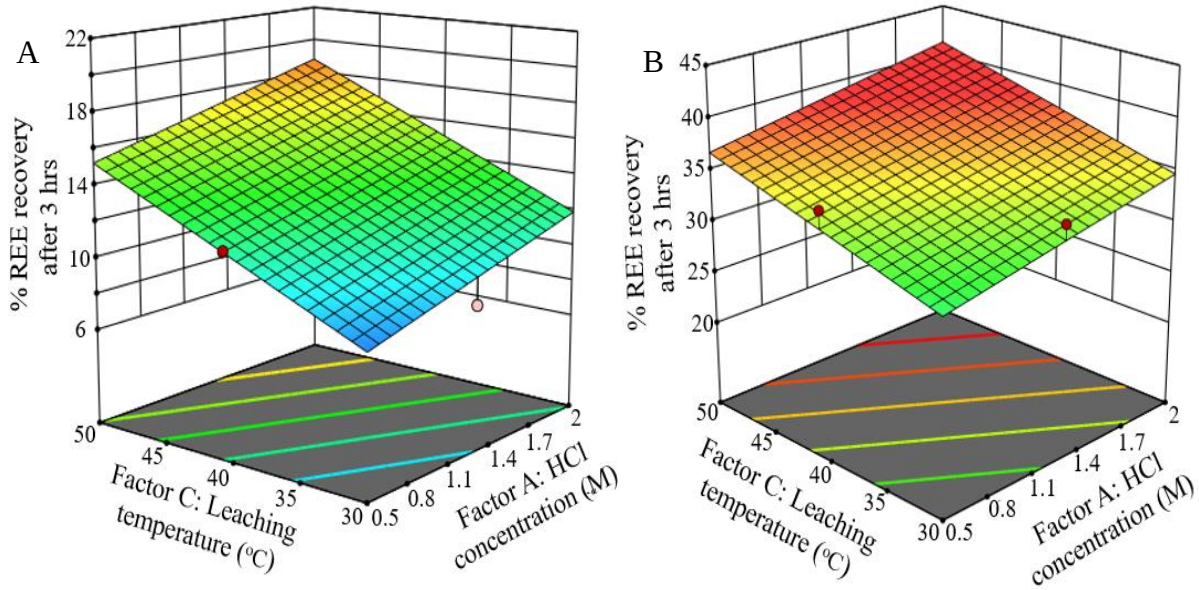


Figure 4-17: 3D surface plots of the relationship between temperature, HCl concentration and their impact on the % REE leaching recovery for RC1(A) and DC1(B).

The contour plots and 3D surface plots from the simultaneous effects of leaching temperatures between 30 °C to 50 °C and solid:liquid ratios ranging from 10 g/l to 40 g/l on the % REE leaching recovery are depicted in Figures 4-18 A and B 4-19 A and B, respectively. The HCl concentration for these tests was kept at 2 M, and it is evident that the % REE leaching recovery increased as the leaching temperature increased to 50 °C. At a leaching temperature of 50 °C and pulp density of 10 g/l, the % REE leaching recovery reached a maximum of 18.8% and 40% for RC1 and DC1, respectively (Figures 4-18 and 4-19). Several studies on REE leaching recovery from coal and different REE-based ores have indicated that REE recovery increased with an increase in leaching temperature and a decrease in solid:liquid ratio (Li *et al.*, 2013; Cao *et al.*, 2018; Amine *et al.*, 2019; Yang, 2019; He *et al.*, 2021; Ji and Zhang, 2021).

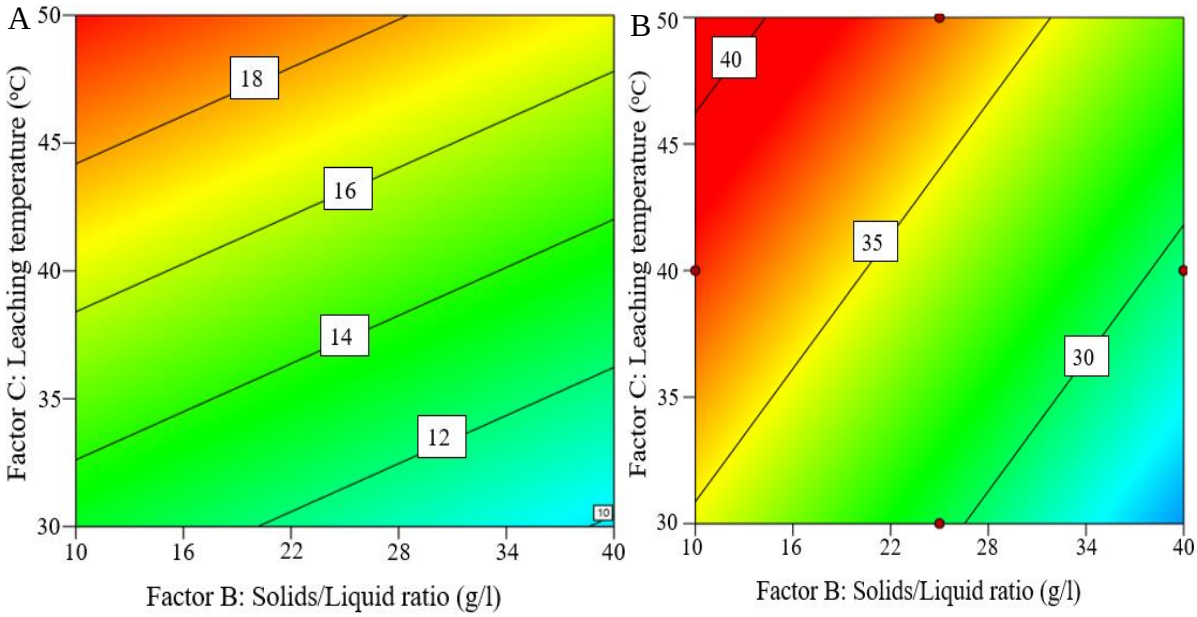


Figure 4-18: Contour plots for the relationship between solid:liquid ratio and leaching temperature with respect to % REE leaching recovery for RC1 (A) and DC1 (B).

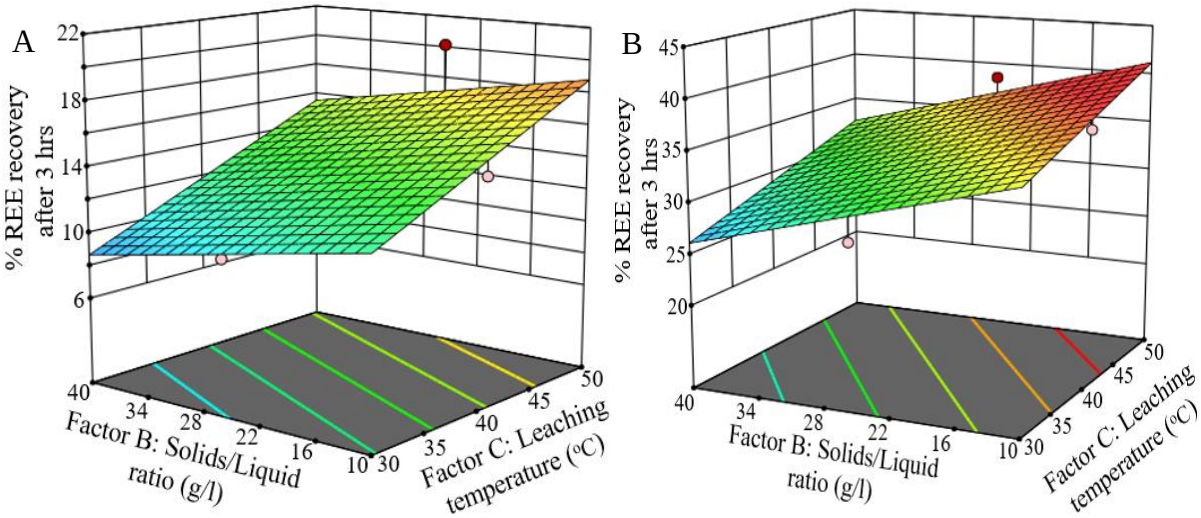


Figure 4-19: 3D surface plots of the relationship between leaching temperature, pulp density (solid:liquid ratio) and their impact on the % REE leaching recovery for the RC1(A) and DC1(B) coals.

Figures 4-20 (A and B) and 4-21 (A and B) depicted the relationship between solid:liquid ratio at 10 g/l to 40 g/l, and the HCl concentration ranging between 0.5 M to 2 M. The leaching temperature was kept at a constant temperature of 50 °C throughout the plots. From the contour plots (Figure 4-20) and 3D surface plots (Figure 4-21), it was observed that an increase in REE recovery was due to an increase in acid concentration and a decrease in the pulp density. This observation was similar to that reported by Chi *et al.* (2006); Cao *et al.* (2018); Amine *et al.*

(2019); Yang, (2019) and He *et al.* (2021), on the influence acid concentration and the pulp density on REE recovery.

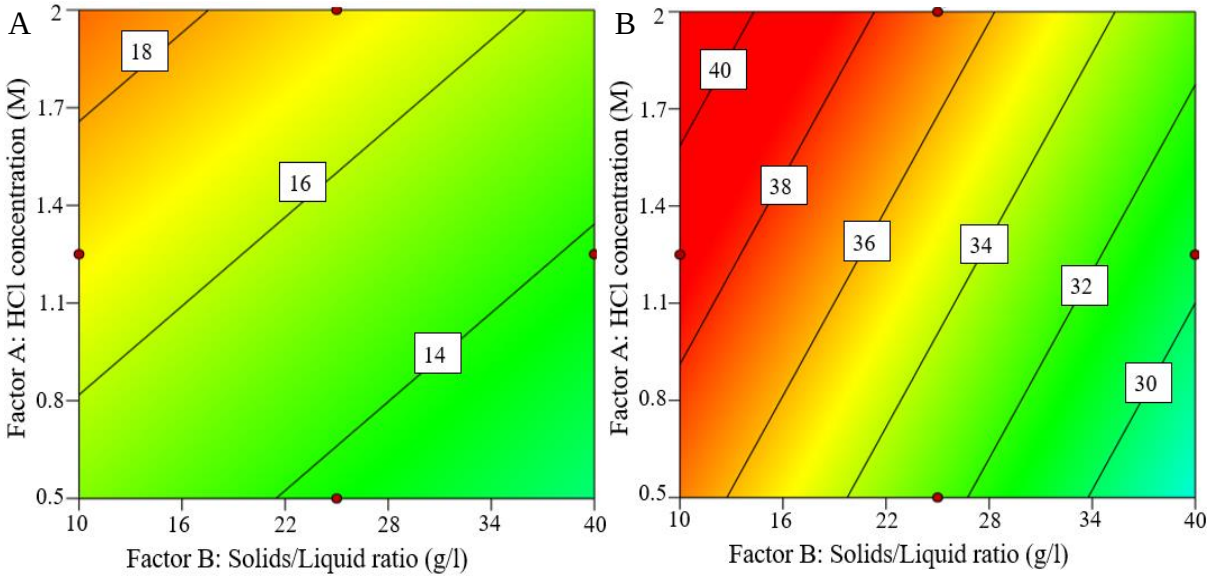


Figure 4-20: ROM (RC1) (A) and Discard (DC1) (B) coals contour plots for the relationship between solid:liquid ratio (g/l) and HCl (M) concentration with respect to REE recovery.

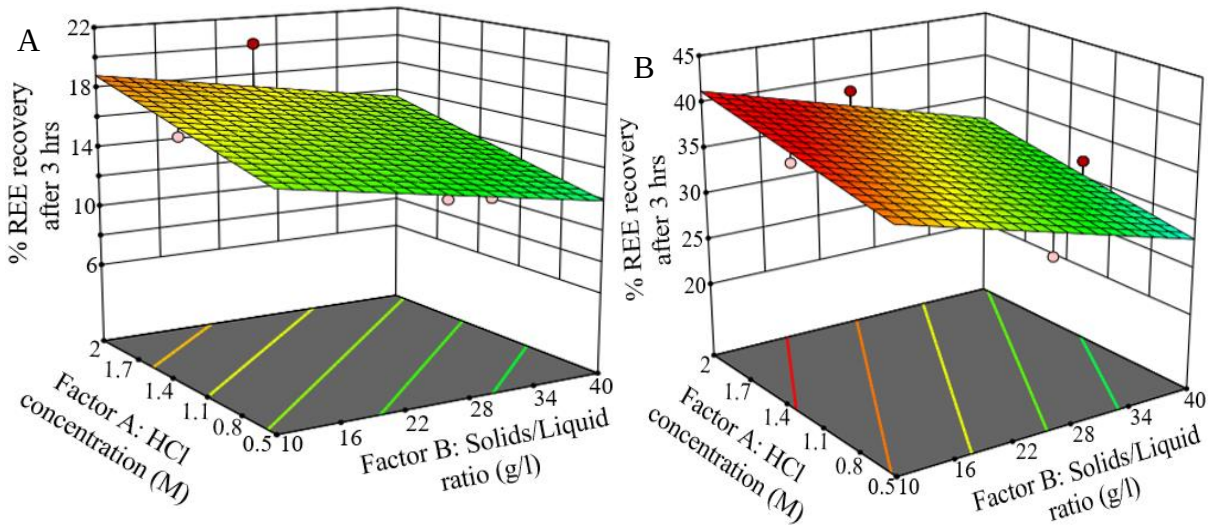


Figure 4-21: 3D surface plots of the relationship between leachate concentration, pulp density (solid:liquid ratio) and their impact on the % REE leaching recovery for the RC1(A) and DC1(B).

The development of the 3D surface response models provided valuable information on the optimisation and % REE leaching recovery of the two coal samples. It was concluded that increasing the HCl concentration and temperature and decreasing the solid:liquid ratio improved the % REE leaching recovery for RC1 and DC1.

4.6.1.7 Determination of the optimal leaching parameters

The determination of the optimal leaching conditions for REE recovery was carried out on DOE according to Table 4-10. To obtain the optimal leaching conditions of factors A (HCl concentration), B (solid:liquid ratio) and C (leachate temperature), a desirability function was employed to maximise the % REE leaching recovery. The application of the desirability function was to provide the conditions which offered the maximum desirability factor (Abdulsalam *et al.*, 2019; Amine *et al.*, 2019), leading to optimal leaching conditions. Table 4-10 illustrates the parameter settings for the desired target response.

Table 4-10: Leaching parameter settings for the optimised response of RC1 and DC1.

Parameter constraints	**Goal**	**Lower limit**	**Upper limit**
A: Concentration (M)	is in range	0.5	2
B: Solid:liquid ratio (g/l)	is in range	10	40
C: Temperature (^{o}C)	is in range	30	50
% REE leaching recovery after 3 hrs	maximise	6.91	20.16

The desirability function operates in an interval of [0, 1], with 1 conforming to the maximum satisfaction and 0 indicating an unacceptable or undesirable response (Amine *et al.*, 2019). Table 4-11 illustrates the optimal leaching solutions, with solution 1 selected for RC1 and DC1 as the % REE leaching recovery was highest in this design space. Additionally, solution 1 for RC1 and DC1 manifested a desirability of 0.90 and 1.00, respectively. Therefore, indicating the optimal runs that provide maximum satisfaction. In conclusion, the optimum leaching process conditions for RC1 and DC1 corresponds to a HCl concentration of 2 M, with a solid:liquid ratio of 10 g/l and a leaching temperature of 50 ^{o}C.

Table 4-11: Leaching conditions of the optimised solution for RC1 and DC1.

Solution	**A: HCl concentration (M)**	**B: Solid:liquid ratio (g/l)**	**C: Temperature (^{o}C)**	**% REE leaching recovery (3 hrs)**	**Desirability**	**Remark**
(RC1) 1	2.00	10.00	50.00	18.81	0.90	**Selected**
(RC1) 2	2.00	10.00	50.00	18.81	0.90	
(RC1) 3	2.00	10.12	50.00	18.80	0.89	
(DC1) 1	2.00	10.00	50.00	41.01	1.00	**Selected**
(DC1) 2	1.98	10.16	49.73	41.03	1.00	
(DC1) 3	1.99	10.10	49.97	41.14	1.00	

The contour plots for the desirability function with respect to HCl concentration, solid:liquid ratio and leaching temperature for both coal samples are displayed in Figures 4-22 and 4-23. A desirability function close to 1 indicated the optimal or ideal region of operation (Abdulsalam, 2019). The desirability functions for RC1 and DC1 were 0.9 (Figures 4-22 A and 4-23 A) and 1 (Figures 4-22 B and 4-23 B), respectively. Combining the desirability functions (Figures 4-22 and 4-23) and % REE leaching recovery contour plots (Figures 4-16, 4-18 and 4-20) illustrated the optimal leaching conditions for RC1 and DC1. These optimal conditions are noted at a HCl concentration of 2 M, a solid:liquid ratio of 10 g/l and a leaching temperature of 50 ^{o}C. At these optimal leaching conditions, the % REE leaching recovery predicted was 18.81% and 41.41% for DC1 and RC1, respectively.

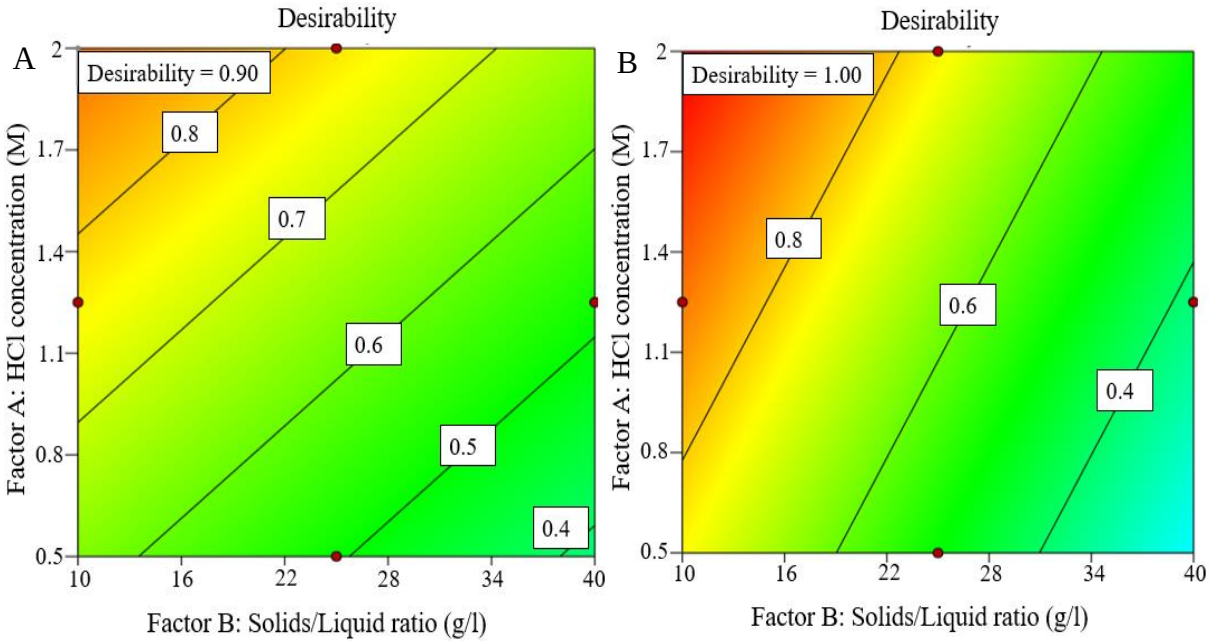


Figure 4-22: Contour plots of desirability for varying solid:liquid ratios and HCl concentrations for RC1 (A) and DC1 (B).

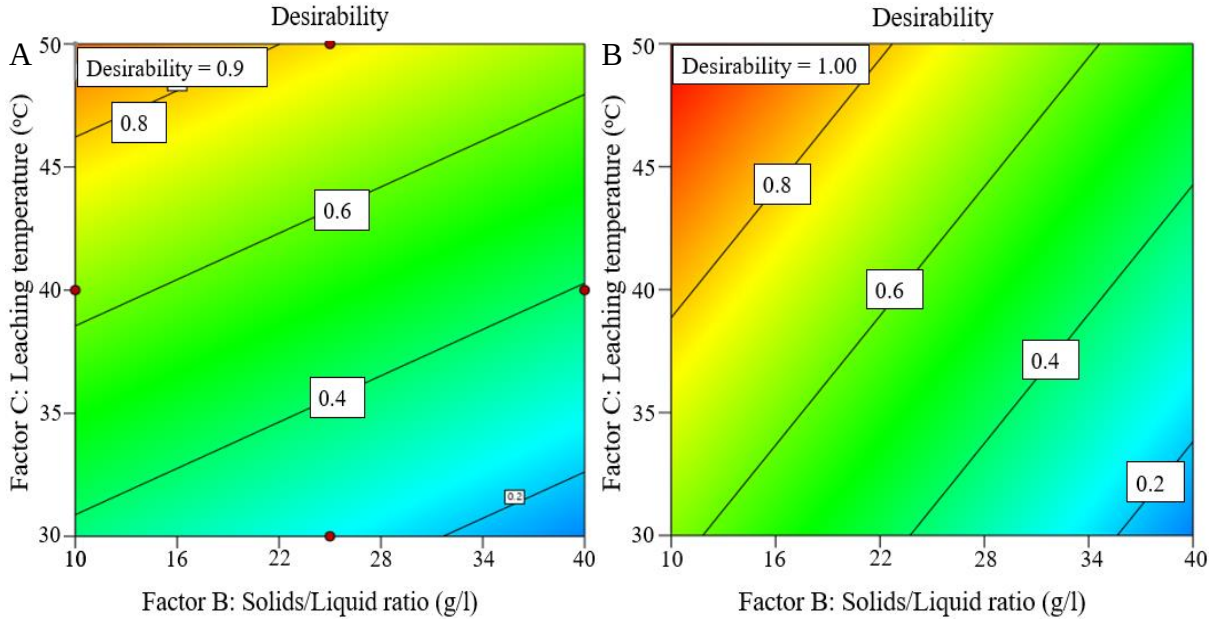


Figure 4-23: Contour plots of desirability for varying solid:liquid ratios and leaching temperatures for RC1 (A) and DC1 (B).

The predicted optimised % REE leaching recovery model (Equations 4-14 and 4-15) and conditions were within a 95% confidence level (Table 4-12). More so, the point prediction provided a standard deviation of 2.93 (RC1) and 1.99 (DC1). Hence, indicating that the predicted and experimental % REE leaching recovery from the optimised leaching conditions (Table 4-12) will not deviate by more than 3% for both samples. The predicted % REE leaching recovery mean and median for RC1 and DC1 are 18.82 and 41.04, respectively (Table 4-12). These values are close to the expected REE recovery percentage for the optimised leaching conditions, illustrating the model's accuracy for the optimised leaching conditions.

Table 4-12: Point prediction table for the optimised selected solutions.

Solution 1 response	**Predicted mean**	**Predicted median**	**Std Dev**	**95% Cl low for mean**	**95% Cl high for mean**
RC1 % REE leaching recovery after 3 hrs	18.82	18.82	2.93	14.53	23.10
DC1 % REE leaching recovery after 3 hrs	41.04	41.04	1.99	38.16	43.91

Std Dev: Standard Deviation; Cl: Confidence level

Based on the model's validity, RC1 and DC1 were subjected to leaching under the optimal conditions achieved (HCl concentration of 2 M, with a solid:liquid ratio of 10 g/l and a leaching temperature of 50 °C). Under these conditions, the experimental % REE leaching recoveries for RC1 and DC1 were 18.95% and 41.53%, respectively. These REE recovery values are close

to the predicted % REE recovery (Tables 4-11 and 4-12). The percentage of absolute error (POAE) was determined by Equation 4-16.

$$POAE = \frac{Experimental\ \%\ REE\ recovery - Predicted\ \%\ REE\ recovery}{Experimental\ \%\ REE\ recovery} \times 100 \quad (4\text{-}16)$$

The error percentages for RC1 and DC1 were 0.74% and 1.25%, respectively. The standard accepted POAE should not be greater than 2.5% to 5%, depending on the type of experiment conducted (Ernest, 2014). Therefore, the POAE achieved shows that the optimised results and solutions are satisfactory and agree with the experimental results.

4.7 Percentage REE recovery under optimised leaching conditions for discard and ROM coals

4.7.1 Effect of HCl on the recovery of REE from RC1 and DC1 coals

The optimal leaching conditions determined by the DOE software were verified. This was carried out by subjecting the RC1 and DC1 with a particle size of - 106 µm to leaching under the optimal parameters (HCl concentration of 2 M, solid:liquid ratio of 10 g/l and at a leaching temperature of 50 ^{o}C). RC1 exhibited an 18.95% leaching recovery of REE, as presented in Figure 4-24. However, 41.35% REE leaching recovery was achieved under the optimal leaching conditions for DC1. As shown in Figure 4-24, the recovery of the REE can be seen to occur instantaneously within the first minute, then gradually increases over three hours with only an increase of 5% (DC1) to 10% (RC1). Studies on REE leaching from coal and other minerals correlate well with the REE recovery rate reported in this study (Bandara and Senanayake, 2015; Kim *et al.*, 2016; Yang *et al.*, 2019; Yang and Honaker, 2020; Zhang and Honaker, 2020). In some of these studies, the recovery of REE was higher as most of these studies are conducted at less than 10 µm (Yang, 2019). However, it can be noted that within the one to ten-minute period, REE were leached into the lixiviate instantaneously.

The optimal leaching conditions predicted by the model (Equations 4-14 and 4-15) were validated, as the model predicted % REE leaching recovery close to the optimal experimental REE leaching recovery. The model predicted % REE leaching recovery was 18.82% for RC1 and 41.04% for DC1, whilst the experimental REE recovery values were 18.94% (RC1) and 41.35% (DC1). As a result, the relevance and adequacy of the model were supported by the experimental results.

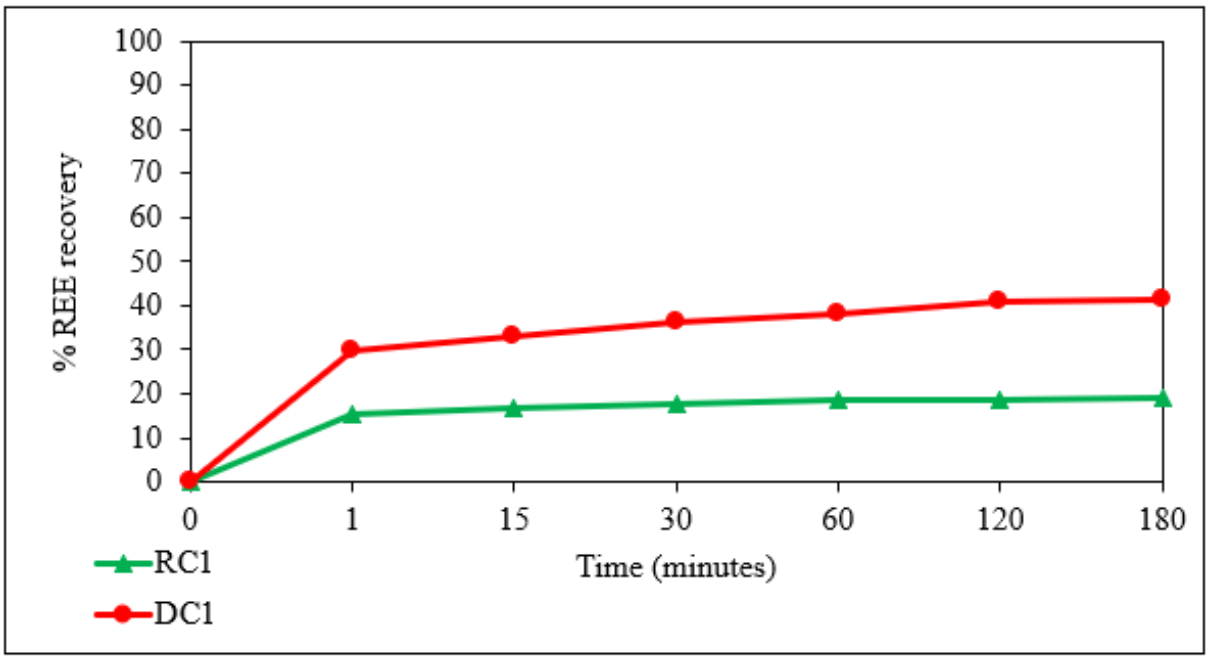


Figure 4-24: RC1 and DC1 % REE leaching recovery under the optimised leaching parameters (HCl concentration of 2 M, solid:liquid ratio of 10 g/l, leaching temperature of 50 ^{o}C, D_{90} = -106 µm, stirrer speed 550 rpm).

The rationale for the low REE leaching recovery of 18.95% and 41.35% (Figure 4-24) from both raw coal samples could be that 2 M HCl only dissolved phosphates (xenotime and monazite), carbonates and sulphate minerals (Figure 4-2). At this concentration, zircon, pyrite and the aluminosilicate minerals (kaolinite) may have failed to dissolve or solubilise completely. REE are also associated with these minerals (Dhawan and Sharma, 2019; Yang, 2019). Hence, the REE attached to the non-soluble minerals may not have been released, as exhibited by the low REE recovery. This was also emphasised in a study by Ji and Zhang (2021), where thermal decomposition was used to solubilise clay minerals prior to leaching.

Under the optimal leaching conditions, DC1 maintained a significantly greater % REE leaching recovery compared to RC1. This may be due to the REE being weakly ion-adsorbed with kaolinite clay minerals. The lower REE recovery from RC1 may be due to the physical encapsulation by the carbon matrices, as shown in the BSE images in Figure 4-3, thereby reducing the interactions between the REE trivalent cations and the Cl^{-} ions in solution. The higher REE recovered from DC1 may also be due to the higher ash (mineral) content and lower carbon content, leading to reduced carbon matrices and increased interactions between leachate and REE-bearing minerals. Laudal (2017) indicated that the high ash Harmon-Hansen coal

manifested a higher REE recovery than the lower ash Hagel-B coal. However, ash yield cannot be directly related to increased REE recovery, as some studies have noted higher recoveries on coals with a lower ash content (Yang, 2019). Therefore, REE in different coal sources may reside either with mineral matter or with organic matter, so the percentage of REE recovery may differ depending on the association of REE. Therefore, in this study, REE have been shown to have a greater affinity for the mineral fraction, as shown by TIMA image analysis (Figure 4-3). This is illustrated by the higher REE recoveries manifested by DC1 (Figure 4-24).

Figure 4-25 depicts the results obtained under the optimal leaching conditions for the % HREE recovery for DC1 and RC1. 77% of HREE were recovered from DC1, whilst RC1 manifested a % HREE recovery of 21.03%. The LREE recovery for both coal samples were lower than the HREE recovery. The % LREE recovery for RC1 and DC1 were 14% and 32%, respectively (Figure 4-25). The higher HREE recovery indicates that the HREE dissolve more rapidly under the optimal leachate conditions within the first minute. However, the LREE display a slow dissolution in solution in the first fifteen minutes, but over time the LREE typically increase in solution.

The results of a higher extraction efficiency of HREE suggest that they form weak ion-adsorbed bonding complexes with the organic or inorganic minerals within the coal. In addition, more HREE were released into the leachate from the DC1 coal, which contains a higher ash content relative to the RC1 coal. This may be because the carbon fraction of RC1 (high carbon) consumes more acid, leaving less HCl available to react with REE.

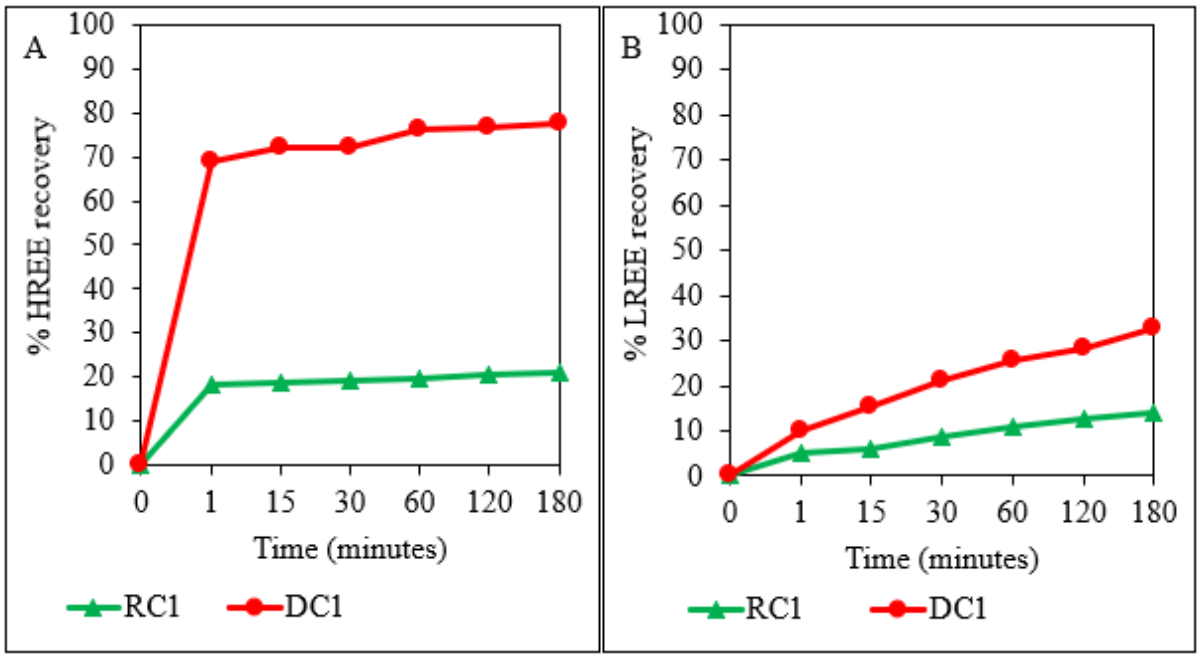


Figure 4-25: RC1 and DC1 % HREE (A) and % LREE (B) leaching recovery under the optimised leaching parameters (HCl concentration of 2 M, solid:liquid ratio of 10 g/l, leaching temperature of 50 ^{o}C, D_{90} = - 106 µm, stirrer speed 550 rpm).

LREE, widely distributed in the inorganic minerals (Figure 4-3), typically exhibit a slower leaching kinetic and a lower % REE leaching recovery. This is considered the result of their stronger attachment to insoluble minerals like silicates, kaolinite, pyrite, magnetite and zircon (Table 4-2). These minerals would require more contact time, more aggressive leaching concentrations and higher temperatures to solubilise these REE-bearing minerals (Laudal *et al.*, 2018). The LREE that were released into solution instantaneously are a result of weaker associations with the mineral matter (Laudal *et al.*, 2018). In retrospect, HREE were dispersed and weakly adsorbed to organic matrices or weakly adsorbed to clayey mineral sites, whereas the LREE formed more stable strongly nested bonds with the mineral fraction, illustrated by their slower REE recovery rate over time.

The high HREE recovery of 77% from DC1 (sourced from discard coal left in tailings dumps) implies that discard coal is a promising potential source for economic gain as no prior mining is required. Secondly, HREE are usually rare and are in higher demand as they are included in CREE, as reported by the USA Department of Energy (Reid, 2018).

4.7.2 Effect of acid type on the percentage REE recovery under optimal leaching parameters

Leaching experiments were conducted at the optimal leaching parameters of 2 M acid, 50 ^{o}C and a solid:liquid ratio of 10 g/l with different inorganic acids. Nitric acid and perchloric acid were used to compare REE leaching and assess differences in the % REE leaching recovery from the HCl leaching process (Figure 4-24). Both RC1 and DC1 were subjected to HNO_3 and $HClO_4$ leaching at 2 M. After three hours of leaching, 15.9% of REE were recovered using the nitric acid lixiviate, whilst the perchloric acid only achieved a 7.08% REE recovery from RC1 (Figure 4-26). The HNO_3 and $HClO_4$ leaching applied to DC1 exhibited a REE recovery of 42.57% and 22.39%, respectively (Figure 4-26). Thus, HNO_3 was more effective than $HClO_4$ for leaching REE.

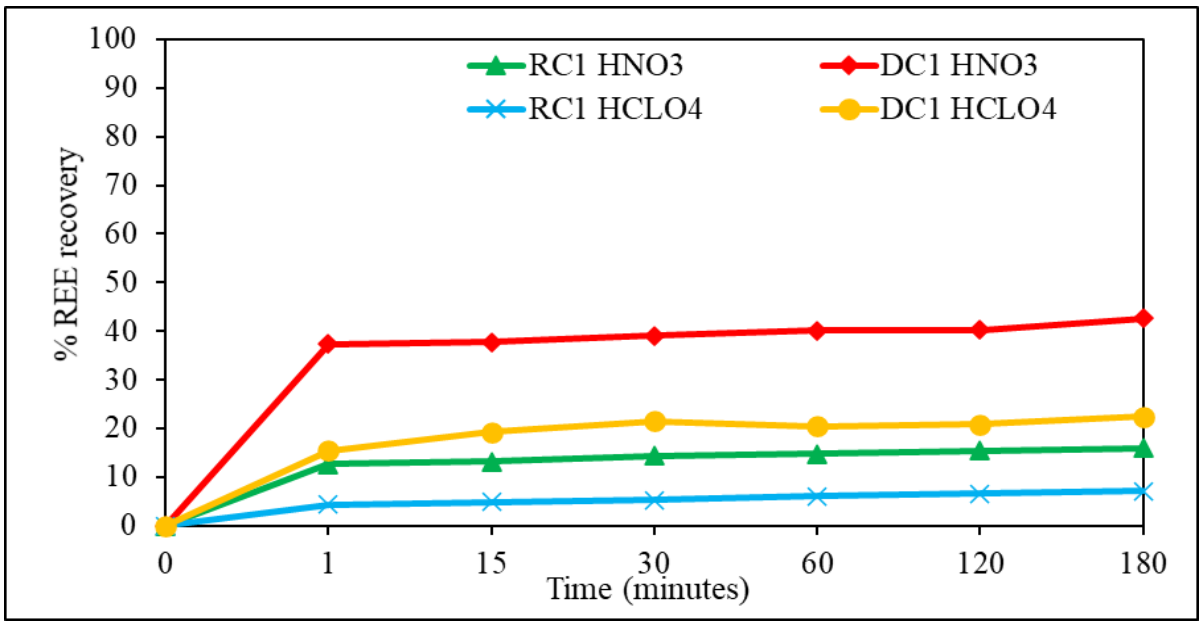


Figure 4-26: RC1 and DC1 % REE leaching recovery under the optimised leaching parameters ($HClO_4/HNO_3$ concentration of 2 M, solid:liquid of 10 g/l, leaching temperature of 50 ^{o}C, D_{90} = - 106 µm, stirrer speed 550 rpm).

Overall, the effectiveness of perchloric acid leaching for REE recovery was lower than nitric acid and hydrochloric acid. The order of proton activity, $HClO_4 > HNO_3 > HCl$ (Bandara and Senanayake, 2015), implies that $HClO_4$ should have produced a greater recovery of REE. Nonetheless, perchlorate (ClO_4^-) ions have a lower association/ability to bind to REE cations (Bandara and Senanayake 2019). Hence the reason for the decrease in the percentage REE recovery during $HClO_4$ leaching. The increase in REE recovery with HCl or HNO_3 leaching is due to the stronger bonding abilities of the NO_3^- and Cl^- ions, even though they exhibit a lower

proton activity (Bandara and Senanayake, 2019). REE cation recovery requires a composite effect of the H_3O^+ hydronium ion, leading to the acidity and solubilisation of the REE-bearing minerals, along with the influence of the anions' (Cl^-, NO_3^-) bonding ability to recover the REE (Bandara and Senanayake, 2019). This indicates why HNO_3 and HCl exhibited similar REE recoveries of 42.57% and 41.35% for DC1, and 15.9% and 18.95% for RC1, respectively. Therefore, it can be concluded that HNO_3 and HCl behaved similarly in the leaching tests on both coal samples.

Figure 4-27 presents the % HREE and LREE leaching recovery from DC1 and RC1 under HNO_3 and $HClO_4$. HNO_3 leaching resulted in a recovery of 93.5% HREE and 20.78% LREE from DC1. $HClO_4$ achieved a 71.23% HREE recovery and 10.84% LREE recovery from DC1. Nitric acid resulted in an HREE recovery of 38.69% and LREE recovery of 10.51% from RC1. The perchloric acid leaching results from RC1 were 16.15% HREE recovery and 4.97% LREE recovery.

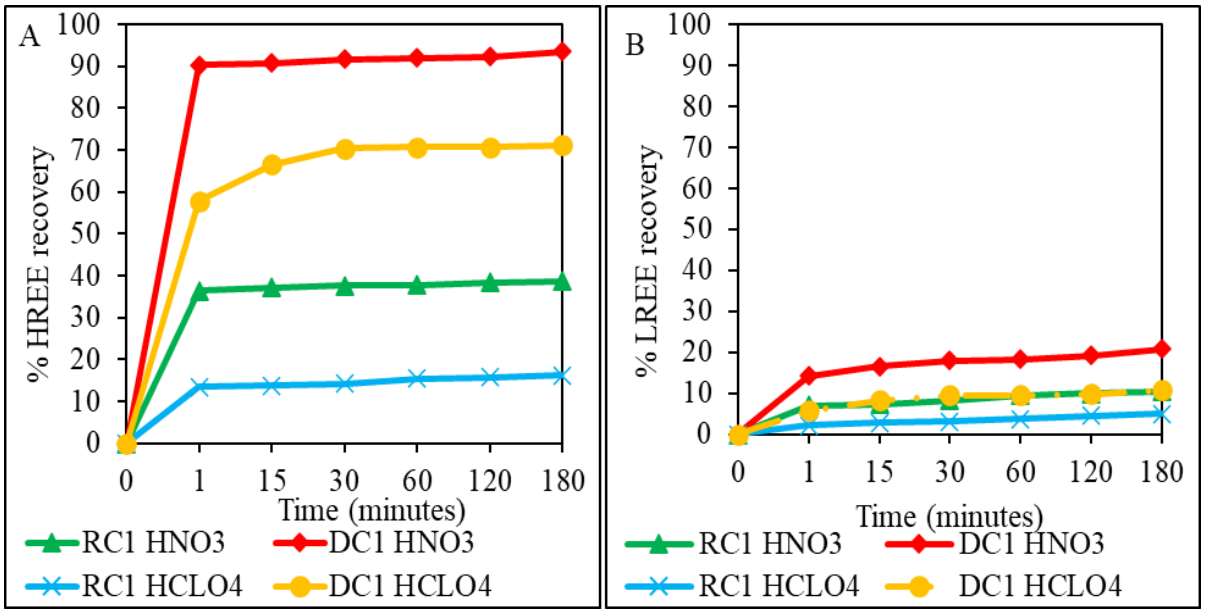


Figure 4-27: RC1 and DC1 % HREE (A) and % LREE (B) leaching recovery under the optimised leaching parameters ($HClO_4/HNO_3$ concentration of 2 M, solid:liquid ratio of 10 g/l, leaching temperature of 50 ^oC, D_{90} = - 106 µm, stirrer speed 550 rpm).

The % HREE leaching recovery for RC1 and DC1 and both lixiviates was greater than the % LREE leaching recovery. This may be as a result of the weak ion-bonding of the HREE with the organic matrices and clay minerals, thus being released instantaneously into the leachate solution (Laudal, 2017). The lower recovery of LREE could be due to its association with less acid-soluble REE minerals. Thus, the recovery of the LREE progressively improves (Figure 4-

27 B) as the mineral slowly decomposes. Laudal *et al*. (2018) suggested that leachate contact time with the raw coal should be increased to 24 hours to maximise LREE recovery.

The perchloric acid leaching of both coal samples revealed a lower % HREE and LREE leaching recovery. As stated in section 4.7.2, this results from the low complexation or bonding abilities of the (ClO_4^-) chlorate anions with the HREE/LREE cations (Bandara and Senanayake, 2015). Secondly, nitric acid attained higher % HREE and LREE recoveries for both coal samples (RC1 and DC1) due to the strong complexation abilities of the nitrate anions with HREE/LREE cations.

Overall, % LREE and % HREE recovery was higher from DC1 (in the perchloric and nitric acid leachates) than RC1, which correlates well with the HCl leaching results. DC1 provided higher recoveries of REE in general than RC1 for all three leachates.

HCl was used in the subsequent optimised leaching test for REE of the calcined samples due to its higher REE recoveries and cost-effectiveness relative to the HNO_3 and $HClO_4$ lixiviates.

4.8 The effect of calcination pre-treatment on the subsequent % REE leaching recovery

Calcination was conducted on RC1 and DC1 to evaluate the influence of the pre-treatment technique on the percentage recovery of REE. RC1 and DC1 were calcined at 500 ^oC, 600 ^oC, 700 ^oC and 800 ^oC. Subsequently, the calcined coals were subjected to optimised leaching parameters (HCl concentration of 2 M, solid:liquid ratio of 10 g/l and leaching temperature of 50 ^oC).

The leaching % REE recovery increased drastically for both coal samples when they were initially subjected to thermal pre-treatment via calcination. At the calcined temperatures of 500 ^oC, 600 ^oC, 700 ^oC and 800 ^oC, a % REE leaching recovery of 84.72%, 89.82%, 94.73% and 86.83% was achieved for RC1, respectively (Figure 4-28 A). At the same temperatures, a % REE leaching recovery of 86.83%, 89.24%, 98.17% and 89.23% was achieved for DC1, respectively (Figure 4-28 B). Calcination improved the leaching rate of REE within the first minute (Figure 4-28).

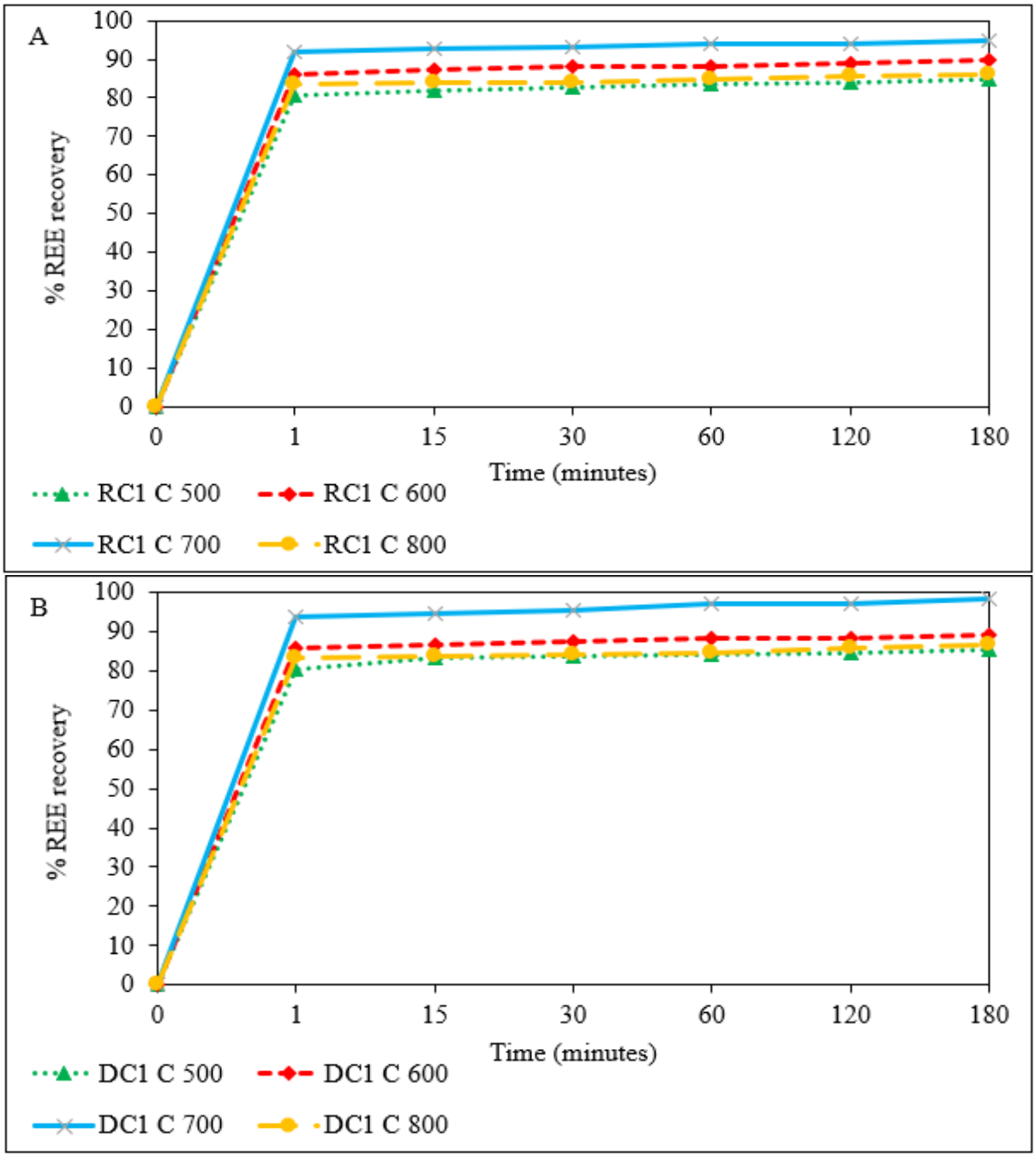


Figure 4-28: The effect of calcination of RC1 (A) and DC1 (B) on the % REE leaching recovery under the optimised leaching parameters (HCl concentration of 2 M, solid:liquid of 10 g/l, leaching temperature of 50 ^{o}C, D_{90} = - 106 µm, stirrer speed 550 rpm).

The percentage recovery of REE leaching increased as the calcination temperature increased from 500 ^{o}C to 700 ^{o}C. The optimal calcination temperature to enhance REE recovery was 700 ^{o}C, supported by the high REE recovery of 94.73% (RC1) and 98.17% (DC1). However, when the calcination temperature was elevated to 800 ^{o}C, the % REE leaching recovery decreased by more than 7% for both coal samples (Figure 4-28). This is similar to the findings of Honaker

et al. (2019), Zhang and Honaker (2019a), Zhang and Honaker (2019b) and Zhang and Honaker (2020). At higher coal calcination temperatures between 750 ^{o}C and 900 ^{o}C, the % REE leaching recovery decreased substantially. During calcination, carbon is removed, increasing the ash and mineral content of the coal (Zhang and Honaker, 2019a). The removal of the carbon matrices prevents the physical encapsulation of the REE-bearing mineral species and reduces the carbon acid consumption or interactions between them (Honaker *et al.*, 2019). Hence, indicates the reason as to why thermal pre-treatment has improved the overall REE leaching recovery in general.

According to Zhang and Honaker (2019a), at a calcination temperature above 800 ^{o}C, the surface area and pore volume of kaolinite declined significantly. In the current study, this elevated temperature reduced the % REE leaching recovery (Figure 4-28). The decrease in surface area and pore volume decreases the leachate interactions with REE. Additionally, due to the pozzolanic nature of clay minerals at 800 ^{o}C to 900 ^{o}C, such as kaolinite, the major REE-bearing mineral was converted to a crystalline mullite form, which encapsulates the REE (Honaker *et al.*, 2019). This form of kaolinite mullite requires very aggressive acid sintering conditions to digest. In retrospect, calcination above 800 °C decreased the percentage of REE recovery, as shown in Figure 4-28, due to mullite formation in clay minerals.

Initially, the % REE recovery under the same optimal conditions for the raw RC1 and DC1 was 18.95% and 41.35%, respectively (Figure 4-24). Correspondingly, through calcination, the % REE leaching recovery increased by 65.77% for RC1 and DC1 (Figure 4-28 A and B). Therefore, indicating the effectiveness of calcination on the improvement of REE recovery. From Figure 4-28, it was observed that the highest % REE leaching recovery occurred within the first minute, suggesting that there was an increase in more soluble forms of REE in leachate following calcination (Zhang and Honaker 2019a). Subsequently, during the following 180 minutes of leaching, the REE recovery increased by only one to five per cent. Thus, indicating that the calcined coal sample required a short leaching contact time for REE recovery. Zhang and Honaker (2019a) and Honaker *et al.* (2019) also noted the rapid recovery of REE leaching within the first five minutes of leaching their calcined coal samples.

Results from Mardon and Hower (2004) indicate that REE present in the coal remain non-volatile even when the coal is in a boiler at 1000 ^{o}C. Thus, no REE were degraded or removed during the calcination stage. In addition, during calcination, REE bound to inorganic minerals

and carbon fractions form REE oxides, making REE forms more soluble. Hence, leading to an improved REE leaching extraction efficiency (Honaker *et al.*, 2019; Zhang and Honaker, 2019a; Ji and Zhang, 2021), confirming the findings of the current study concerning the higher percentage of leaching recovery from calcinated coal. Overall, calcination increases the % REE leaching recovery from 500 ^{o}C to 700 ^{o}C, with 700 ^{o}C the optimal calcination temperature for enhancing REE recovery in the RC1 and DC1.

4.8.1 The effect of calcination pre-treatment on the subsequent % HREE and LREE leaching recovery

Thermal calcination at 500 ^{o}C to 800 ^{o}C improved the % HREE and % LREE leaching recovery (Figures 4-29 and 4-30). Raw RC1 subjected to optimised leaching conditions resulted in an HREE and LREE recovery of 21.03% and 14.04%, respectively (Figure 4-25 A and B). Subsequently, RC1 calcinated at 500 ^{o}C, 600 ^{o}C, 700 ^{o}C and 800 ^{o}C resulted in 60.55%, 72.91%, 79.35% and 72.04% HREE leaching recovery, respectively (Figure 4-29 A). In order of the same calcination temperatures, LREE recovery for RC1 was 83.31%, 87.62%, 94.24% and 88.56% (Figure 4-30 A).

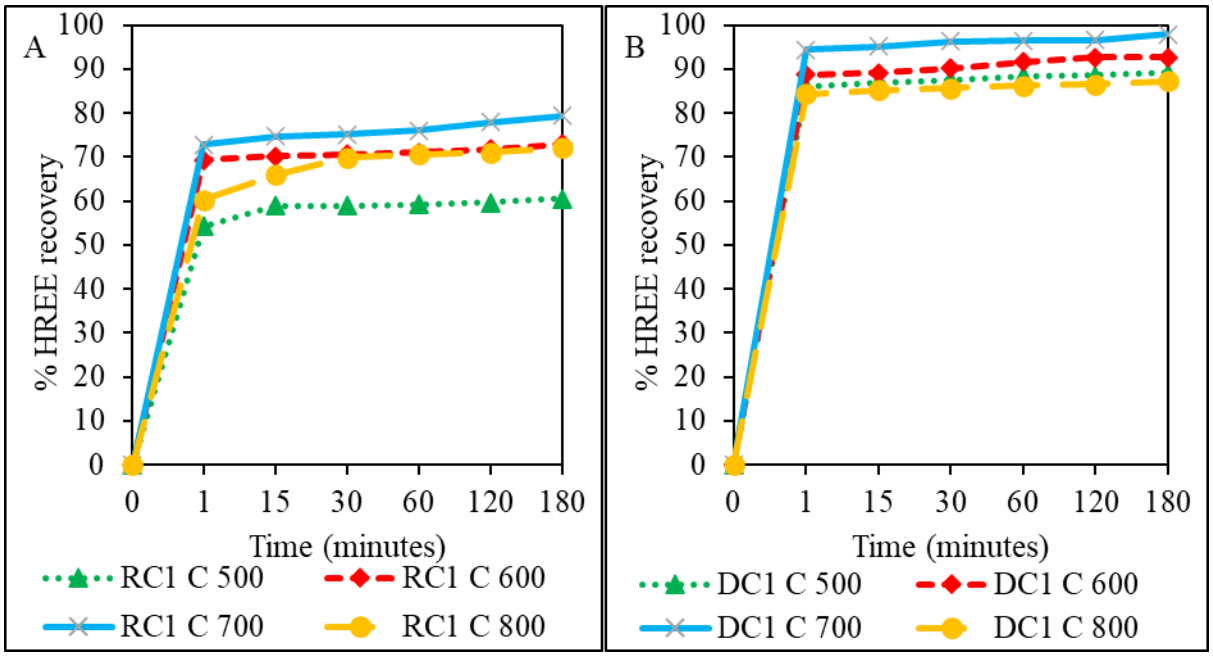


Figure 4-29: Calcined RC1 (A) and DC1 (B) % HREE leaching recovery under the optimised leaching parameters of (HCl concentration of 2 M, solid:liquid ratio of 10 g/l, leaching temperature of 50 ^{o}C, D_{90} = - 106 µm, stirrer speed 550 rpm).

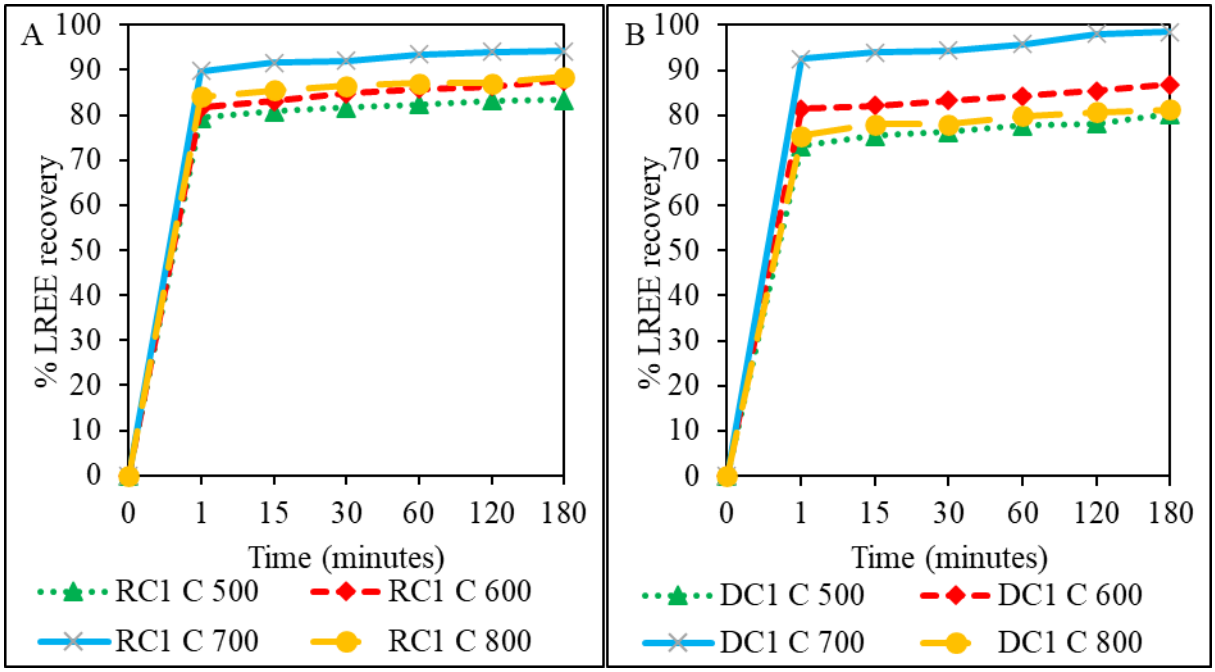


Figure 4-30: Calcined RC1 (A) and DC1 (B) % LREE leaching recovery under the optimised leaching parameters of (HCl concentration of 2 M, solid:liquid ratio of 10 g/l, leaching temperature of 50 °C, D_{90} = - 106 µm, stirrer speed 550 rpm).

Raw DC1 subjected to the optimal leaching conditions resulted in 77.37% HREE recovery and 32.50% LREE recovery (Figure 4-25 A and B). Upon calcination at 500 °C, 600 °C, 700 °C and 800 °C the % HREE leaching recovery increased to 89.08%, 92.69%, 97.9% and 87.31%, respectively (Figure 4-29 B). The % LREE leaching recovery also increased to 80.25%, 86.82%, 98.49% and 81.27% for the same calcination temperatures, respectively (Figure 4-30 B).

The best calcination temperature for improving the % HREE and % LREE leaching recovery was 700 °C (Figures 4-29 and 4-30). At this temperature, the % HREE leaching recovery for RC1 and DC1 was 79.35% and 97.9%, respectively. The high recovery observed in HREE relative to the LREE from the two coal samples was due to the HREE being weakly associated or ion-adsorbed to the carbon matrices and surfaces of the clay minerals (Laudal *et al.*, 2018). Upon calcination at 700 °C, most of the carbon was removed, leaving behind HREE oxides, which readily dissolved into the leachate and improved the % HREE leaching recovery overall (58% for RC1 and 20.53% for DC1).

The low LREE recovery from both raw coal samples could be attributed to the LREE being associated and distributed with non-soluble minerals (Figure 4-25 B) (Laudal *et al.*, 2018). Typically, these non-soluble minerals include silicates, kaolinite, pyrite, magnetite and zircon,

which are present in the raw RC1 and DC1 coals (Zhang and Honaker, 2020) (Table 4-2). The calcination of RC1 at 700 ^{o}C increased the % LREE leaching recovery to 94.24% from 14.04%. At the same calcination temperature, the % LREE leaching recovery for DC1 improved from 32.50% to 98.49%. This suggests that calcination destroyed the kaolinite layer structure, increasing the liberation of previously encapsulated LREE minerals (Zhang and Honaker 2020). More so, it converts the LREE-bearing minerals into oxides, which are more soluble during acid leaching, resulting in an improved % LREE recovery (Honaker *et al.*, 2019).

4.9 Summary

The discard coal, waste from the tailings dump, is more of a potential source for REE than the ROM coal. In addition, as there is no prior mining required for the discard coal and its higher HREE and LREE recovery, this could be a source of future economic benefits to the mining houses. The ROM coal can also be used for REE extraction but will require further liberation due to the carbon matrices masking the REE. Calcination of both coals further improves REE recovery and its potential as a future source for REE extraction in the country.

CHAPTER 5: CONCLUSION AND RECOMMENDATIONS

5.1 Overview

Globally, the demand for coal-fired energy is still at an all-time high. Coal mining in South Africa is one of the largest sectors, continuously producing and generating large quantities of waste. Pollution from this sector includes acid mine drainage, leaching of heavy metals from coal tailing dumps, coarse discard stockpiles, spontaneous combustion and sulphur dioxide released into the atmosphere. With increasing global demand for REE and China's export restrictions, extraction of REE from coal waste as a secondary source was investigated.

In this study, a ROM coal sample and discard coal sample were prepared and characterised for their REE concentration, distribution, and association with the coal constituents. The study also employed leaching, coupled with modelling and optimisation for the recovery of REE. Different lixiviates (HCl, HNO_3 and $HClO_4$) were also used under the optimised leaching conditions. The two samples pre-treated by calcination were subjected to the optimum leaching conditions. This was carried out to view the effect of thermal pre-treatment on the recovery of REE. The objectives of this research were accomplished; the findings are reported below.

5.2 Key findings of the research

1) The mineralogy and characterisation analysis of the South African discard (DC1) and ROM (RC1) coal sample revealed the following:
    - The two samples were classified as medium rank C bituminous shale coals with a high ash content (> 50%) and low total carbon content (< 34.30%).
    - In both samples, LREE manifested a higher association with mineral matter, particularly pyrite, and less association with kaolinite, xenotime, monazite and the organic fraction
    - HREE showed a weak ion-adsorbed association with clay minerals (kaolinite) finely dispersed in the organic matrix fractures of both samples.
    - The TREE contents for RC1 and DC1 were 225 ppm and 245 ppm, respectively. This was well above the cut-off grade of 130 ppm for TREE in coals.
    - The PSD of REEs ranges from 5 µm to 106 µm (in the -106 µm milled samples fraction).
    - Both coals had a $C_{outlook}$ coefficient greater than 0.88. Hence, both samples are considered a promising source for REE recovery.

2) Results of experimental leaching tests (DOE) have shown that:
    - The % REE leaching recovery improved as the HCl concentration increased from 0.5 M to 2 M.
    - The % REE leaching recovery increased as the leaching temperature increased from 30 ^{o}C to 50 ^{o}C and when the solid:liquid ratio decreased from 40 g/l to 10 g/l.
    - Statistical analysis indicated that the three leaching factors (concentration, temperature and solid/liquid ratio) are significant. Furthermore, all three factors were noted to regulate the REE leaching per cent recovery model.
    - The optimal leaching parameters were achieved at a concentration of 2 M, a solid:liquid ratio of 10 g/l and a temperature of 50 ^{o}C.
    - The REE leaching recovery under the optimal parameters for the untreated RC1 and DC1 coal samples was 18.95% and 41.35%, respectively.
    - The % HREE leaching recovery for both coal samples was greater than the % LREE leaching recovery. Thus, suggesting HREE are weakly ion-adsorbed onto clay minerals and carbon matrices, whilst LREE form stronger bonds with non-acid-soluble minerals.

3) The results of the different lixiviates ($HClO_4$, HNO_3 and HCl) used on the RC1 and DC1 coals, based on optimal leaching parameters, demonstrated the following:
    - The leaching efficiency of $HClO_4$ for REE recovery was significantly lower compared to HCl and HNO_3.
    - The complexation capacity of the ClO_4^- anions with REE cations was lower than that of the Cl^- and NO_3^- anions. This results in a lower REE recovery for $HClO_4$ leaching.
    - HNO_3 and HCl leaching showed a similar percent REE recovery of approximately 41% for DC1.
    - The best acid was HCl due to its higher percent REE recovery, and it is significantly cheaper than nitric acid.

4) The results of the calcination pre-treatment of RC1 and DC1 under the optimum leaching parameters for REE recovery indicated the following:
    - The concentration of REE in RC1 and DC1 improved significantly as calcination temperatures increased from 500 ^{o}C to 800 ^{o}C. At 700 °C, the REE concentration was 347 ppm (RC1) and 363 ppm (DC1). At 800 °C, the REE concentration increased to 362 ppm (RC1) and 390 ppm (DC1).
    - The % REE leaching recovery increased as the calcination temperatures of both samples increased from 500 ^{o}C to 700 ^{o}C.
    - The optimal calcination temperature for REE recovery was 700 ^{o}C. This was demonstrated by the high REE recovery of 94.73% (RC1) and 98.17% (DC1). At the calcination temperature of 700 ^{o}C, the % LREE leaching recovery was 94.24% (RC1) and 98.49% (DC1), whilst the % HREE leaching recovery was 79.35% (RC1) and 97.9% (DC1).
    - Calcination also reduced leaching time, as most REE were released in the 1- to 15-minute interval.
    - The % LREE leaching recovery improved significantly after calcination, suggesting that the REE-bearing minerals were solubilised and oxidised during calcination.

In summary, the two South African shale coal samples assessed in the study, may be used for REE extraction. The discard coal (based in the DC1 results) has a significantly higher potential for REE recovery than the ROM coal (based on the RC1 results), as it exhibited greater REE abundance and recovery. In addition, this sample represents a potentially economically viable secondary REE resource, as it will assist in waste reduction. The use of discard coal for REE extraction will create new opportunities for economic gains for the mining sector and reduce pollution and environmental degradation.

5.3 Recommendations for future studies

Suggestions for further research based on the results from this research include:

- A two-stage leaching process should be conducted. The first stage will remove the identified contaminant elements and the second stage will seek to enrich REE from the calcined coal discard.

- A pilot-scale plant employing the physical separation method, followed by calcination, leaching and REE precipitation for high purity REE products should be developed.

REFERENCES

Abdulsalam, J. (2019). Development of activated carbons from South African coal waste for application in natural gas storage. *PhD thesis*. University of the Witwatersrand.

Abdelnour, S.A., Abd El-Hack, M.E., Khafaga, A.F., Noreldin, A.E., Arif, M., Chaudhry, M.T., Losacco, C., Abdeen, A., Abdel-Daim, M.M., (2019). Impacts of rare earth elements on animal health and production: Highlights of cerium and lanthanum', *Science of the Total Environment*. Elsevier B.V., pp. 1021−1032. doi: 10.1016/j.scitotenv.2019.02.270.

Abdulsalam, J., Mulopo, J., Oboirien, B., Bada, S., Falcon, R., (2019). Experimental evaluation of activated carbon derived from South Africa discard coal for natural gas storage', *International Journal of Coal Science & Technology 2019 6:3*. Springer, 6(3), pp. 459−477. doi: 10.1007/S40789-019-0262-5.

Akdogan, G., Bradshaw, S., Dorfling, C., Bergmann, C., Ghosh, T., Campbell, Q., (2019) 'Characterization of rare earth elements by XRT sorting products of a South African coal seam', *International Journal of Coal Preparation and Utilization*. Routledge, pp. 1–17. doi: 10.1080/19392699.2019.1685506.

Akinyemi, S. A., Gitari, W. and Petrik, L. F. (2012) 'Mineralogy and Geochemistry of Sub-Bituminous Coal and Its Combustion Products from Mpumalanga Province, South Africa', *Analytical chemistry*, (December), pp. 1–46. doi: 10.5772/3086.

Al-Ani, T., Molnár, F., Lintinen, P., Leinonen, S., (2018). minerals Geology and Mineralogy of Rare Earth Elements Deposits and Occurrences in Finland', https://doi.org/10.3390/min8080356

Alaoui, A., El Kacemi, K., El Ass, K., Kitane, S., (2015). Application of Box-Behnken design to determine the optimal conditions of reductive leaching of MnO2 from manganese mine tailings', *Russian Journal of Non-Ferrous Metals*. Allerton Press Incorporation, 56(2), pp. 134–141. doi: 10.3103/S1067821215020029.

Alonso, E., Sherman, A.M., Wallington, T.J., Everson, M.P., Field, F.R., Roth, R., Kirchain, R.E., (2012). Evaluating rare earth element availability: A case with revolutionary demand from clean technologies', *Environmental Science and Technology*. https://doi.org/10.1021/es3011354

Amine, M., Asafar, F., Bilali, L., Nadifiyine, M., 2019. Hydrochloric Acid Leaching Study of Rare Earth Elements from Moroccan Phosphate', *Journal of Chemistry*. Hindawi Limited, 2019. doi: 10.1155/2019/4675276.

ASTM D-5142, (2010), "Standard Test Methods for Proximate Analysis of the Analysis Sample of Coal and Coke by Instrumental Procedures," *ASTM International*, DOI: 10.1520/D5142-04.

ASTM D-2013, (2007), "Standard Practice for Preparing Coal Samples for Analysis", *ASTM International*.

ASTM D3682-13, (2013), "Standard Test Method for Major and Minor Elements in Combustion Residues from Coal Utilization Processes" *ASTM International.*

Aubert, D., Stille, P. and Probst, A. (2001) 'REE fractionation during granite weathering and removal by waters and suspended loads: Sr and Nd isotopic evidence', *Geochimica et Cosmochimica Acta*. Pergamon, 65(3), pp. 387–406. doi: 10.1016/S0016-7037(00)00546-9.

Baioumy, H., Farahat, M., Arifin, M.H., Noor, M., Bin Anuar, A., Al-Kahtany, K., (2021) 'Hypogene kaolin deposits from felsic intrusive rocks (Peninsular Malaysia) with special reference to rare earth elements and stable isotopes geochemistry', *Geosciences Journal*, pp. 1–14. doi: 10.1007/s12303-021-0003-9.

Bandara, A. M. T. S. and Senanayake, G. (2015) 'Leachability of rare-earth, calcium and minor metal ions from natural Fluorapatite in perchloric, hydrochloric, nitric and phosphoric acid solutions: Effect of proton activity and anion participation', *Hydrometallurgy*. Elsevier B.V., 153(2015), pp. 179–189. doi: 10.1016/j.hydromet.2015.02.002.

Bandara, A. M. T. S. and Senanayake, G. (2019) 'Dissolution of calcium, phosphate, fluoride and rare earth elements (REEs) from a disc of natural fluorapatite mineral (FAP) in perchloric, hydrochloric, nitric, sulphuric and phosphoric acid solutions: A kinetic model and comparative batch leaching of major and minor elements from FAP and RE-FAP concentrate', *Hydrometallurgy*. Elsevier, 184, pp. 218–236. doi: 10.1016/J.HYDROMET.2018.09.002.

Bao, Z. and Zhao, Z. (2008) 'Geochemistry of mineralization with exchangeable REY in the weathering crusts of granitic rocks in South China', *Ore Geology Reviews*, 33(3–4), pp. 519–535. doi: 10.1016/j.oregeorev.2007.03.005.

Behera, S. K., Chakraborty, S. and Meikap, B. C. (2017) 'Removal of ash from low grade Indian coal by chemical leaching technique', *Mineral Processing and Extractive Metallurgy Review*. Taylor & Francis, 39(1), pp. 59–67. doi: 10.1080/08827508.2017.1391247.

Blumenthal, W. B. (1973) 'Chlorides of zirconium oxide', *Journal of the Less-Common Metals*. Elsevier Sequoia S.A, 30(0), pp. 39–46.

Chen, J., Algeo, T.J., Zhao, L., Chen, Z.Q., Cao, L., Zhang, L., Li, Y., (2015). Diagenetic uptake of rare earth elements by bioapatite, with an example from Lower Triassic conodonts

of South China', *Earth-Science Reviews*. Elsevier, 149, pp. 181–202. doi: 10.1016/J.EARSCIREV.2015.01.013.

Chen, S., Feng, Z., Wang, M., Zhao, L., Yu, Z., Xia, C., Huang, X., (2020). Leaching kinetic study of sulfuric acid roasted mixed-type rare earth concentrate for reducing the solid-waste production and chemical consumption', *Journal of Cleaner Production*. Elsevier Ltd, 260, p. 120989. doi: 10.1016/j.jclepro.2020.120989.

Chen, W., Honghui, H., Bai, T., Jiang, S., (2017). Geochemistry of Monazite within Carbonatite Related REE Deposits', *Resources*. MDPI AG, 6(4), p. 51. doi: 10.3390/resources6040051.

Colina, F. G., Esplugas, S. and Costa, J. (2013) 'British Ceramic Transactions High temperature reaction of kaolin with inorganic acids'. doi: 10.1179/096797801681468.

Chi, R., Tian, J., Zhu, G., Wu, Y., Li, S., Wang, C., Zhou, Z.A., (2006). Kinetics of rare earth leaching from a mangnese-removed weathered rare-earth mud in hydrochloric acid solutions', *Separation Science and Technology*, 41(6), pp. 1099–1113. doi: 10.1080/01496390600632503

Dai, S., Finkelman, R.B., 2018. Coal as a promising source of critical elements: Progress and future prospects. Int. J. Coal Geol. 186, 155–164. https://doi.org/10.1016/J.COAL.2017.06.005

Dai, S., Li, D., Chou, C.L., Zhao, L., Zhang, Y., Ren, D., Ma, Y., Sun, Y., (2008.) Mineralogy and geochemistry of boehmite-rich coals: New insights from the Haerwusu Surface Mine, Jungar Coalfield, Inner Mongolia, China', *International Journal of Coal Geology*. 74, 185–202. https://doi.org/10.1016/j.coal.2008.01.001

Dai, S., Jiang, Y., Ward, C.R., Gu, L., Seredin, V. V., Liu, H., Zhou, D., Wang, X., Sun, Y., Zou, J., Ren, D., 2012. Mineralogical and geochemical compositions of the coal in the Guanbanwusu Mine, Inner Mongolia, China: Further evidence for the existence of an Al (Ga and REE) ore deposit in the Jungar Coalfield', *International Journal of Coal Geology*. Elsevier B.V., 98, pp. 10–40. doi: 10.1016/j.coal.2012.03.003.

Dai, S., Graham, I.T., Ward, C.R., (2016). A review of anomalous rare earth elements and yttrium in coal. Int. *International Journal of Coal Geology*. https://doi.org/10.1016/j.coal.2016.04.005

Dai, S., Xie, P., Jia, S., Ward, C.R., Hower, J.C., Yan, X., French, D., (2017). Enrichment of U-Re-V-Cr-Se and rare earth elements in the Late Permian coals of the Moxinpo Coalfield, Chongqing, China: Genetic implications from geochemical and mineralogical data', *Ore Geology Reviews*. Elsevier B.V., 80, pp. 1–17. doi: 10.1016/j.oregeorev.2016.06.015.

Dai, S., Graham, I. T. and Ward, C. R. (2016) 'A review of anomalous rare earth elements and yttrium in coal', *International Journal of Coal Geology*. Elsevier B.V., pp. 82–95. doi:

10.1016/j.coal.2016.04.005.

Dai, S., Hower, J.C., Finkelman, R.B., Graham, I.T., French, D., Ward, C.R., Eskenazy, G., Wei, Q., Zhao, L., (2020). Organic associations of non-mineral elements in coal: A review', *Internation Journal of Coal Geology* 218, 103347. https://doi.org/10.1016/j.coal.2019.103347

Dhawan, H. and Sharma, D. K. (2019) 'Advances in the chemical leaching (inorgano-leaching), bio-leaching and desulphurisation of coals', *International Journal of Coal Science & Technology 2019 6:2*. Springer, 6(2), pp. 169–183. doi: 10.1007/S40789-019-0253-6.

Dreyer, J. (1994) 'Total utilization of coal resources: The Grootgeluk Experience', *SAIMM*, 3, pp. 153–164.

Dushyantha, N., Batapola, N., Ilankoon, I.M.S.K., Rohitha, S., Premasiri, R., Abeysinghe, B., Ratnayake, N., Dissanayake, K., (2020). The story of rare earth elements (REEs): Occurrences, global distribution, genesis, geology, mineralogy and global production', *Ore Geology Reviews*. Elsevier B.V. doi: 10.1016/j.oregeorev.2020.103521.

Dushyantha, N., Hemalal, P.V.A., Jayawardena, C.L., Ratnayake, A.S., Ratnayake, N., (2019). Application of geochemical techniques for prospecting unconventional phosphate sources: A case study of the lake sediments in Eppawala area Sri Lanka. *Journal of Geochemical Exploration.* 201, 113–124. https://doi.org/10.1016/j.gexplo.2019.02.010

Eberhard, A. (2011) The future of South African coal: Market, investment and policy challenges. Available at: http://pesd.stanford.edu (Accessed: 2 December 2020).

Ekmann, J. M. (2012) 'Rare Earth Elements in Coal Deposits – a Prospectivity Analysis *', *NETL report*, 80270(September), pp. 22–26.

Epshtein, S. A., Borodich, F. M. and Bull, S. J. (2015) 'Evaluation of elastic modulus and hardness of highly inhomogeneous materials by nanoindentation', *Applied Physics A: Materials Science and Processing*. Springer Verlag, 119(1), pp. 325–335. doi: 10.1007/s00339-014-8971-5.

Equeenuddin, S.M., Tripathy, S., Sahoo, P.K., Ranjan, A., (2016). Geochemical characteristics and mode of occurrence of trace elements in coal at West Bokaro coalfield', *International Journal of Coal Science and Technology*. Springer International Publishing, 3(4), pp. 399–406. doi: 10.1007/S40789-016-0146-X.

Ernest, Z. (2014) '*What percent error is too high'* | *Socratic*. Available at: https://socratic.org/questions/what-percent-error-is-too-high (Accessed: 5 October 2021).

Falcon, R. and Ham, A. (1988) 'The characteristics of Southern African coals', *South African Institute of Mining and Metallurgy*, 88(05), pp. 145–161. Available at: https://www.researchgate.net/publication/285190168_The_characteristics_of_Southern_Afric

an_coals (Accessed: 22 September 2020).

Falcon, R. (1986) ‘A brief review of the origin, formation, and distribution of coal in Southern Africa’ *South African Institute of Mining and Metallurgy*.

Faure, K. (1993) ‘Mineralogy and Geochemistry of the Carbonaceous Mudstones, and Coal Petrogenesis of the Grootegeluk Formation in the Waterberg Coalfteld, South Africa’.PhD Thesis. University of Cape Town p. 220.

Faure, K., Armstrong, R.A., Harris, C., Willis, J.P., (1996). Provenance of mudstones in the Karoo supergroup of the Ellisras basin, South Africa, Geochemical evidence’, *Journal of African Earth Sciences*, 23(2), pp. 189–204.doi: 10.1016/S0899-5362(96)00061-9.

Faure, K., Willis, J. P. and Dreyer, J. C. (1996) ‘The Grootegeluk Formation in the Waterberg Coalfield, South Africa: Facies, palaeoenvironment and thermal history - Evidence from organic and clastic matter’, *International Journal of Coal Geology*, 29(1–3), pp. 147–186. doi: 10.1016/0166-5162(95)00029-1.

Finkelman, R. B., Dai, S. and French, D. (2020) *The importance of minerals in coal as the hosts of chemical elements: A review*.

Finkelman, R. B., Palmer, C. A. and Wang, P. (2018) ‘Quantification of the modes of occurrence of 42 elements in coal’, *International Journal of Coal Geology*. Elsevier B.V., 185, pp. 138–160. doi: 10.1016/j.coal.2017.09.005.

Gao, L. and Chen, Y. (2010) ‘A study on the rare earth ore containing scandium by high gradient magnetic separation’, *Journal of Rare Earths*. The Chinese Society of Rare Earths, 28(4), pp. 622–626. doi: 10.1016/S1002-0721(09)60167-8.

Garside, M. (2021) • *Rare earth reserves worldwide as of 2020, by country*, *StatistaGarside, M. (2021) • Rare earth reserves worldwide as of 2020, by country, Statista. Available at: https://www.statista.com/statistics/277268/rare-earth-reserves-by-country/ (Accessed: 15 October 2021).* Available at: https://www.statista.com/statistics/277268/rare-earth-reserves-by-country/ (Accessed: 15 October 2021).

Georgakopoulos, A., Iordanidis, A. and Kapina, V. (2003) ‘Study of low rank greek coals using FTIR spectroscopy’, *Energy Sources*. Taylor and Francis Ltd., 25(10), pp. 995–1005. doi: 10.1080/00908310390232442.

Goodarzi, F., Sanei, H., Stasiuk, L.D., Bagheri-Sadeghi, H., Reyes, J., (2006). A preliminary study of mineralogy and geochemistry of four coal samples from northern Iran’, *International Journal of Coal Geology*. Elsevier, 65(1–2), pp. 35–50. doi: 10.1016/J.COAL.2005.04.014.

Goodenough, K. M., Wall, F. and Merriman, D. (2018) ‘The Rare Earth Elements: Demand, Global Resources, and Challenges for Resourcing Future Generations’, *Natural Resources*

Research. Springer New York LLC, 27(2), pp. 201–216. doi: 10.1007/s11053-017-9336-5.

Goonan, T. (2011) *Rare Earth Elements-End Use and Recyclability Scientific Investigations Report 2011-5094*. Virginia.

Van Gosen, Bradley S, Philip L. Verplanck, R. R. S. and Gambogi, J. (2017) 'Critical mineral resources of the United States— Economic and environmental geology and prospects for future supply: U.S. Geological Survey Professional Paper 1802, p. O1– O31',. doi: 10.3133/pp1802O.

Gottlieb, P. and Dosbaba, M. (2015) 'the Tima Automated Mineral Analyzer for the Characterization of Ore Deposits', (September).

Gupta, C. and Krishnamurthy, N. (2005) *Extractive Metallurgy of Rare Earths*. Mumbai: CRC Press. Available at: www.crcpress.com (Accessed: 15 October 2020).

Gupta, C. and Krishnamurthy, N. (1992) 'Extractive metallurgy of rare earths', *International Materials Reviews*, 37(1), pp. 197–248. doi: 10.1179/imr.1992.37.1.197.

Gupta, N. and Li, B. (2016) 'Hydrophobic-hydrophilic separation (HHS) process for recovery and dewatering and dewatering of ultrfine coal', Conference Paper, in *SME Annual Meeting*.

Gupta, T., Ghosh, T., Akdogan, G., Bandopadhyay, S., (2019). Maximizing REE enrichment by froth flotation of Alaskan coal using Box-Behnken design', *Mining Engineering*. Society for Mining, Metallurgy and Exploration, 71(8), pp. 53–54. doi: 10.1007/s42461-019-0048-8.

Güler, T., Şahbudak, K., Çetinkaya, S., Akdemir, Ü., (2010). FTIR Spectroscopy Study on the Electrochemistry of Pyrite-Cu Interaction in the Presence of Dithiophosphinate at pH 9.2', *International Mineral Processing Symposium*, (October), pp. 321–329.

Haque, N., Hughes, A., Lim, S., Vernon, C., (2014) 'Rare earth elements: Overview of mining, mineralogy, uses, sustainability and environmental impact', *Resources*, 3(4), pp. 614–635. doi: 10.3390/resources3040614.

He, X., Liu, X., Nie, B., Song, D., (2017). FTIR and Raman spectroscopy characterization of functional groups in various rank coals', *Fuel*. Elsevier Ltd, 206, pp. 555–563. doi: 10.1016/J.FUEL.2017.05.101.

Heier, S. (2014) *Grid Integration of Wind Energy: Onshore and Offshore Conversion Systems - Siegfried Heier - Google Books*. 3rd edn. Edited by G. Roth. Kassel: Wiley. Available at: https://books.google.co.za/books?hl=en&lr=&id=d0FsAwAAQBAJ&oi=fnd&pg=PT16&ots=qwgP5qEDHC&sig=cr51U8kxp6LPjeGfW38UK7CRQDo&redir_esc=y#v=onepage&q&f=false (Accessed: 17 October 2020).

Holland, M.J., Cadle, A.B., Pinheiro, R., Falcon, R.M.S., (1989). Depositional environments and coal petrography of the Permian Karoo Sequence: Witbank Coalfield, South Africa',

International Journal of Coal Geology, 11(2), pp. 143–169. doi: 10.1016/0166-5162(89)90003-7.

Honaker, R., Groppo, J., Zhang, W., Bhagavatula, A., Rezaee, M., (2016). Recovery of Rare Earth Elements From Coal and Coal By- Products', (April). doi: 10.1130/abs/2017am-303789.

Honaker, R. and Groppo, J. (2016) 'Rare Earth Element Production from Coal'.

Honaker, R.Q., Groppo, J., Yoon, R.H., Luttrell, G.H., Noble, A., Herbst, J., (2017). Process evaluation and flowsheet development for the recovery of rare earth elements from coal and associated byproducts', *Minerals and Metallurgical Processing*. Society for Mining, Metallurgy and Exploration, 34(3), pp. 107–115. doi:10.19150/mmp.7610.

Honaker, R. Q., Zhang, W. and Werner, J. (2019) 'Acid Leaching of Rare Earth Elements from Coal and Coal Ash: Implications for Using Fluidized Bed Combustion to Assist in the Recovery of Critical Materials', *Energy and Fuels*. American Chemical Society, 33(7), pp. 5971–5980. doi: 10.1021/acs.energyfuels.9b00295.

Hoshino, M., Sanematsu, K. and Watanabe, Y. (2016) 'REE Mineralogy and Resources', in *Handbook on the Physics and Chemistry of Rare Earths*. Elsevier B.V., pp. 129–291. doi: 10.1016/bs.hpcre.2016.03.006.

Huang, Q., Noble, A., Herbst, J., Honaker, R., (2018). Liberation and release of rare earth minerals from Middle Kittanning, Fire Clay, and West Kentucky No. 13 coal sources', *Powder Technology*. Elsevier B.V., 332, pp. 242–252. doi: 10.1016/j.powtec.2018.03.063.

Humphries, M. (2010) *Rare Earth Elements: The Global Supply Chain , Congressional Research Service*. Available at: https://books.google.co.za/books?hl=en&lr=&id=uzkYstWv_HYC&oi=fnd&pg=PA1&otswapfOMyDl8&sig=5SnyjzkhoZEmNB7-3K-VBgAye0s&redir_esc=y#v=onepage&q&f=false (Accessed: 17 October 2020).

Humphries, M. (2013) 'Rare earth elements: The global supply chain', *Rare Earth Minerals: The Global Supply Chain*, pp. 1–20.

IEA (2019) *Coal 2019 – Analysis and forecasts to 2024*, *Fuel Report*. Available at: https://www.iea.org/reports/coal-2019 (Accessed: 25 November 2020).

ISO13909-4 standard, (2001), Hard coal and coke-Mechanical sampling-Part 4: Coal-Preparation of test samples, *International Organisation for Standardisation.*

ISO 12902 method, (2001), Solid mineral fuels Determination of total carbon, hydrogen and nitrogen Instrumental methods, *International Organisation for Standardisation.*

ISO 19579 standard, (2006), Solid mineral fuels-Determination of sulphur by IR spectrometry Instrumental methods, *International Organisation for Standardisation,* 75.160.10 Solid fuels.

ISO 7404-part 2 method, (2009), Methods for the petrographic analysis of bituminous coal and anthracite-Part 2: Preparation of coal samples, *International Organisation for Standardisation.*

ISO 7404-part 3 standard, (2001), Methods for the petrographic analysis of coals-Part 3: Method of determining maceral group composition, *International Organisation for Standardisation.*

Jeffrey, L. S. (2005) 'Characterization of the coal resources of South Africa', *Journal of The South African Institute of Mining and Metallurgy*, 105(2), pp. 95–102.

Ji, B. and Zhang, W. (2021) 'Rare earth elements (REEs) recovery and porous silica preparation from kaolinite', *Powder Technology*. Elsevier, 391, pp. 522–531. doi: 10.1016/J.POWTEC.2021.06.028.

Jordens, A., Marion, C., Langlois, R., Grammatikopoulos, T., Sheridan, R.S., Teng, C., Demers, H., Gauvin, R., Rowson, N.A., Waters, K.E., (2016). 'Beneficiation of the Nechalacho rare earth deposit. Part 2: Characterisation of products from gravity and magnetic separation', *Minerals Engineering*. Elsevier Ltd, 99, pp. 96–110. doi: 10.1016/j.mineng.2016.04.007.

Jordens, A., Cheng, Y. P. and Waters, Kristian E. (2013) 'A review of the beneficiation of rare earth element bearing minerals', *Minerals Engineering*. Elsevier Ltd, 41, pp. 97–114. doi: 10.1016/j.mineng.2012.10.017.

Kanungo, S. B. (1999) 'Rate process of the reduction leaching of manganese nodules in dilute HCl in presence of pyrite: Part II: Leaching behavior of manganese', *Hydrometallurgy*. Elsevier, 52(3), pp. 331–347. doi: 10.1016/S0304-386X(99)00022-5.

Karayigit, A.I., Gayer, R.A., Querol, X., Onacak, T., (2000) 'Contents of major and trace elements in feed coals from Turkish coal-fired power plants', *International Journal of Coal Geology*, 44(2), pp. 169–184. doi: 10.1016/S0166-5162(00)00009-4.

Ketris, M. P. and Yudovich, Y. E. (2009) 'Estimations of Clarkes for Carbonaceous biolithes: World averages for trace element contents in black shales and coals', *International Journal of Coal Geology*. Elsevier B.V., 78(2), pp. 135–148. doi: 10.1016/j.coal.2009.01.002.

Khanchi, A.R., Sedighi, H., Ansar, S., Fasihi, J., (2014) 'Preconcentration of rare earth elements from Iranian monazite ore by spiral separator using multi-response optimization method', *International Journal of Mining Science and Technology*, 24(1), pp. 117–121. doi: 10.1016/j.ijmst.2013.12.020.

Kim, R., Cho, H., Han, K.N., Kim, K., Mun, M., (2016) 'Optimization of acid leaching of rare-earth elements from mongolian apatite-based ore', *Minerals*, 6(3). doi: 10.3390/min6030063.

Kiser, M.J., Luttrell, G.H., Adel, G.T., Keles, S., Ripepi, N.S., (2015) *New Methodologies for the Characterization and Separation of Rare Earth Elements Present in Coal*.

Kolker, A., Scott, C., Hower, J.C., Vazquez, J.A., Lopano, C.L., Dai, S., (2017) 'Distribution

of rare earth elements in coal combustion fly ash, determined by SHRIMP-RG ion microprobe', *International Journal of Coal Geology*. Elsevier, 184(June), pp. 1–10. doi: 10.1016/j.coal.2017.10.002.

Kołodyńska, D., Fila, D., Gajda, B., Gęga, J., Hubicki, Z., (2019) 'Rare Earth Elements—Separation Methods Yesterday and Today', in *Applications of Ion Exchange Materials in the Environment*. Springer International Publishing, pp. 161–185. doi: 10.1007/978-3-030-10430-6_8.

Kossovich, E.L., Borodich, F.M., Epshtein, S.A., Galanov, B.A., (2020) 'Indentation of bituminous coals: Fracture, crushing and dust formation', *Mechanics of Materials*. Elsevier B.V., 150, p. 103570. doi: 10.1016/j.mechmat.2020.103570.

Kraber, S. (2013) 'Getting Started: Stat-Ease Resources New to Design of Experiments?', *2013 Stat-Ease*, pp. 1–53. Available at: http://www.statease.com/beginner.html•Webinars:http://www.statease.com/webinar.html•Articles:http://www.statease.com/articles.html•SoftwareTutorials:http://www.statease.com/dx8_man.html (Accessed: 13 September 2021).

Kumari, A. *et al.* (2015) 'Process development to recover rare earth metals from monazite mineral: A review', *Minerals Engineering*. Elsevier Ltd, 79(August), pp. 102–115. doi: 10.1016/j.mineng.2015.05.003.

Kuppusamy, V. K., Kumar, A. and Holuszko, M. (2019) 'Simultaneous Extraction of Clean Coal and Rare Earth Elements From Coal Tailings Using Alkali-Acid Leaching Process', *Journal of Energy Resources Technology, Transactions of the ASME*. American Society of Mechanical Engineers (ASME), 141(7). doi: 10.1115/1.4043328.

Laudal, D. A. (2017) 'Evaluation Of Rare Earth Element Extraction From North Dakota Coal-Related Feed Stocks'. Available at: https://commons.und.edu/theses (Accessed: 31 August 2021).

Laudal, D.A., Benson, S.A., Addleman, R.S., Palo, D., (2018) 'Leaching behavior of rare earth elements in Fort Union lignite coals of North America', *International Journal of Coal Geology*. Elsevier, 191(March), pp. 112–124. doi: 10.1016/j.coal.2018.03.010.

Li, B., Zhuang, X., Querol, X., Moreno, N., Yang, L., Shangguan, Y., Li, J., (2019) 'Mineralogy and Geochemistry of Late Permian Coals within the Tongzi Coalfield in Guizhou Province, Southwest China', *Minerals*. MDPI AG, 10(1), p. 44. doi: 10.3390/min10010044.

Li, L. Z. H. I. and Yang, X. (2014) 'China's Rare Earth Ore Deposits and Beneficiation Techniques', *1st European Rare Earth Resources Conference*, pp. 26–36.

Li, M., Zhang, X.-W., Liu, Z.-G., Wang, M.-T., Liu, J., Yang, J.-P., (2013) 'Mixed rare earth

concentrate leaching with HCl-$AlCl_3$ solution', *Rare Metals*, 32(3), pp. 312–317. doi: 10.1007/s12598-013-0034-0.

De Lima, I. B. and Leal Filho, W. (2015) *Rare Earths Industry - 1st Edition*. 1st edn, *Elsevier*. 1st edn. Edited by I. B. De Lima and W. Leal Filho. Hamburg, Roriama: Elsevier. Available at: https://www.elsevier.com/books/rare-earths-industry/borges-de-lima/978-0-12-802328-0 (Accessed: 15 October 2020).

Lin, R., Bank, T., Roth, E., Granite, E., Soong, Y., (2017) 'Organic and inorganic association of rare earth elements in coal', *34th Annual International Pittsburgh Coal Conference: Coal - Energy, Environment and Sustainable Development, PCC 2017*, 2017-Septe, pp. 1–20.

Lin, R., Soong, Y., Roth, E., Bank, T.L., Howard, B., Granite, E., (2017) 'Recovery of Rare Earth Elements From Coal and Coal By-Products', (April). doi: 10.1130/abs/2017am-303789.

Lolon, S. and Rahman, F. (2014) *(PDF) Overview of Rare Earth Elements in Indonesia*, *Coal Asia*. Available at: https://www.researchgate.net/publication/280302337_Overview_of_Rare_Earth_Elements_in_Indonesia (Accessed: 16 November 2020).

Long, K. R, Van Gosen, B.S., Foley, N., Cordier, D., (2010) *The Principal Rare Earth Elements Deposits of the United States—A Summary of Domestic Deposits and a Global Perspective*, *USGS Scientific Investigations Report 2010–5220*. Available at: https://pubs.usgs.gov/sir/2010/5220/ (Accessed: 10 November 2020).

Long, K. R. (2011) *The Future of Rare Earth Elements-Will These High-Tech Industry Elements Continue in Short Supply?* Virginia. Available at: http://seeker401.wordpress.com/2010/11/18/experts-speak-about-a-rare-earth- (Accessed: 17 October 2020).

Long, K.R., Van Gosen, B.S., Foley, N., Cordier, D., (2012) 'The principal rare earth elements deposits of the United States: A summary of domestic deposits and a global perspective', in *Non-Renewable Resource Issues: Geoscientific and Societal Challenges*. Springer Netherlands, pp. 131–155. doi: 10.1007/978-90-481-8679-2_7.

Luttrell, G.H., Kiser, M.J., Yoon, R.H., Bhagavatula, A., Rezaee, M., Honaker, R.Q., (2016) 'Rare Earth element concentrations in product streams of coal preparation plants in the eastern United States', in *2016 SME Annual Conference and Expo: The Future for Mining in a Data-Driven World*. Phoenix: Society for Mining, Metallurgy and Exploration, pp. 710–712. Available at: https://pennstate.pure.elsevier.com/en/publications/rare-earth-element-concentrations-in-product-streams-of-coal-prep (Accessed: 26 November 2020).

Mabuza, M., Premlall, K. and Daramola, M. O. (2020) 'Physicochemical characterization of

South African coals upon short-term flue gas exposure using conventional and advanced techniques', *Materials Science for Energy Technologies*. Elsevier, 3, pp. 25–35. doi: 10.1016/J.MSET.2019.09.008.

Maledi, N. (2017) 'Characterisation of Mineral Matter in South African Coals Using Micro-Raman Spectroscopy and Other Techniques', p. 331.

Mancheri, N.A., Sprecher, B., Bailey, G., Ge, J., Tukker, A., (2019) 'Effect of Chinese policies on rare earth supply chain resilience', *Resources, Conservation and Recycling*. Elsevier B.V., 142, pp. 101–112. doi: 10.1016/j.resconrec.2018.11.017.

Mardon, S. M. and Hower, J. C. (2004) 'Impact of coal properties on coal combustion by-product quality: Examples from a Kentucky power plant', *International Journal of Coal Geology*, 59(3–4), pp. 153–169. doi: 10.1016/J.COAL.2004.01.004.

Middleton, A., Park, D.M., Jiao, Y., Hsu-Kim, H., (2020) 'Major element composition controls rare earth element solubility during leaching of coal fly ash and coal by-products', *International Journal of Coal Geology*. Elsevier B.V., 227, p. 103532. doi: 10.1016/j.coal.2020.103532.

Mills, S. J. (2010) *Coal use in the new economies of China, India and South Africa*, *Africa*. IEA Clean Coal Centre.

Moghise, M., Pourrahim, M., Rezai, B., Gharabaghi, M., (2016) 'Concentration and recycling of rare earth elements (REEs) from iron mine waste using a combination of physical separation methods', *Journal of Mining and Environment*, 7(2), pp. 195–203. doi: 10.22044/jme.2016.521.

Moldoveanu, G. A. and Papangelakis, V. G. (2013) 'Recovery of rare earth elements adsorbed on clay minerals: II. Leaching with ammonium sulfate', *Hydrometallurgy*. Elsevier B.V., 131–132(March 2020), pp. 158–166. doi: 10.1016/j.hydromet.2012.10.011.

Montross, S.N., Yang, J., Britton, J., McKoy, M., Verba, C., (2020) 'Leaching of Rare Earth Elements from Central Appalachian Coal Seam Underclays', *Minerals*, 10(577), pp. 1–20. doi: 10.3390/min10060577.

Morris, L. (2011) 'Direct drive vs. gearbox: Progress on both fronts', *Power Engineering (Barrington, Illinois)*, 115(3), pp. 38–42.

Moumakwa, O. (2010) 'The Future Role of the Waterberg Coalfield in South Africa's coal industry, Directorate: Mineral Economics'. Available at: http://www.dme.gov.za (Accessed: 16 February 2021).

Mudd, G. M. and Jowitt, S. M. (2016) 'Rare earth elements from heavy mineral sands: assessing the potential of a forgotten resource', *Applied Earth Science*. Taylor and Francis Ltd.,

125(3), pp. 107–113. doi: 10.1080/03717453.2016.1194955.

Munir, M.A.M., Liu, G., Yousaf, B., Ali, M.U., Abbas, Q., Ullah, H., (2018) 'Enrichment of Bi-Be-Mo-Cd-Pb-Nb-Ga, REEs and Y in the Permian coals of the Huainan Coalfield, Anhui, China', *Ore Geology Reviews*. Elsevier B.V., 95, pp. 431–455. doi: 10.1016/j.oregeorev.2018.02.037.

Naumov, A. (2008) 'Review of the world market of rare-earth metals', *Russian Journal of Non-Ferrous Metals*, 49(1), pp. 14–22. doi: 10.1007/s11981-008-1004-6.

Neary, C. R. and Highley, D. E. (1984) 'The Economic Importance of the Rare Earth Elements', in *Developments in Geochemistry*. Elsevier, pp. 423–466. doi: 10.1016/B978-0-444-42148-7.50017-4.

Pandey, B. D. (2011) 'Rare Metals Extraction from Non-ferrous Resources in India: Present Status and Prospects of R&D', in Dr. T. R., M., Dr. Abhilash, and S. Majumdar (eds) *15th International Conference on Non -ferrous metals*. Kolkata, pp. 1–15.

Park, S. and Liang, Y. (2019) 'Bioleaching of trace elements and rare earth elements from coal fly ash', *International Journal of Coal Science and Technology*. Springer Singapore, 6(1), pp. 74–83. doi: 10.1007/s40789-019-0238-5.

Peelman, S., Kooijman, D., Sietsma, J., Yang, Y., (2018) 'Hydrometallurgical Recovery of Rare Earth Elements from Mine Tailings and WEEE', *Journal of Sustainable Metallurgy*. Springer International Publishing, 4(3), pp. 367–377. doi: 10.1007/s40831-018-0178-0.

Peiravi, M., Ackah, L., Guru, R., Mohanty, M., Liu, J., Xu, B., Zhu, X., Chen, L., (2017) 'Chemical extraction of rare earth elements from coal ash', *Minerals and Metallurgical Processing*, 34(4), pp. 170–177. doi: 10.19150/mmp.7856.

Pooe, D. and Mathu, K. (2011) 'The South African coal mining industry: A need for a more efficient and collaborative supply chain', *Journal of Transport and Supply Chain Management*. AOSIS, 5(1). doi: 10.4102/jtscm.v5i1.80.

Pourret, O., Davranche, M., Gruau, G., Dia, A., (2007) 'Rare earth elements complexation with humic acid', *Chemical Geology*. Elsevier, 243(2), pp. 128–141. doi: 10.1016/j.chemgeo.2007.05.018ï.

Prime, J. (2019) 'IEA Coal information overview and statistical report'.

Ratshomo, K. (2016) 'South African coal sector report, Directorate: Energy data collection, management and analysis', Pretoria. Available at: http://www.energy.gov.za (Accessed: 2 December 2020).

Reid, I. (2018) 'Non-energy uses of Coal', (October).

Resende, L. V. and Morais, C. A. (2010) 'Study of the recovery of rare earth elements from

computer monitor scraps - Leaching experiments', *Minerals Engineering*. Elsevier Ltd, 23(3), pp. 277–280. doi: 10.1016/j.mineng.2009.12.012.

Roskill (2017) *Rare Earths Global Industry, Markets & Outlook report*. Available at: https://roskill.com/news/rare-earths/ (Accessed: 17 November 2020).

Rozelle, P.L., Khadilkar, A.B., Pulati, N., Soundarrajan, N., Klima, M.S., Mosser, M.M., Miller, C.E., Pisupati, S. V., (2016) 'A Study on Removal of Rare Earth Elements from U.S. Coal Byproducts by Ion Exchange', *Metallurgical and Materials Transactions E*. Springer US, 3(1), pp. 6–17. doi: 10.1007/s40553-015-0064-7.

Saxby, J. D. (2000) 'Minerals in coal', in *Organic Matter and Mineralisation: Thermal Alteration, Hydrocarbon Generation and Role in Metallogenesis*. Springer Netherlands, pp. 314–328. doi: 10.1007/978-94-015-9474-5_15.

Schofield, A. and Haskin, L. (1964) 'Rare-earth distribution patterns in eight terrestrial materials', *Geochimica et Cosmochimica Acta*. Pergamon, 28(4), pp. 437–446. doi: 10.1016/0016-7037(64)90117-6.

Scott, A. C. (2002) 'Coal petrology and the origin of coal macerals: A way ahead?', *International Journal of Coal Geology*, 50(1–4), pp. 119–134. doi: 10.1016/S0166-5162(02)00116-7.

Seredin, V. V. (1996) 'Rare earth element-bearing coals from the Russian Far East deposits', *International Journal of Coal Geology*. Elsevier B.V., 30(1–2), pp. 101–129. doi: 10.1016/0166-5162(95)00039-9.

Seredin, V. V. (2010) 'A new method for primary evaluation of the outlook for rare earth element ores', *Geology of Ore Deposits*. Maik Nauka-Interperiodica Publishing, 52(5), pp. 428–433. doi: 10.1134/S1075701510050077.

Seredin, V. V. and Dai, S. (2012) 'Coal deposits as potential alternative sources for lanthanides and yttrium', *International Journal of Coal Geology*. Elsevier B.V., 94, pp. 67–93. doi: 10.1016/j.coal.2011.11.001.

Shannon, R. D. (1976) *Revised Effective Ionic Radii and Systematic Studies of Interatomie Distances in Halides and Chaleogenides, Acta Cryst*. Wilmington.

Shen, Y., Moomy, R. and Eggert, R. G. (2020) 'China's public policies toward rare earths, 1975–2018', *Mineral Economics*. Springer, 33(1–2), pp. 127–151. doi: 10.1007/s13563-019-00214-2.

Soltani, F., Abdollahy, M., Javad Koleini, S.M., Moradkhani, D., (2017) 'Selection of an appropriate leaching method for light REEs from Esfordi flotation concentrate based on mineral characterization', *Journal of the Southern African Institute of Mining and Metallurgy*.

The Southern African Institute of Mining and Metallurgy, 117(5), pp. 443–450. doi: 10.17159/2411-9717/2017/V117N5A6.

Soundarrajan, N., Pulati, N., Klima, M.S., Ityokumbul, M., Pisupati, S. V., (2015) *Separation of rare earth elements from coal and coal products*. Available at: https://edx.netl.doe.gov/dataset/netl-ree-technical-reports/revision_resource/a2c1d4be-eae7-a2a7-a547-850c15db2815.

Strümpel, C., McCann, M., Beaucarne, G., Arkhipov, V., Slaoui, A., Švrček, V., del Cañizo, C., Tobias, I. (2007) 'Modifying the solar spectrum to enhance silicon solar cell efficiency-An overview of available materials', *Solar Energy Materials and Solar Cells*. North-Holland, 91(4), pp. 238–249. doi: 10.1016/j.solmat.2006.09.003.

Suárez-Ruiz, I. and Ward, C. R. (2008) 'Basic Factors Controlling Coal Quality and Technological Behavior of Coal', in *Applied Coal Petrology*. Elsevier Ltd, pp. 19–59. doi: 10.1016/B978-0-08-045051-3.00002-6.

Szabadvary, F. (1988) 'Chapter 73 The history of the discovery and separation of the rare earths', *Handbook on the Physics and Chemistry of Rare Earths*. Elsevier, pp. 33–80. doi: 10.1016/S0168-1273(88)11005-2.

Taole, R. L., Falcon, R. M. S. and Bada, S. O. (2015) 'The impact of coal quality on the efficiency of a spreader stoker boiler', *Journal of the Southern African Institute of Mining and Metallurgy*. South African Institute of Mining and Metallurgy, 115(12), pp. 1159–1165. doi: 10.17159/2411-9717/2015/v115n12a3.

Taylor, G.H; Teichmüller, M.; Davis A.; C.F.K. Diessel; R. Littke; P. Robert, 1998. Organic petrology : a new handbook incorporating some revised parts of Stach's Textbook of coal petrology 704.

Taylor, S. and McLennan, S. (1985) *The continental crust: Its composition and evolution* . 1st edn. United States. Available at: https://www.osti.gov/biblio/6582885 (Accessed: 7 June 2021).

Teimouri, S. (2020) *Feasibility study on the use of imidazolium-based ionic liquids in the extraction of gold*. Masters thesis. University of the Witwatersrand.

TheCoalHub (2020) *Coal production regions China , The coal Industry portal*. Available at: https://thecoalhub.com/top-3-provinces-contribute-70-of-chinas-coal-output-in-jan-may.html (Accessed: 26 November 2020).

Thompson, W. *et al.* (2011) 'Mineralogical studies in assisting beneficiation of Rare Earth Element Minerals from Carbonatite deposits', in *10th International Congress for Applied Minerology*. Randburg, pp. 1–8.

Tunsu, C., Petranikova, M., Ekberg, C., Retegan, T., (2016) 'A hydrometallurgical process for the recovery of rare earth elements from fluorescent lamp waste fractions', *Separation and Purification Technology*. Elsevier, 161, pp. 172–186. doi: 10.1016/j.seppur.2016.01.048.

van Breugel, Y., Cowan, A. K. and Tsikos, H. (2019) 'Geochemical Study of Weathered Coal, a Co-Substrate for Bioremediation of South African Coal Discard Dumps', *Minerals*. MDPI AG, 9(12), p. 772. doi: 10.3390/min9120772.

Vijayalakshmi, R., Mishra, S.L., Singh, H., Gupta, C.K., (2001) 'Processing of xenotime concentrate by sulphuric acid digestion and selective thorium precipitation for separation of rare earths', *Hydrometallurgy*. Elsevier, 61(2), pp. 75–80. doi: 10.1016/S0304-386X(00)00159-6.

Wadsworth, M. E. and Miller, J. D. (1979) 'Hydrometallurgical Processes', in *Rate Processes of Extractive Metallurgy*. Springer US, pp. 133–244. doi: 10.1007/978-1-4684-9117-3_4.

Wagner, N. J. and Matiane, A. (2018) 'Rare earth elements in select Main Karoo Basin (South Africa) coal and coal ash samples', *International Journal of Coal Geology*. Elsevier, 196(June), pp. 82–92. doi: 10.1016/j.coal.2018.06.020.

Wagner, N., Malumbazo, N. and Falcon, R. M. . (2018) *Southern African Coals and Carbons: Definitions and Applications of Organic* . Cape Town: Struik Nature. Available at: https://books.google.co.za/books/about/Southern_African_Coals_and_Carbons.html?id=6QkAvgEACAAJ&redir_esc=y (Accessed: 7 June 2021).

Wang, W., Qin, Y., Sang, S., Zhu, Y., Wang, C., Weiss, D.J., (2008) 'Geochemistry of rare earth elements in a marine influenced coal and its organic solvent extracts from the Antaibao mining district, Shanxi, China', *International Journal of Coal Geology*, 76(4), pp. 309–317. doi: 10.1016/j.coal.2008.08.012.

Ward, C. R. (2002) 'Analysis and significance of mineral matter in coal seams', *International Journal of Coal Geology*. Elsevier, 50(1–4), pp. 135–168. doi: 10.1016/S0166-5162(02)00117-9.

Ward, C. R. and Suárez-Ruiz, I. (2008) 'Introduction to Applied Coal Petrology', in *Applied Coal Petrology*. Elsevier Ltd, pp. 1–18. doi: 10.1016/B978-0-08-045051-3.00001-4.

What is coal? | World Coal Association (no date). Available at: https://www.worldcoal.org/coal/what-coal (Accessed: 16 September 2020).

Whitcomb, P. (2018) 'Exciting New Features in Design-Expert-V11 and Beyond". Presented by Pat Whitcomb Founder and Principle', in *Stat-Ease European User Conference 2018*.

de Wit, D. R. (2015) 'An African Rare Earth Story'

Wood, L. (2019) *South Africa Coal Mining Report 2019 including Coal Testing and*

Laboratories, *CISION PR newswire*. Available at: https://www.prnewswire.com/news-releases/south-africa-coal-mining-report-2019-including-coal-testing-and-laboratories-300945607.html (Accessed: 25 November 2020).

WorldCoalInstitute (2005) 'the Coal Resource a Comprehensive Overview of Coal the Coal Resource Where Does Coal Come From ? What Is It', *World Coal Institute*, pp. 1–44. doi: 10.1017/CBO9781107415324.004.

Xiuyi, T. (2011) 'Mineral matter in coal', Coal, Oil Shale, Natural Bitumen, Heavy oil and Peat, I(86), pp. 1–6.

Yang, X., Satur, J. V., Sanematsu, K., Laukkanen, J., Saastamoinen, T., (2015) 'Beneficiation studies of a complex REE ore', *Minerals Engineering*. Elsevier Ltd, 71(November), pp. 55–64. doi: 10.1016/j.mineng.2014.10.005.

Yang, X. (2019) 'Leaching Characteristics of Rare Earth Elements From Bituminous Coal-Based Sources', p. 159.

Yang, X. and Honaker, R. (2020) 'Leaching kinetics of rare earth elements from fire clay seam coal', *Minerals*, 10(6). doi: 10.3390/min10060491.

Yang, X., Werner, J. and Honaker, R. Q. (2019) 'Leaching of rare Earth elements from an Illinois basin coal source', *Journal of Rare Earths*. Elsevier Ltd, 37(3), pp. 312–321. doi: 10.1016/j.jre.2018.07.003.

Yin, Y., Yin, H., Wu, Z., Qi, C., Tian, H., Zhang, W., Hu, Z., Feng, L., (2019) 'Characterization of coals and coal ashes with high Si content using combined second-derivative infrared spectroscopy and Raman spectroscopy', *Crystals*. MDPI AG, 9(10). doi: 10.3390/CRYST9100513.

Zaimes, G.G., Hubler, B.J., Wang, S., Khanna, V., (2015) 'Environmental life cycle perspective on rare earth oxide production', *ACS Sustainable Chemistry and Engineering*. American Chemical Society, 3(2), pp. 237–244. doi: 10.1021/sc500573b.

Zeng, F. (2008) *HEAVY OIL AND PEAT-Vol. I-The Origin of Coal and World Reserves-Fangui*.

Zhang, W., Rezaee, M., Bhagavatula, A., Li, Y., Groppo, J., Honaker, R., (2015) 'A review of the occurrence and promising recovery methods of rare earth elements from coal and coal by-products', *International Journal of Coal Preparation and Utilization*, 35(6), pp. 295–330. doi: 10.1080/19392699.2015.1033097.

Zhang, W., Honaker, R. and Groppo, J. (2017) 'Concentration of rare earth minerals from coal by froth flotation', *SME Annual Conference and Expo 2017: Creating Value in a Cyclical Environment*, 34(3), pp. 647–651.

Zhang, W. and Honaker, R. Q. (2018) ‘Rare earth elements recovery using staged precipitation from a leachate generated from coarse coal refuse’, *International Journal of Coal Geology*. Elsevier, 195(November 2017), pp. 189–199. doi: 10.1016/j.coal.2018.06.008.

Zhang, W., Noble, A., Yang, X., Honaker, R., (2020) ‘A comprehensive review of rare earth elements recovery from coal-related materials’, *Minerals*. MDPI AG, p. 451. doi: 10.3390/min10050451.

Zhang, W. and Honaker, R. (2019a) ‘Calcination pretreatment effects on acid leaching characteristics of rare earth elements from middlings and coarse refuse material associated with a bituminous coal source’, *Fuel*. Elsevier Ltd, 249, pp. 130–145. doi: 10.1016/j.fuel.2019.03.063.

Zhang, W. and Honaker, R. (2019b) ‘Enhanced leachability of rare earth elements from calcined products of bituminous coals’, *Minerals Engineering*. Elsevier, 142(13), p. 105935. doi: 10.1016/j.mineng.2019.105935.

Zhang, W. and Honaker, R. (2020) ‘Characterization and recovery of rare earth elements and other critical metals (Co, Cr, Li, Mn, Sr, and V) from the calcination products of a coal refuse sample’, *Fuel*. Elsevier, 267(January), p. 117236. doi: 10.1016/j.fuel.2020.117236.

Zhou, B., Li, Z. and Chen, C. (2017) ‘Global potential of rare earth resources and rare earth demand from clean technologies’, *Minerals*, 7(11), pp. 1–14. doi: 10.3390/min7110203.

APPENDICES

Appendix A1

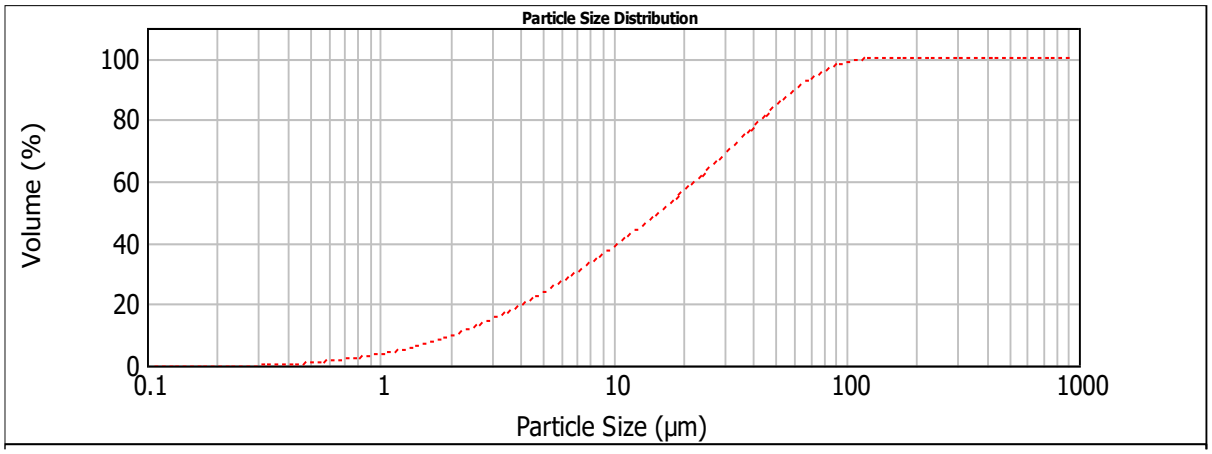


Figure A1-1: PSD curve for RC1 coal sample calcined at 500°C.

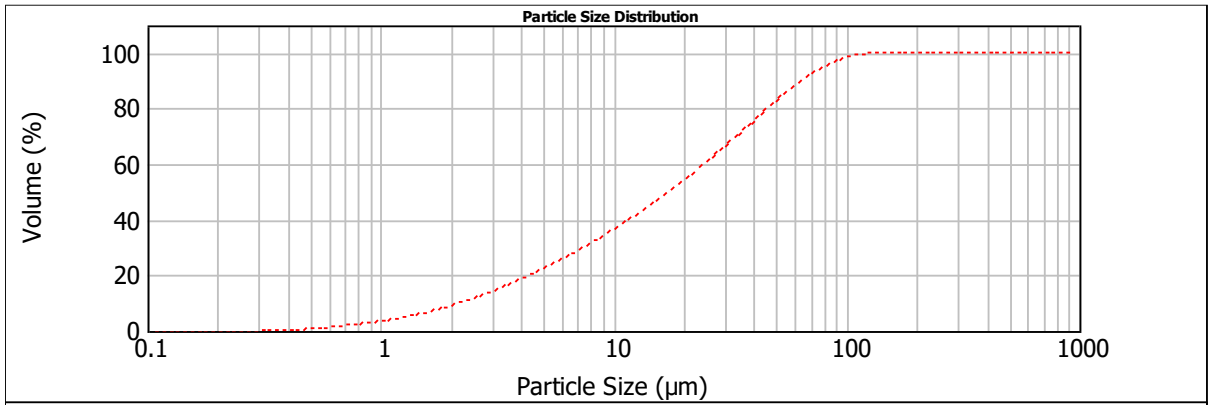


Figure A1-2: PSD curve for RC1 coal sample calcined at 600°C.

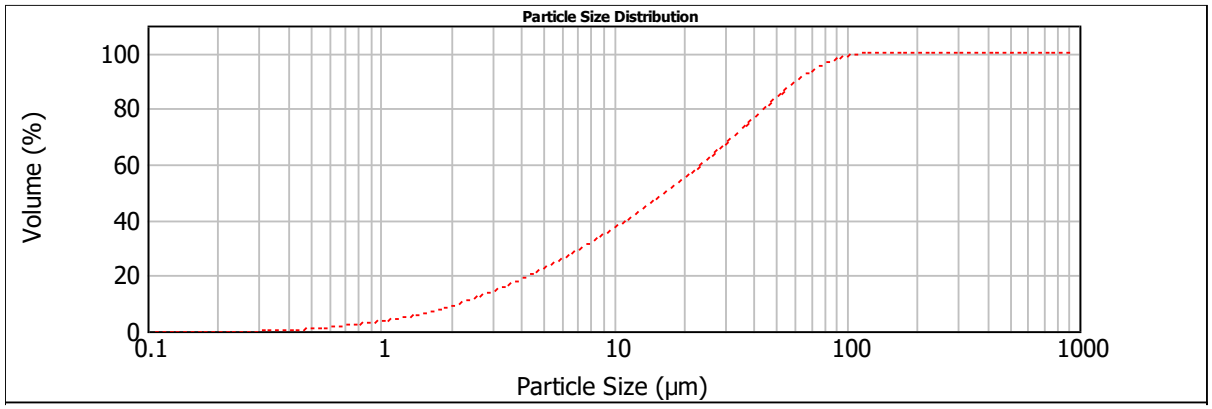


Figure A1-3: PSD curve for RC1 coal sample calcined at 700°C.

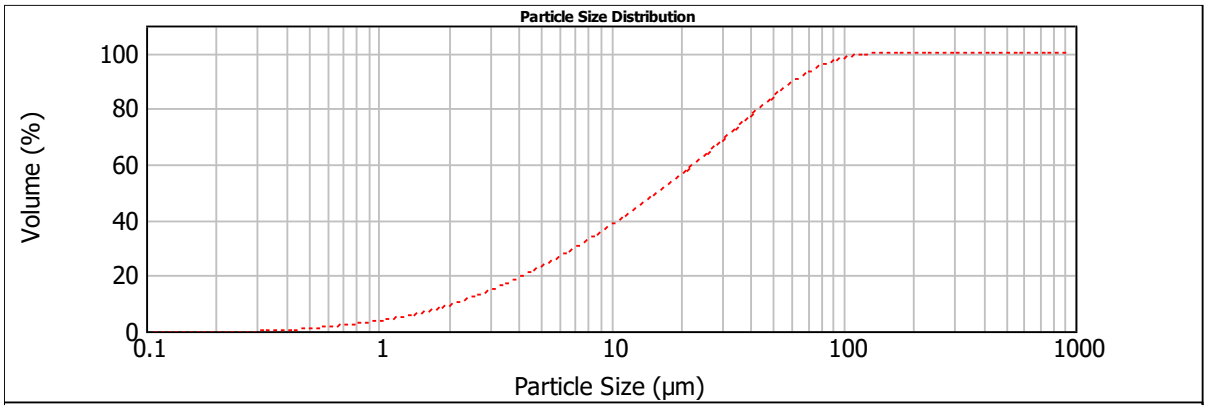


Figure A1-4: PSD curve for RC1 coal sample calcined at 800°C.

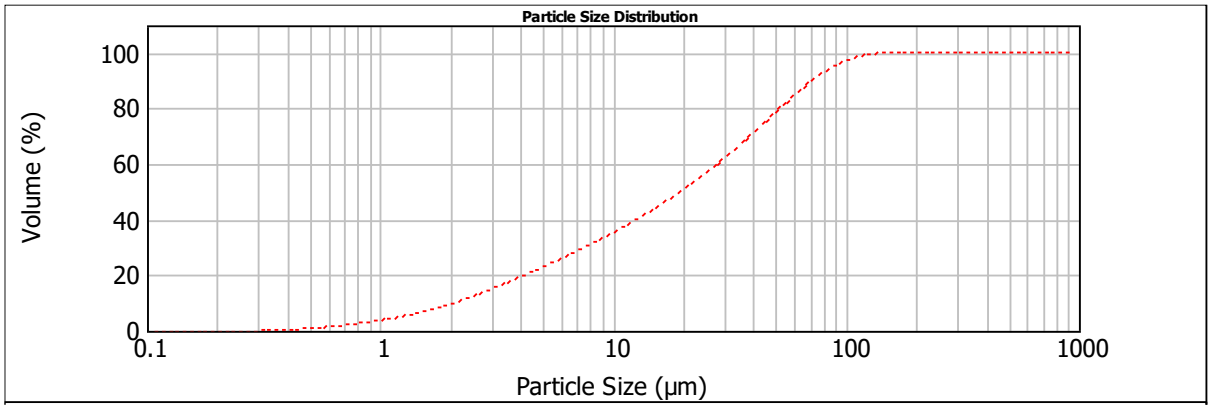


Figure A1-5: PSD curve for DC1 coal sample calcined at 500°C.

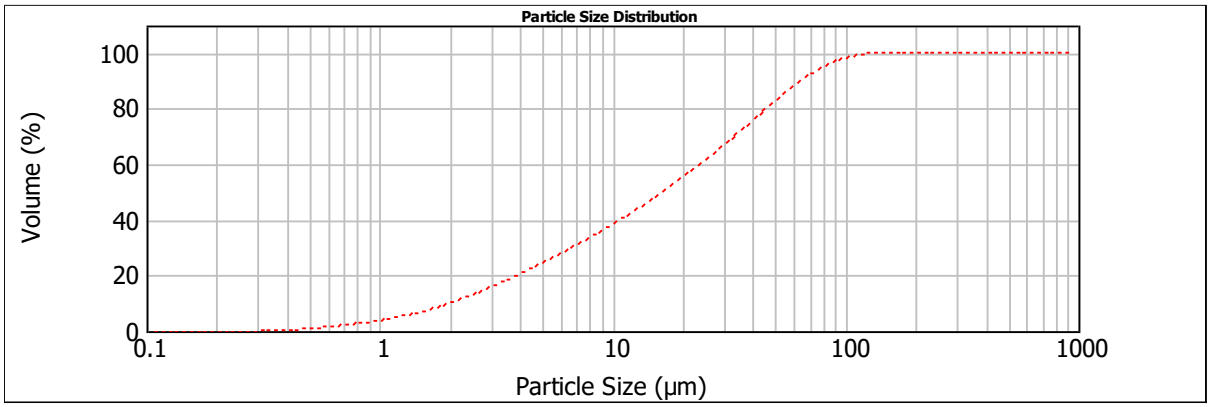


Figure A1-6: PSD curve for DC1 coal sample calcined at 600°C.

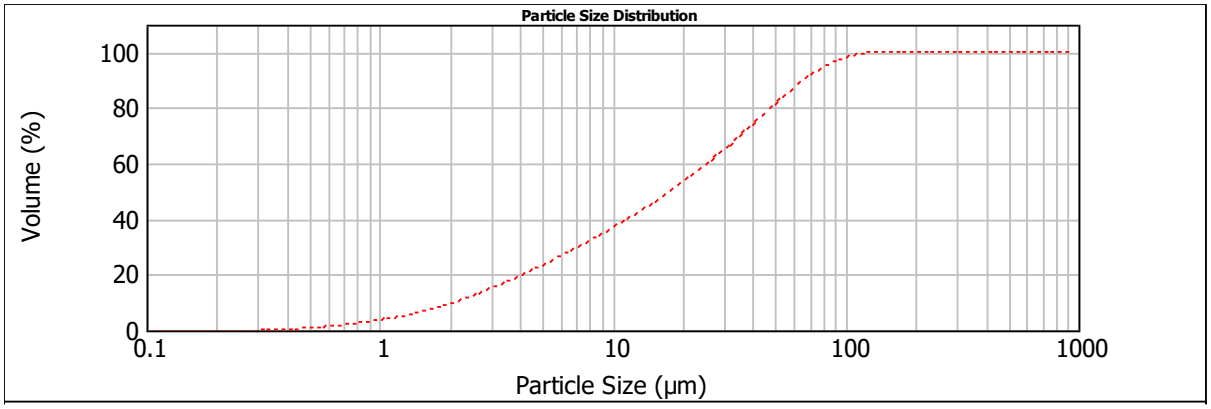


Figure A1-7: PSD curve for DC1 coal sample calcined at 700°C.

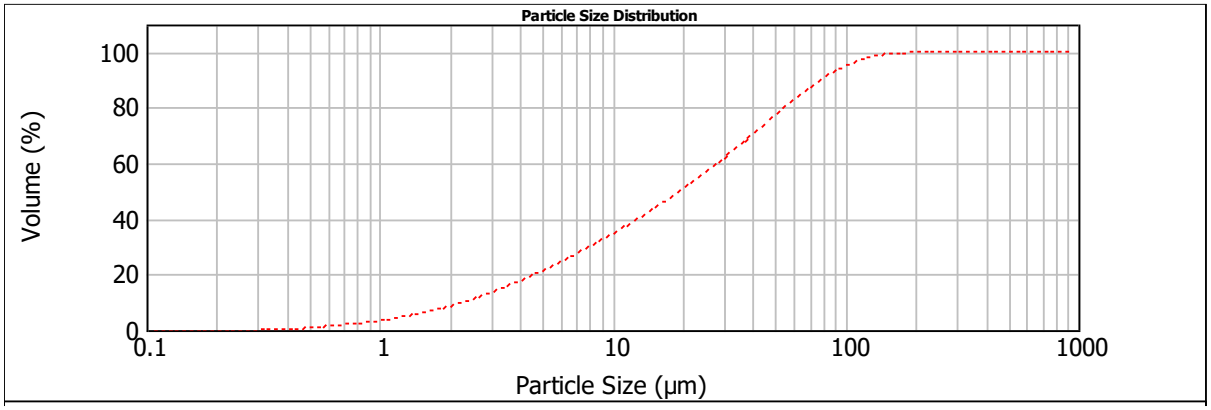


Figure A1-8: PSD curve for DC1 coal sample calcined at 800°C.